6-2017

Facies Architecture and Provenance of a Boulder-Conglomerate Submarine Channel System, Panoche Formation, Great Valley Group: A Forearc Basin Response to Middle Cretaceous Tectonism in the California Convergent Margin

T. J. Greene

Kathleen D. Surpless
Trinity University, ksurples@trinity.edu

Research Paper

GEOSPHERE

GEOSPHERE; v. 13, no. 3

doi:10.1130/GES01422.1

15 figures; 1 plate; 3 tables; 1 supplemental file

CORRESPONDENCE: tjgreene@csuchico.edu

CITATION: Greene, T.J., and Surpless, K.D., 2017, Facies architecture and provenance of a boulder-conglomerate submarine channel system, Panoche Formation, Great Valley Group: A forearc basin response to middle Cretaceous tectonism in the California convergent margin: Geosphere, v. 13, no. 3, doi:10.1130/GES01422.1.

Received 26 August 2016
Revision received 22 December 2016
Accepted 15 March 2017

Facies architecture and provenance of a boulder-conglomerate submarine channel system, Panoche Formation, Great Valley Group: A forearc basin response to middle Cretaceous tectonism in the California convergent margin

Todd J. Greene[1] and Kathleen D. Surpless[2]

[1]Department of Geological and Environmental Sciences, California State University, Chico, 400 West 1st Street, Chico, California 95929-0205, USA
[2]Department of Geosciences, Trinity University, One Trinity Place, San Antonio, Texas 78212, USA

ABSTRACT

Tectonic reorganization induced by a rapid increase in plate motion obliquity and rate beginning at ca. 100 Ma affected California's Andean-style convergent margin, with concomitant changes in the accretionary prism of the Franciscan Complex, the Great Valley forearc basin, and the Sierran continental arc. Using facies analysis and a combined provenance approach, we suggest that this ca. 100 Ma tectonic signal is preserved in a Cenomanian (Upper Cretaceous) boulder-conglomerate outcrop along the San Luis Reservoir (SLR) in the southern Great Valley, which represents the thickest and coarsest deep-water deposit ever described in the Great Valley Group (GVG). We document a 1.8-km-thick by 4-km-long depositional-dip profile of an interpreted SE-directed (axial) submarine channel system that is part of a conglomeratic package that stretches 20 km along the east-central Diablo Range. Our facies analysis of the SLR area documents five facies associations within four aggradational channel complex sets, followed by regional abandonment.

Sandstone petrography and mudrock geochemical data suggest a dissected continental Sierra Nevadan arc source. Conglomerate clast counts show abundant ophiolitic-type clasts that may be derived from the Coast Range Ophiolite and/or the Western Sierra Nevada Metamorphic Belt. Detrital-zircon geochronology data also indicate western and central Sierra Nevadan sources; however, we interpret an anomalous (relative to other Cenomanian localities) 105–95 Ma zircon population to indicate the initial erosional products from the volcanic carapace associated with the Late Cretaceous magmatic flare-up within the eastern Sierran arc. This flare-up has been linked to an increase in arc-parallel plate motion that induced deformation along shear zones in the eastern Sierra Nevada, allowing for widespread plutonism. Our provenance interpretation makes the SLR area the earliest Upper Cretaceous GVG locality to receive significant detritus from the flare-up, effectively linking tectonic plate motion changes and coarse-grained, deep-water forearc sedimentation.

INTRODUCTION

California's Late Jurassic through Paleocene history includes one of the best long-lived examples of Andean-style convergent margin tectonics in the geologic record (Bailey et al., 1964; Dickinson and Seely, 1979; Ingersoll, 1979, 1982; Ingersoll and Dickinson, 1981; Dickinson, 1995; Ducea, 2001). Moreover, the mid-Cenozoic conversion to transform tectonics of the San Andreas fault system uplifted and exposed a rich record of continuous forearc sedimentation and accretionary prism tectonics (Atwater, 1970; Dickinson and Rich, 1972; Mansfield, 1979; Short and Ingersoll, 1990; Williams et al., 1998). From east to west, the major tectonic elements include the volcanic arcs of the Sierra Nevada–Klamath mountains, the forearc basin of the Great Valley (represented by the Great Valley Group [GVG]), and the accretionary prism of the Franciscan Complex (Fig. 1; Hamilton, 1969; Dickinson, 1970, 1976; Ernst, 1970; Hsü, 1971; Maxwell, 1974; Schweickert and Cowan, 1975). Numerous studies of each tectonic element have helped resolve the details of the margin that involves changes in magmatism, accretionary tectonics, and basin subsidence (Ingersoll, 1978, 1979, 1982; Dickinson and Seely, 1979; Ingersoll and Dickinson, 1981; Moxon and Graham, 1987; DeGraaff-Surpless et al., 2002; Williams and Graham, 2013; Surpless, 2014; Sharman et al., 2015; Wakabayashi, 2015; and many others).

The transition between the Early and Late Cretaceous (ca. 100 Ma) has received particular attention as an opportunity to examine how a convergent system responded to changes in plate motion rates and direction. Many studies have documented an overall increase in plate convergence rate and plate motion parallel to the arc (obliquity) occurring 100–90 Ma (Page and Engebretson, 1984; Engebretson et al., 1985; Liu et al., 2008). Others suggest that these plate motion changes led to induced deformation in the eastern Sierran arc, resulting in increased rates of magmatism (Glazner, 1991; Tikoff and Teyssier, 1992; McNulty, 1995; Greene and Schweickert, 1995; Tikoff and Greene, 1997; Tobisch et al., 2000; Memeti et al., 2014; Paterson and Ducea, 2015), as well as accelerated phases of accretion in the prism (Wakabayashi, 2015). Studies of forearc basin stratigraphy have also recognized various sedimentary

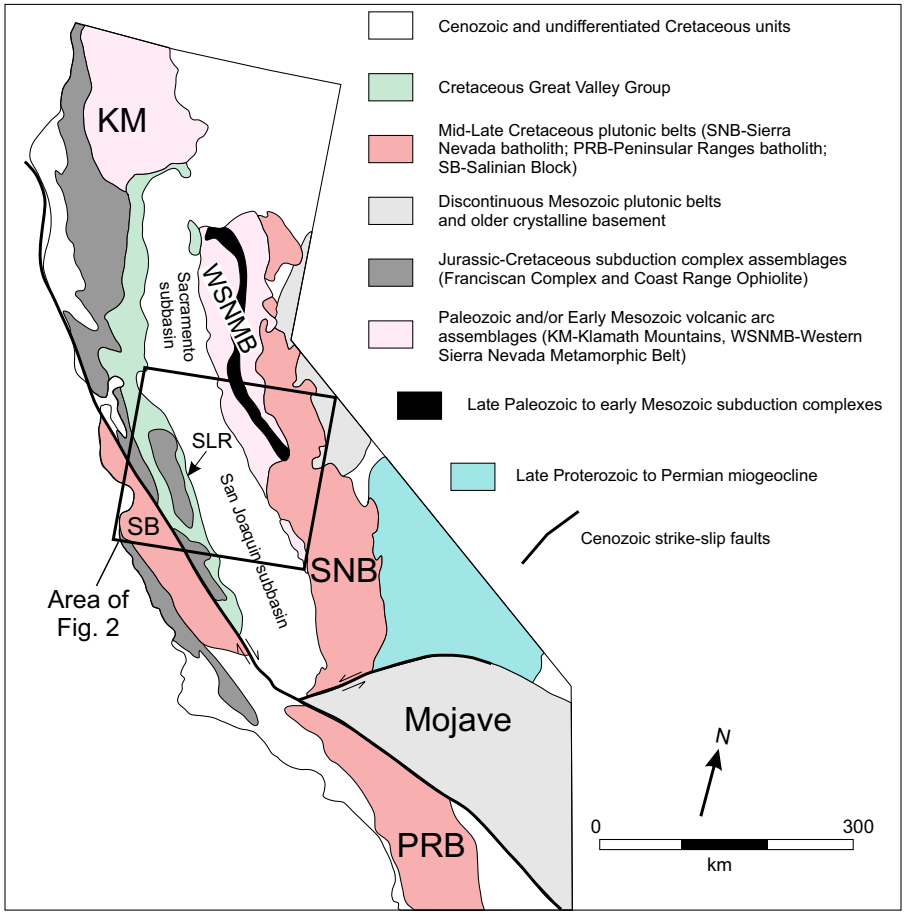

Figure 1. Map showing the major terranes of California and location of the San Luis Reservoir (SLR) within the San Joaquin subbasin of the Great Valley forearc basin. Map after Wyld et al. (2006) and Surpless (2014).

responses at ca. 100 Ma, though most studies have focused on the northern Great Valley (Sacramento subbasin). These include recognition of unconformities (Williams and Graham, 2013), deformation (Chuber, 1961), accelerated subsidence (Moxon and Graham, 1987), and abrupt shifts in provenance (Ingersoll, 1983; Surpless, 2014).

In the southern portion of the forearc (San Joaquin subbasin), however, recognizing a potential ca. 100 Ma signal has been more elusive due to inaccessible burial depths, a bias toward more proximal facies in outcrop, and a general lack of integrative studies (Moxon, 1990). As a result, paleogeographic models may be overly simplistic and therefore overlook potential responses to plate motion changes. For example, Ingersoll (1979) summarizes the San Joaquin subbasin as generally deepening to bathyal depths by ca. 100 Ma (base of Cenomanian), followed by transverse submarine canyons and overlapping submarine fan deposits. Our results suggest more complexity, with larger axial submarine channelized systems, slumping channel walls, and possible emergent accretionary outer-arc ridges.

We use facies analysis to document a previously unrecognized submarine channelized system in the San Luis Reservoir (SLR) area of the eastern Diablo Range; this system is ideally positioned to help address this ca. 100 Ma transitional period of the forearc and improve paleogeographic models for the San Joaquin subbasin (Fig. 2; Schilling, 1962; Ingersoll, 1976, 1978, 1979; Bennison, 1991; Bennison et al., 1991). The boulder-conglomerate succession is ~1.8 km thick along a 4 km transect that lies within an even larger 20-km-long, depositional-dip exposure of a southeast-directed (axial) submarine channelized system (Fig. 3).

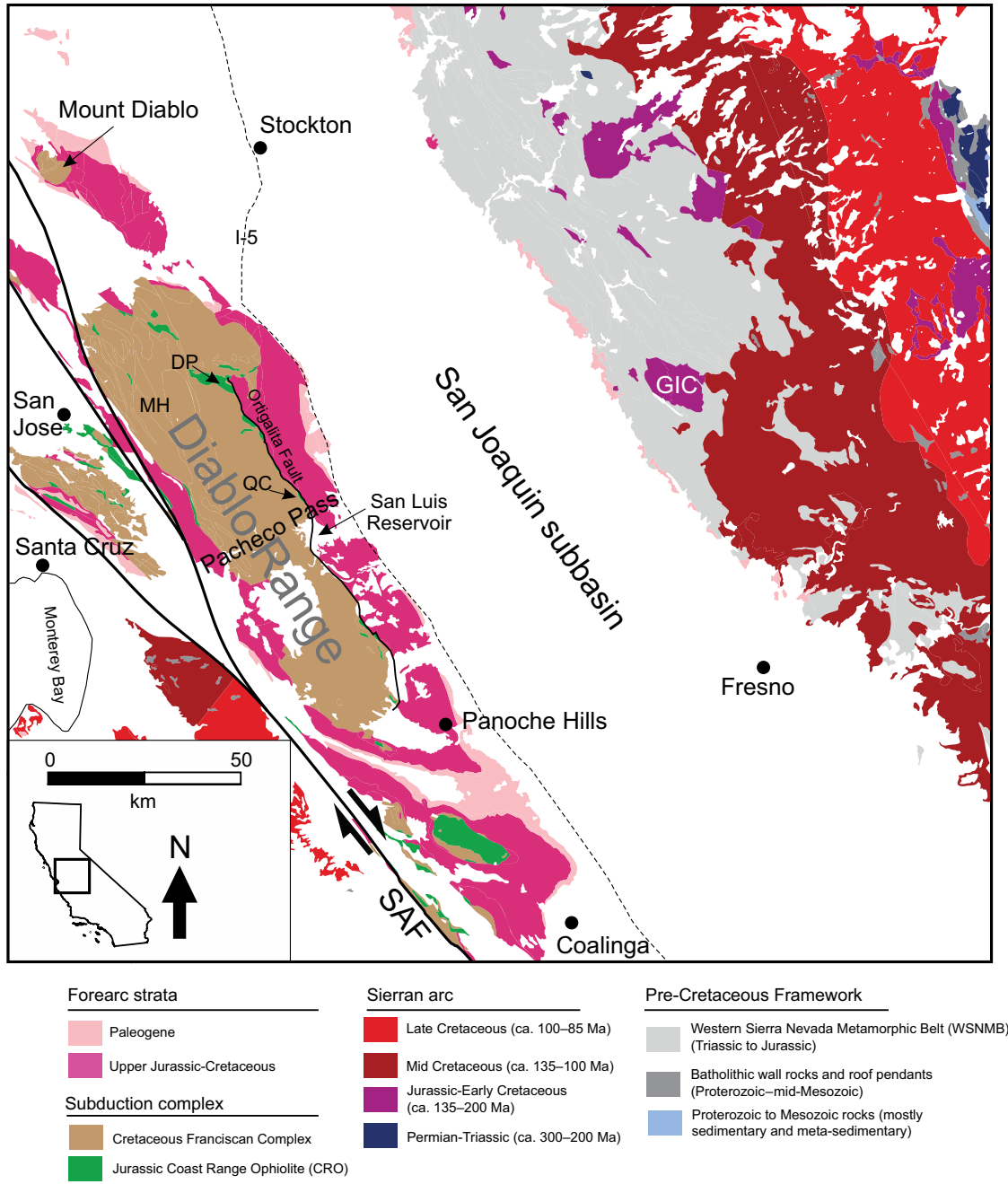

Figure 2. Generalized geologic framework of a portion of the San Joaquin subbasin showing potential sources for the Cenomanian San Luis Reservoir (SLR) deposits. (Abbreviations: GIC—Guadalupe Igneous Complex, SAF—San Andreas fault, DP—Del Puerto ophiolite, MH—Mount Hamilton, QC—Quinto Creek ophiolite). White area designates Neogene–Holocene stratigraphy. Map adapted from Sharman et al. (2015).

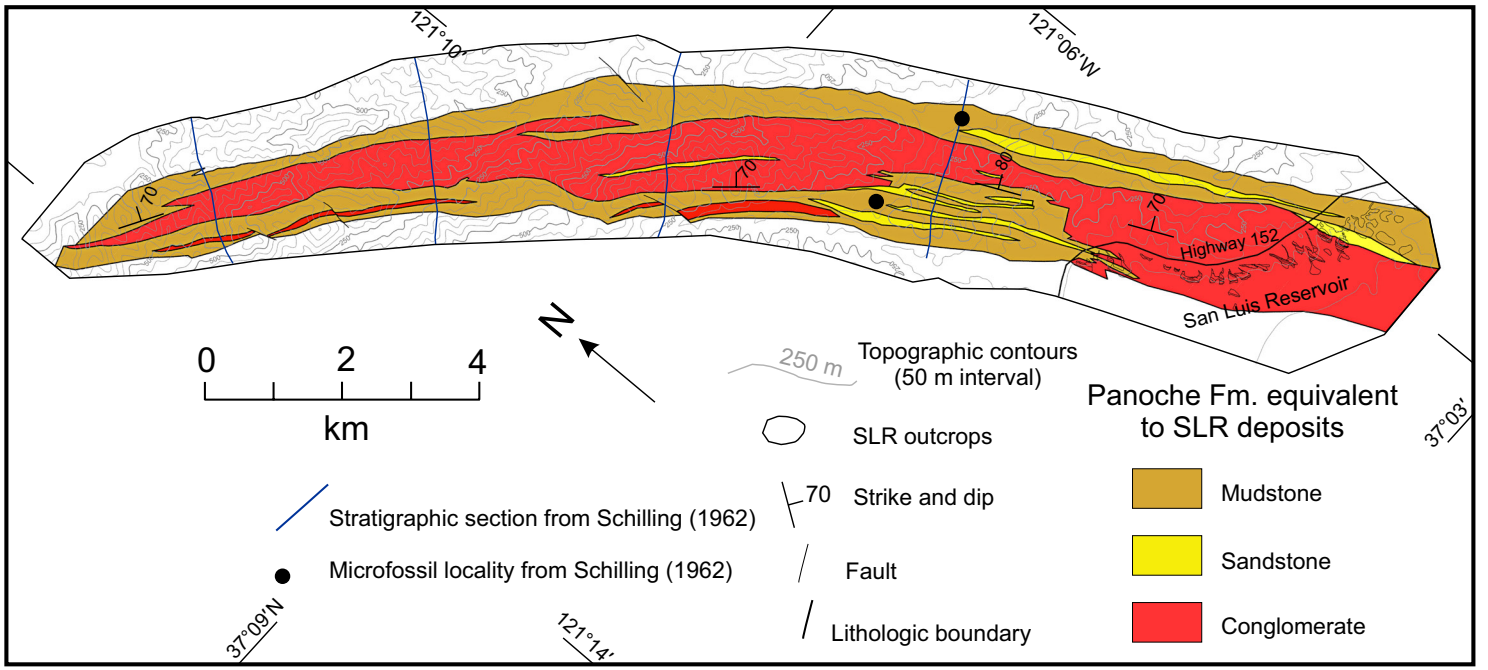

Figure 3. Geologic map of the lower portion of Member C of the Panoche Formation (Schilling, 1962) equivalent to the San Luis Reservoir (SLR) study area in the central Diablo Range. Lithologic units are modified from Dibblee (2007a, 2007b, 2007c). Note the 20-km-long conglomeratic deposits extending north of the SLR area and the microfossil localities used to interpret a lower-middle bathyal paleowater depth.

We combine our facies analysis with a combination of provenance indicators from mudrock geochemistry, sandstone composition, conglomerate clast counts, and detrital-zircon geochronology and compare our results to larger, basin-wide data sets (e.g., DeGraaff-Surpless et al., 2002; Surpless, 2014; Sharman et al., 2015).

Our integrated provenance results define a mixed source for detritus within the submarine channelized system: (1) local ophiolitic sources that we interpret to be derived from either proximal outer-arc high uplifts of the Coast Range Ophiolite (CRO) or from the Western Sierra Nevada Metamorphic Belt (WSNMB); and (2) Sierran-arc sources, including a contemporaneous volcanic carapace linked to eastern Sierran magmatism induced by deformation related to plate motion changes. The 105–95 Ma detrital-zircon population in the channelized deposits is not prevalent in coeval GVG deposits to the north and south (e.g., Sharman et al., 2015) and could indicate that the SLR submarine channelized system was depositionally linked to subaerial systems that tapped the eastern Sierra volcanic carapace. We interpret that this Cenomanian paleogeography in the San Joaquin subbasin resulted from large-scale tectonic reorganization of the arc-forearc-prism system at ca. 100 Ma.

BACKGROUND

Most of the southern GVG exposures lie along N-S–trending strike ridges on the far western portion of the San Joaquin subbasin in fault contact with the Franciscan Complex of the eastern Coast Ranges or unconformably on ophiolitic fragments of the Jurassic CRO (Fig. 2; Bailey et al., 1970; Cady, 1975; Hopson et al., 1981, 2008; Robertson, 1989; Bartow and Nilsen, 1990; Stern and Bloomer, 1992). In the eastern San Joaquin subbasin, the GVG rests unconformably on a compilation of metamorphosed Jurassic island arc terranes and ophiolitic fragments of the WSNMB (Fig. 2; Cady, 1975; Hopson et al., 1981; Saleeby, 1982; Schweickert et al., 1999; Ernst et al., 2008; Schweickert, 2015), which includes Early and mid-Cretaceous plutons of the Sierran arc (Saleeby et al., 1989a). Beneath the central San Joaquin subbasin, perhaps at the prominent magnetic high along the axis of the basin (Cady, 1975), the amalgam of the WSNMB and Sierran plutons transitions into ophiolitic basement that some have referred to as the Great Valley Ophiolite (GVO; Jachens et al., 1995; Godfrey et al., 1997; Godfrey and Klemperer, 1998). For simplicity here, we refer to the ophio-

litic basement underlying the western portion of the San Joaquin subbasin as the CRO.

Following the assembly of the Jurassic basement terranes, reinitiation of subduction in Late Jurassic time (Schweickert and Cowan, 1975; Saleeby, 1981; Ingersoll and Schweickert, 1986) coincided with the development of the Great Valley forearc basin (combined Sacramento and San Joaquin subbasins; Fig. 2). The forearc basin widened and filled through Cretaceous time due to westward and upward growth of the Franciscan accretionary prism and the eastward migration of the Sierra Nevada magmatic arc (Evernden and Kistler, 1970; Dickinson and Rich, 1972; Dickinson and Seely, 1979; Ingersoll, 1979; Graham and Ingersoll, 1981). The Great Valley forearc stratigraphy is now represented by the GVG, which consists of up to 15 km of mostly deep-water deposits that eventually shoaled to fill the basin by Paleogene time (Fig. 4; Moxon, 1990). The forearc formed a westward-thickening, asymmetric basin (Bartow and Nilsen, 1990; Williams, 1997) as fluvial systems from the Sierran-Klamath arc transitioned to deltaic environments along narrow shelves, eventually bringing sediment into the deep-water setting. Paleocurrents indicate the basin filled longitudinally (north to south), most likely affected by the outboard outer-arc high of the subduction complex (Ojakangas, 1964, 1968; Ingersoll, 1976, 1979; Dickinson and Seely, 1979; Cherven, 1983; Moxon, 1990; Williams, 1997). The forearc basin was subdivided by the Stockton Arch during the Paleogene into successor basins referred to as the Sacramento subbasin in the north and the San Joaquin subbasin in the south (Fig. 2; Dickinson et al., 1979).

Geology of the Diablo Range

Within the San Joaquin subbasin, the SLR deposits are located in the eastern portion of the Diablo Range along Pacheco Pass (Fig. 2; Bartow and Nilsen, 1990). The Diablo Range is an antiform with GVG rocks flanking the Franciscan core along vertical faults (Page, 1981; Blake et al., 1984; Elder and Miller, 1993; Ernst, 1993; Ingersoll et al., 1999). The Diablo Range has probably been a positive feature since at least latest Cretaceous (Maastrichtian) time (Nilsen and Clarke, 1975; Mitchell et al., 2010). The most recent uplift phase was associated with the arrival of the Mendocino Triple Junction between 12 and 8 Ma and San Andreas transform tectonics (Atwater, 1970; Bartow and Nilsen, 1990; Ingersoll et al., 1999).

The San Luis Reservoir covers a faulted contact (Ortigalita fault) between the Franciscan and CRO rocks to the west and the GVG rocks to the east (Bennison et al., 1991). The best pre-reservoir geologic map of the area derives from Schilling's (1962) unpublished dissertation. Schilling (1962) documented up to 3.6-km-thick conglomerate in the Panoche Formation (Cenomanian and Turonian) across 20 km of GVG strike ridges. Mapping by Dibblee (2007a, 2007b, 2007c) also documented extensive Panoche-aged conglomerate along the ridges to the north of San Luis Reservoir (Fig. 3). Detailed unpublished maps by Vic Cherven (2015, personal commun.) documented five submarine fan sequences to the north of San Luis Reservoir; his lowest fan, called the Crevison Peak Fan, is equivalent to the exposures described in this study.

Great Valley Group Stratigraphy

Great Valley Group (GVG) stratigraphy is mainly defined by biostratigraphic zonations of Goudkoff (1945) and modified by others (Fig. 4; Chuber, 1961, 1962; Douglas, 1966; Ingersoll, 1976, 1990; Almgren, 1986; Moxon, 1990). Using a variety of outcrop and subsurface data sets, Moxon (1990) divided the Mesozoic and Cenozoic GVG into six major supersequences, three of which are relevant to this study: (1) JK (Upper Jurassic–Lower Cretaceous: Tithonian to Valanginian); (2) LK (Lower Cretaceous: Hauterivian to Albian); and (3) UK-1 (Upper Cretaceous: Cenomanian to Campanian). Although both subbasins of the Great Valley contain variable thicknesses of the JK and UK-1 supersequences, the LK supersequence is conspicuously absent or very thin from the San Joaquin subbasin, implying some degree of uplift and erosion prior to deposition of UK-1 in Cenomanian time (Hopson et al., 1981; Ingersoll, 1988).

Previous work by Anderson and Pack (1915), Schilling (1962), and Moxon (1990) placed the SLR deposits of our study into the lower portion of Member C of the Cenomanian and Turonian Panoche Formation (Goudkoff's [1945] H and I zones), largely based on micropaleontological analysis (Fig. 4; note that this is distinct from the subsurface nomenclature used in the San Joaquin subbasin, where the term "Panoche Formation" describes younger Cretaceous strata [Hosford Scheirer and Magoon, 2007]). In addition, using the model of Sliter and Baker (1972) and Sliter (1975), Moxon (1990) placed the SLR deposits in middle-lower bathyal paleowater depths (1500–2500 m); he based this on Schilling's (1962) report of a variety of benthic foraminifera genera, including the indicative middle-lower bathyal genus *Glomospira* (cf. Haig, 1979; Williams, 1997). Cenomanian coarse-grained, deep-water deposits also occur to the south within the Redil Shale (Papanatas Conglomerate) near the Panoche Hills and the Juniper Ridge Conglomerate near Coalinga (Fig. 2; Payne, 1962; Moxon, 1990; Hickson and Lowe, 2002).

Provenance Trends of Great Valley Group (GVG) Deposits

Previous provenance work in the San Joaquin subbasin has established trends in sandstone composition, mudrock geochemistry, and detrital-zircon geochronology of deep-water deposits. These studies confirm earlier interpretations that the southern Sierra Nevada source area shifted eastward and was uplifted, deeply eroded, and unroofed throughout Cretaceous time (Sams and Saleeby, 1988; Linn et al., 1992; House et al., 1998; DeGraaff-Surpless et al., 2002).

The earliest provenance studies on GVG deposits recognized distinct vertical trends that were defined by sandstone framework grain components

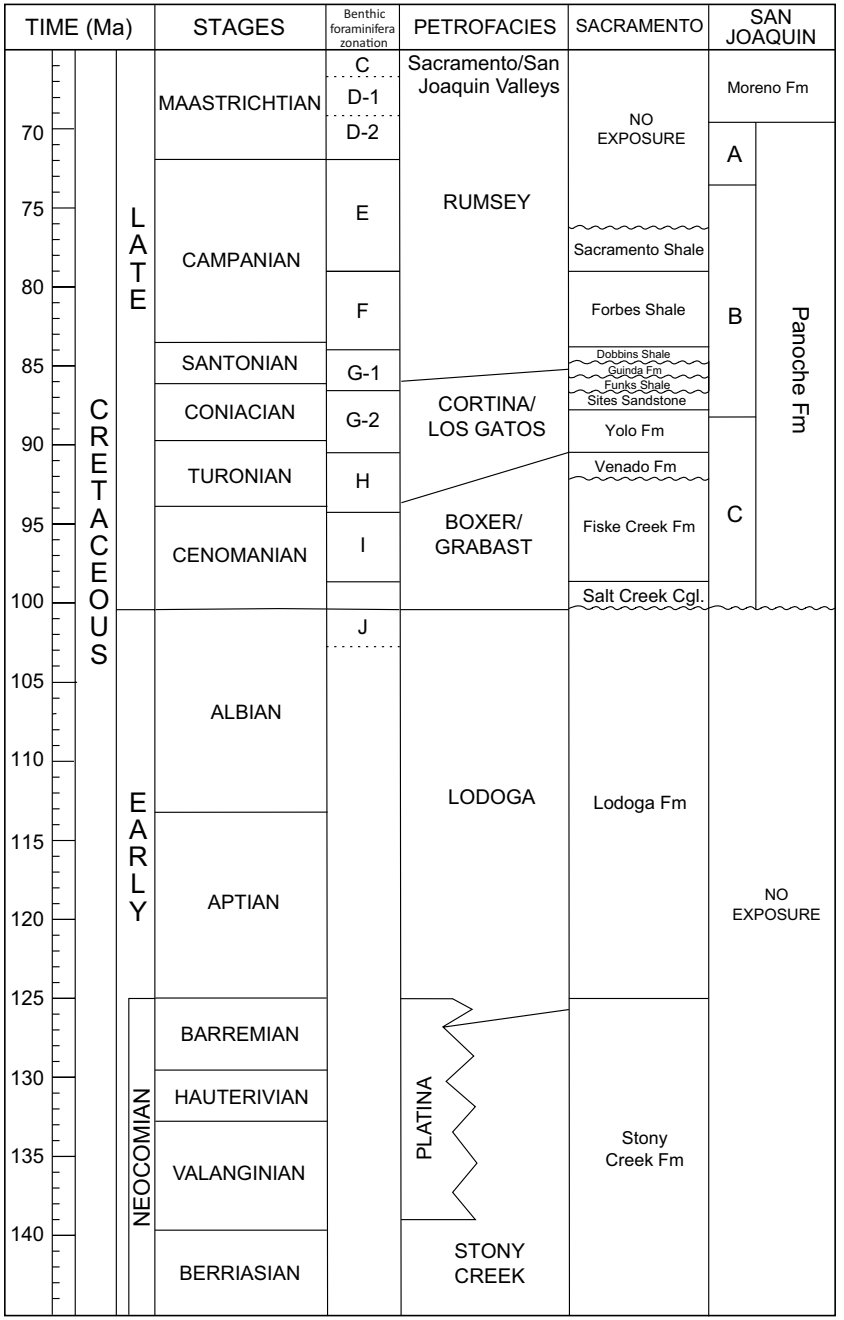

Figure 4. Cretaceous petrofacies and stratigraphic nomenclature for portions of the Sacramento and San Joaquin subbasins. Wavy lines indicate unconformities and dashed lines indicate uncertainty in time. Cretaceous stages are from Gradstein et al. (2012); petrofacies from Ingersoll (1979, 1983); Sacramento subbasin stratigraphy is from Cache Creek and subsurface combined (Williams and Graham, 2013); San Joaquin subbasin stratigraphy is from the Pacheco Pass area (Fig. 2; Schilling, 1962; Moxon, 1990); benthic foraminifera zones from Goudkoff (1945), as modified by Almgren (1986) and Berry (1974).

(Ojakangas, 1968; Dickinson and Rich, 1972; Ingersoll, 1978, 1979, 1981, 1983; Mansfield, 1979; Graham and Ingersoll, 1981). Ingersoll (1983) statistically organized these data into eight sandstone petrofacies. Ingersoll (1983) suggested that these large-scale changes in sandstone composition reflected alternating periods of erosion and build-up of the volcanic edifice in the Sierra-Klamath source region and can therefore be used as laterally continuous stratigraphic markers across the basin. In addition to documenting a general unroofing trend of the arc, Ingersoll (1983) also concluded that the sources for the San Joaquin subbasin were more "continental" than Sacramento subbasin sources, based on higher proportions of metamorphic grains and felsic volcanic grains in San Joaquin samples.

Following Ingersoll (1983), Surpless (2014) grouped the sandstone petrofacies into a Lower Cretaceous and an Upper Cretaceous "super-petrofacies" based on conglomerate clast counts, sandstone composition, mudrock geochemistry, and detrital-zircon age populations. The San Joaquin sandstone and mudrock provenance results are consistent with previous studies (e.g., Linn et al., 1992) and also indicate that more mafic, volcanic sources in Lower Cretaceous samples transitioned to more felsic plutonic, metamorphic, and continental crustal sources in Upper Cretaceous samples. Moreover, Surpless (2014) reported that Lower Cretaceous San Joaquin samples include abundant Precambrian detrital-zircon grains (25%), and their Mesozoic age spectra have a single, dominant zircon age peak at 162 Ma. In contrast, Upper Cretaceous San Joaquin samples have very few Precambrian grains (4%) and a more broadly distributed Mesozoic age spectra with peaks at ca. 104 Ma, 121 Ma, and 148 Ma (Surpless, 2014). The SLR samples from our study fill a data-poor spatial sampling gap and will be compared to both Ingersoll's (1983) petrofacies and Surpless's (2014) super-petrofacies trends.

Sharman et al.'s (2015) extensive study of Mesozoic–Cenozoic detrital-zircon age spectra throughout California highlights important changes in both space and time that are relevant to this study of the SLR area. Cenomanian–Coniacian GVG strata of Sharman et al. (2015) include very few post–100 Ma zircons despite a contemporaneous 100–85 Ma igneous flare-up in the eastern Sierra, perhaps due to a drainage divide that blocked sediment from the eastern Sierran arc from reaching basinal settings (cf. DeGraaff-Surpless et al., 2002). Sharman et al.'s (2015) post-Coniacian strata contain abundant post–100 Ma zircon, indicating unroofing of the eastern Sierran source. In contrast, Cenomanian SLR strata from this study do contain post–100 Ma zircons, suggesting the presence of isolated pathways from eastern Sierran sources into the SLR area during Cenomanian time (see data and discussion below; cf. House et al., 1998).

METHODS

We measured a total of 21 detailed stratigraphic sections along the northeastern shoreline of the San Luis Reservoir (Fig. 5; Plate 1). Each section was measured at meter-scale and includes sedimentologic data with interpreted lithofacies and facies associations. For five localities, conglomerate clast counts of ~200 clasts greater than 5 cm diameter were counted within ~2 m^2. For two localities, paleocurrent directions were measured on ~100 imbricated clasts. Data were corrected for bed attitude and plotted on rose diagrams with a 5° bin size (Plate 1). Submeter GPS data were used to map individual outcrop boundaries, faults, facies associations contacts, measured stratigraphic section pathways, and sample localities. We also utilized small fixed-wing plane photographs and drone aerial photomosaics to assist in locating and mapping significant stratigraphic contacts. The drone aerial photomosaics were stitched together using Adobe Photoshop software and a lens correction add-on to correct for "fisheye" distortion.

Petrographic data were collected for seven massive, medium-grained sandstones. Point-counting methods followed a modified Gazzi-Dickinson method (Dickinson, 1970; Dickinson and Suczek, 1979; Dickinson et al., 1983). Half of each thin-section slide was stained to aid in plagioclase and potassium feldspar identification. Approximately 300 sand-sized grains (>0.0625 mm in diameter) were counted for each thin section. Table 1 lists the raw point data and the recalculated detrital modes that were plotted in Q-F-L, Lm-Lv-Ls, and Qp-Lv-Lsm ternary plots (see Table 1 for definitions of sandstone abbreviations). Data were also re-calculated to compare to Ingersoll's (1983) statistically defined petrofacies parameters.

Five mudrock samples from the SLR deposits were analyzed for geochemistry by inductively coupled plasma–mass spectrometry (ICP-MS) and X-ray fluorescence (XRF) at Washington State University following the procedures of Knaack et al. (1994) and Johnson et al. (1999; data presented in Tables 2 and 3). Graphs of major and trace elements are compared to previously established GVG trends of Surpless (2014).

Seven detrital-zircon samples were collected throughout the SLR study area for U-Pb isotopic analysis (see Fig. 5 for sample locations). Zircons were recovered using standard separation techniques (e.g., Gehrels et al., 2008), and a random subset of zircon grains from each sample was mounted in a 1-inch epoxy round with grains of Sri Lanka, FC-1, and R33 primary zircon standards. Sample mounts were polished to a depth of ~20 microns and imaged using backscattered electron imaging to guide selection of spot locations. U-Pb dating was completed at the University of Arizona LaserChron Center using laser ablation ICP-MS following methods described in Gehrels et al. (2008) and Gehrels and Pecha (2014).

All reported uncertainties are at 1 sigma and include only measurement errors. Common lead correction is based on measured ^{204}Pb, and common Pb composition is interpreted from Stacey and Kramers (1975). Grains with greater than 10% internal (measurement) uncertainty (1 sigma) in ^{206}Pb/^{238}U ages and grains with more than 20% discordance or more than 5% reverse discordance are not considered further (20 grains; 1.5% of the 1343 grains analyzed). Ages reported are ^{206}Pb/^{238}U ages for grains younger than 900 Ma and ^{207}Pb/^{206}Pb ages for grains 900 Ma and older (all U-Pb data in Supplemental Table DR1[1]).

Data Source Information

TITLE	descriptive title of the dataset	Table DR1. Detrital zircon U-Pb geochronologic analyses (San Luis Reservoir, California, USA)
ABSTRACT	brief description of dataset, please aim for <250 words	Seven detrital zircon samples were collected throughout San Luis Reservoir study area for U-Pb isotopic analysis. Zircons were recovered using standard separation techniques (e.g., Gehrels et al., 2008), and a random subset of zircon grains from each sample was mounted in a 1-inch epoxy round with grains of Sri Lanka, FC-1, and R33 primary zircon standards. Sample mounts were polished to a depth of about 20 microns and imaged using backscattered electron imaging to guide selection of spot locations. U-Pb dating was completed at the University of Arizona LaserChron Center using laser ablation inductively coupled plasma mass spectrometry following methods described in Gehrels et al. (2008) and Gehrels and Pecha (2014).The purpose of the dataset was to better understand the provenance of Eocene deep-water deposits.
AUTHOR	name of the author(s) of the dataset (Last, First)	Greene, Todd J.; Surpless, Kathleen D.
Institution	institution of the author	California State University - Chico; Trinity University
Release Date	date when the data is available to the public (if left blank, available)	
Creator	person who fills out this template	Greene, Todd J.
CONTACT INFO	contact email for the creator of the template	tgreene@csuchico.edu

Related Publication #1	information about a publication related to the dataset (e.g. journal article that cites all or part of the dataset)	
Title		Facies architecture and provenance of a boulder-conglomerate submarine channel system, Panoche Formation, Great Valley Group: a fore-arc basin response to middle Cretaceous tectonism in the California convergent margin
Authors		Greene, Todd J.; Surpless, Kathleen D.
Publication Year		2017
Journal		Geosphere
Volume		
Issue		
Pages		
DOI		

Related Publication #2	information about a publication related to the dataset (e.g. journal article that cites all or part of the dataset)	
Title		
Authors		
Publication Year		
Journal		
Volume		
Issue		
Pages		
DOI		

[1]Supplemental Table DR1. Detrital zircon U-Pb geochronologic analyses (San Luis Reservoir, California, USA. Please visit http://doi.org/10.1594/IEDA/100637 to obtain the supplemental item from the Interdisciplinary Earth Data Alliance, EarthChem Library.

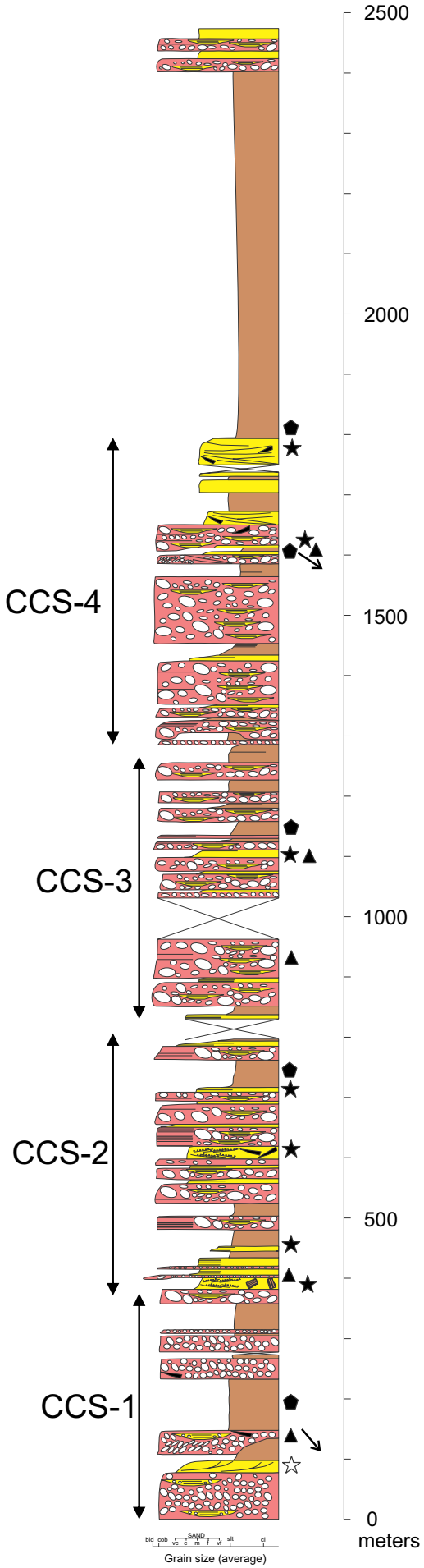

Figure 5. Composite stratigraphic section of the SLR deposits with sample locations and channel complex sets (CCS). Filled stars—detrital-zircon analysis + sandstone petrography; star outline—sandstone petrography only; pentagon—mudstone geochemistry; triangle—conglomerate clast count; arrow—paleocurrent data pointing in mean paleocurrent direction. See Plate 1 for further explanation of symbols and detailed sedimentologic and stratigraphic data and interpretations.

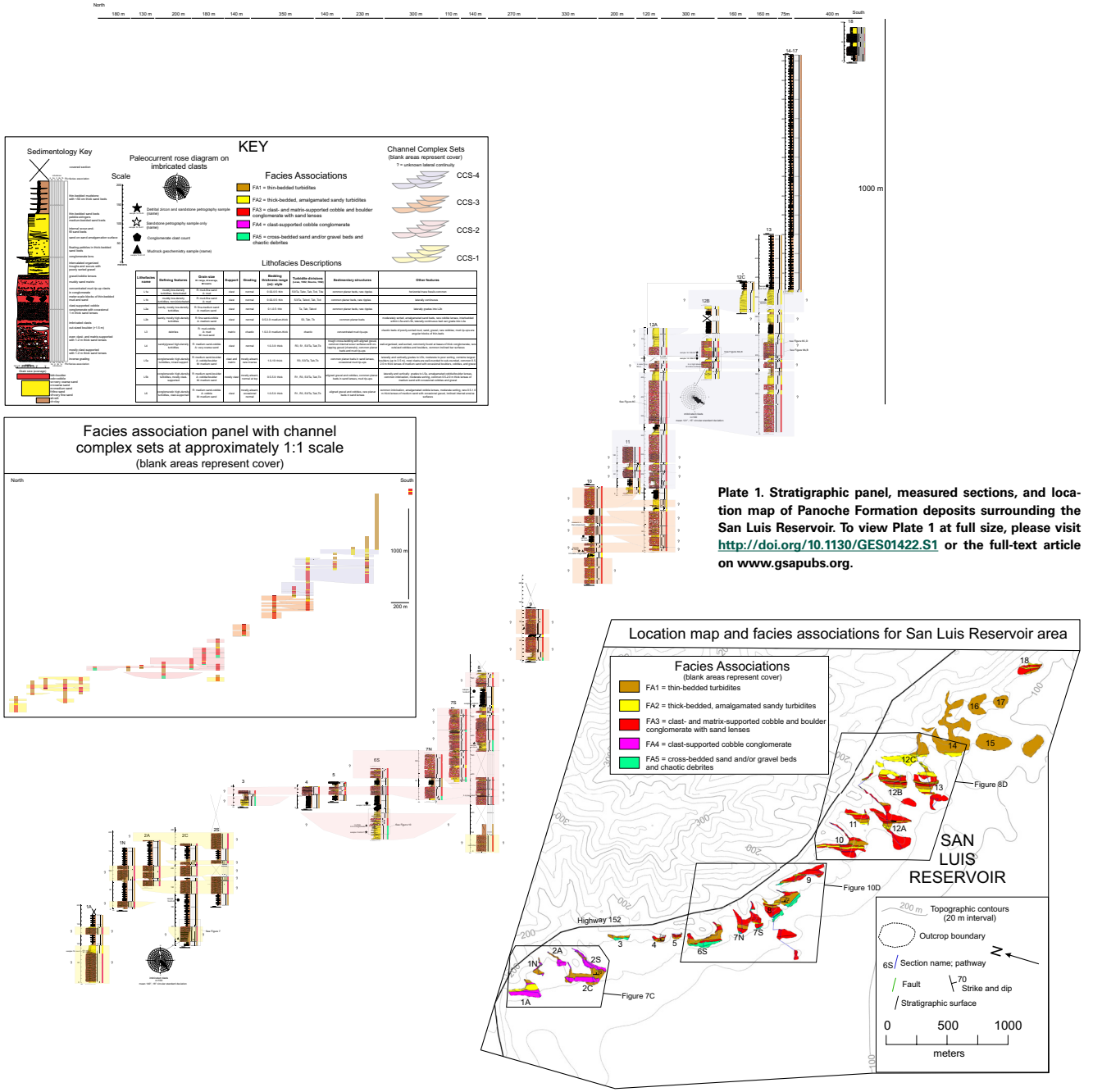

Plate 1. Stratigraphic panel, measured sections, and location map of Panoche Formation deposits surrounding the San Luis Reservoir. To view Plate 1 at full size, please visit http://doi.org/10.1130/GES01422.S1 or the full-text article on www.gsapubs.org.

TABLE 1. RAW AND RECALCULATED SANDSTONE POINT-COUNT DATA

Sample name	Location																		Q-F-L plot			Qp-Lv-Lsm plot			Lv-Ls-Lm plot		
	Latitude (N)	Longitude (W)	Qm	Qp	P	K	M	Ls	Lv	Lm	MISC	Inter.	Total	Lm/Lv	P/F (%)	FMWK%M (%)	Lv/L (%)	Qp/Q (%)	QFL %Q	QFL %F	QFL %L	QpLvLsm %Qp	QpLvLsm %Lv	QpLvLsm %Lsm	LvLsLm %Lv	LvLsLm %Ls	LvLsLm %Lm
14-12C-01	37°4′47″	121°5′55″	49	10	64	27	9	11	44	55	5	12	286	1.25	70.3	3.3	40.0	16.9	22.7	35.0	42.3	8.3	36.7	55.0	40.0	10.0	50.0
14-12B-02	37°4′49″	121°6′4″	75	12	78	32	15	3	23	40	2	4	284	1.74	70.9	5.4	34.8	13.8	33.1	41.8	25.1	15.4	29.5	55.1	34.8	4.5	60.6
14-10-02	37°5′3″	121°6′32″	71	11	65	29	11	12	30	41	7	16	293	1.37	69.1	4.0	36.1	13.4	31.7	36.3	32.0	11.7	31.9	56.4	36.1	14.5	49.4
14-08-02	37°5′12″	121°6′55″	56	5	73	27	20	10	37	48	3	23	302	1.30	73.0	7.2	38.9	8.2	23.8	39.1	37.1	5.0	37.0	58.0	38.9	10.5	50.5
14-08-03	37°5′12″	121°7′0″	75	10	47	25	16	11	31	49	3	13	280	1.58	65.3	6.0	34.1	11.8	34.3	29.0	36.7	9.9	30.7	59.4	34.1	12.1	53.8
14-06-03	37°5′26″	121°7′11″	40	5	75	25	16	12	48	59	5	9	294	1.23	75.0	5.6	40.3	11.1	17.0	37.9	45.1	4.0	38.7	57.3	40.3	10.1	49.6
14-06-01	37°5′28″	121°7′14″	57	9	57	16	16	21	47	53	5	8	289	1.13	78.1	5.7	38.8	13.6	25.4	28.1	46.5	6.9	36.2	56.9	38.8	17.4	43.8
													Average	1.37	71.7	5.3	37.6	12.7	26.9	35.3	37.8	8.8	34.4	56.9	37.6	11.3	51.1
													Standard deviation	0.22	4.2	1.3	2.5	2.7	6.3	5.1	7.6	4.0	3.6	1.6	2.5	4.0	5.1

Note: Qm—monocrystalline quartz; Qp—polycrystalline quartz; F—total feldspar; P—plagioclase feldspar; K—potassium feldspar; M—micaceous grains; Ls—sedimentary lithic grains; Lv—volcanic lithic grains; Lm—metamorphic lithic grains; MISC—miscellaneous grains; Inter.—interstitial; Total—total counts; FMWK—framework grains (all grains excluding interstitial grains); L—total lithic grains (Ls + Lm + Lv); Q—total quartz (Qp + Qm); Lsm—sedimentary and metasedimentary lithic grains (Ls + Lm).

TABLE 2. MUDROCK MAJOR-ELEMENT GEOCHEMICAL DATA

Sample name	Location		SiO_2 (%)	TiO_2 (%)	Al_2O_3 (%)	Fe_2O_3 (%)	MnO (%)	MgO (%)	CaO (%)	Na_2O (%)	K_2O (%)	P_2O_5 (%)	Total (%)
	Latitude (N)	Longitude (W)											
14-13-01	37°4′47″	121°5′53″	56.44	0.76	16.13	6.84	0.06	3.98	1.55	1.63	2.49	0.14	90.01
14-12B-01	37°4′51″	121°6′5″	57.97	0.69	14.85	6.43	0.04	2.93	1.58	1.68	2.20	0.17	88.55
14-10-01	37°4′58″	121°6′29″	58.14	0.73	15.40	4.89	0.03	2.45	1.40	1.36	2.25	0.15	86.79
14-08-01	37°5′10″	121°6′52″	59.24	0.69	16.02	5.85	0.04	3.13	1.10	1.00	2.25	0.10	89.42
15-2C-01	37°5′54″	121°7′33″	60.77	0.79	16.65	5.41	0.03	2.15	1.08	1.09	2.27	0.11	90.34

RESULTS

Stratigraphic Architecture

We use a process-based hierarchical scheme that defines six main lithofacies (three lithofacies are subdivided into two sublithofacies; Fig. 6 and Plate 1), which we group into five facies associations (FA). We correlate stratigraphic surfaces across outcrop localities by reasonably matching lithostratigraphic packages; these correlations have variable uncertainty due to cover and/or faults. Finally, we use the lateral and vertical stacking of depositional facies to outline the overall depositional setting and fill history.

Lithofacies

We divide lithofacies by grouping similar beds and bed sets that are sedimentologically distinguishable from one another using previously established process-based criterion for sediment gravity flows (Bouma, 1962; Lowe, 1982, 2004, and references therein). Our main divisions are based on sediment-support mechanism (clast support and matrix support), caliber (dominant clast size), concentration of dominant clast-size (low-density versus high-density), grading, average bedding thickness, and degree of bioturbation. See Plate 1 (Lithofacies Descriptions) and Figure 6 for definitions and examples for the six lithofacies and sublithofacies.

TABLE 3. MUDROCK TRACE-ELEMENT GEOCHEMICAL DATA

Sample name	Ba (ppm)	Ce (ppm)	Cr (ppm)	Cu (ppm)	Hf (ppm)	La (ppm)	Nb (ppm)	Nd (ppm)	Ni (ppm)	Pb (ppm)	Rb (ppm)	Sc (ppm)	Sr (ppm)	Th (ppm)	V (ppm)	Y (ppm)	Zn (ppm)	Zr (ppm)
14-13-01	923.4	46.7	159.8	86.3	3.8	25.8	11.9	24.8	98.2	16.8	101.5	21.1	177.2	9.5	163.5	24.2	13.3	138.7
14-12B-01	648.6	39.6	123.7	61.1	3.6	23.2	10.0	22.7	71.3	13.5	92.2	19.7	160.5	8.9	163.1	24.0	107.9	129.4
14-10-01	667.3	46.5	113.2	59.0	4.4	26.5	11.0	24.3	49.5	10.4	92.2	19.2	164.2	10.7	134.8	26.2	98.0	152.9
14-08-01	638.6	32.5	142.9	76.3	3.4	17.6	8.4	17.3	88.9	9.8	95.5	20.4	89.8	7.1	175.2	20.0	125.1	125.2
15-2C-01	597.6	52.6	127.6	62.5	4.4	25.4	11.0	23.1	74.4	13.6	91.7	17.1	154.8	10.4	142.4	20.3	102.2	161.3

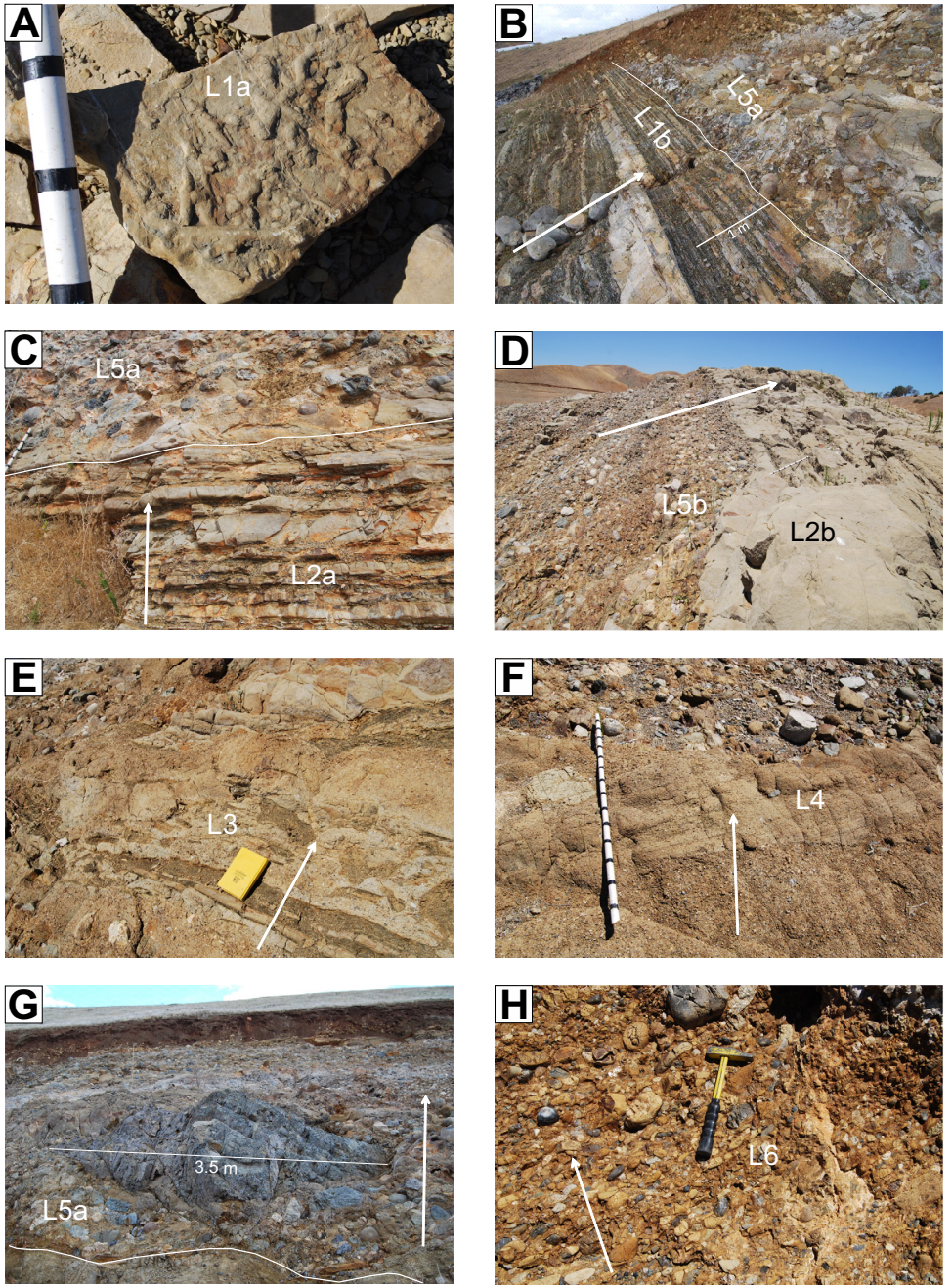

Figure 6. Lithofacies examples from the San Luis Reservoir (SLR) deposits. Arrows show stratigraphic-up direction, and the 1.5 m black-and-white staff shows 10 cm intervals. See Lithofacies Descriptions (Plate 1) for detailed descriptions. (A) L1a, bedding surface view showing horizontal burrows. (B) L1b with overlying L5a. (C) L2a underlying L5a. (D) L2b cutting down into L5b. (E) L3 with floating rip-up clasts. (F) L4 with cross-bedded sands and gravels. (G) L5a with 3.5 m out-sized boulder clast. (H) L6 with imbricated cobbles.

Facies Associations

- **Facies Association 1 (FA1): Thin-Bedded Turbidites**

Description. FA1 contains the highest proportion of siltstone and mudstone (Plate 1). These thin-bedded turbidites are dominated by L1a and L1b, with occasional to rare thicker sandy beds (not exceeding 1 m thick) of L2a and L2b (Figs. 6A and 6B). FA1 is mostly adjacent to the coarser facies associations (Fig. 7). The bases of FA1 packages are generally gradational with the underlying facies association, and the tops of FA1 packages are usually sharp and often erosional with respect to the overlying facies association. Thickness of FA1 ranges from 3 to 85 m (average = 24 m; n = 22). The top of the entire sediment fill is capped by a 620-m-thick FA1 package that contains the only occurrence of L1a (bioturbated thin-bedded turbidites).

Interpretation. FA1 deposits were generally formed from the fine-grained tops of turbidity currents. These beds were either deposited laterally adjacent to migrating axial channels (channel margin or overbank; cf. McHargue et al., 2011) or on the tops of channel bodies during abandonment with varying degrees of hemipelagic fallout. The lack of both climbing-rippled beds and soft-sediment deformation (i.e., high sedimentation rates) suggests the FA1 beds are not associated with typical gull-winged, proximal levees (Dykstra and Kneller, 2009; Kane and Hodgson, 2011). However, common rip-up blocks of the more cohesive FA1 beds occur within the coarser conglomeratic facies, suggesting slumping and/or erosion of confining channel walls.

- **Facies Association 2 (FA2): Thick-Bedded, Amalgamated Sandy Turbidites**

Description. FA2 deposits mostly contain sharply upward-fining, amalgamated medium-grained sandstone of the L2a and L2b lithofacies (Figs. 6C and 6D; Plate 1). Tab (Bouma divisions) beds with internal erosive surfaces dominate FA2, but thin gravel stringers with rare out-sized boulders and cobbles, as well as sporadic mud rip-up clasts (L3) also occur (Fig. 6E). In general, the bases and tops of FA2 are gradual and serve as transitional stages between FA3 and FA1, representing thick fining-upward packages. However, FA2 can also be interbedded and laterally adjacent to the coarser FA3 (Fig. 8). Thickness of FA2 ranges from 3 to 57 m (average = 16 m; n = 18).

Interpretation. FA2 sediments were deposited by high- and low-density sandy turbidity currents and are associated with coarser conglomeratic facies. However, FA2 can occur as either the beginning stages of channel abandonment (Figs. 9A and 9B) or as part of progressive channel migration (cf. Hubbard et al., 2009). In the former case, FA2 represents the beginning of the waning stages within larger channelized packages. Most of the larger caliber sediments have been deposited up-system, leaving flows internally stratified; the basal, more concentrated sandy portions eventually deposit out of suspension, leaving the finer-grained tails to continue downstream or be stripped off to the overbank environment (Posamentier and Walker, 2006). In the latter case, FA2 could represent sandy portions that were off-axis to laterally adjacent coarser, on-axis channels (McHargue et al., 2011; Macauley and Hubbard, 2013; Bain and Hubbard, 2016). Relative to on-axis deposits (see FA3 interpretation), the FA2 off-axis beds are thinner, contain less amalgamation, and have a lower proportion of coarse material. Although both cases exist in the SLR area, the lack of outcrop exposure prohibits determining which depositional mechanism was responsible for these sandy deposits.

- **Facies Association 3 (FA3): Clast- and Matrix-Supported Cobble and Boulder Conglomerate with Sand Lenses**

Description. FA3 is the most prevalent and heterogeneous facies association in the study area (Plate 1). The most widespread lithofacies in FA3 are the sandy-matrix conglomeratic lithofacies (L5a and L5b) in which the average clast diameter reaches boulder in size, with many clasts exceeding 1.0 m diameter (largest is 3.5 m; Fig. 6G). Most clasts are extrabasinal (well- rounded to subrounded), though angular mud rip-up clasts are common, and "raft-blocks" (up to 6 m wide) of thin-bedded turbidites (L1b) occasionally appear. Textures vary between even proportions of clast-supported and matrix-supported (L5a) to mostly clast-supported (L5b), with frequent imbricated clasts in the latter (Fig. 6H; Plate 1). Pervasive medium-grained sandy lenses exist throughout both lithofacies L5a and L5b (Figs. 8 and 9). These sporadically distributed lenses range from 0.5 to 2.0 m in thickness and contain traction structures (mostly Tb), as well as pebble stringers, mud rip-up clasts (L3), and occasional floating boulders. Other sandy lithofacies (L2a and L2b) are interbedded with the conglomeratic lithofacies (L5a and L5b). Although the L2a and L2b lithofacies are very similar to the sand lenses within L5a and L5b, the main differences are that L2a and L2b are more laterally continuous, and they commonly fine upwards to the thin-bedded L1b lithofacies.

FA3 has sharp, planar bases (though one example displays nearly 12 m of erosional relief; section 12A, Plate 1) and gradual coarse-tail graded tops that merge into FA2. Internal erosional surfaces are very common in FA3, although individual channel dimensions are difficult to determine due to the highly amalgamated nature of the L5a and L5b lithofacies. Based on thickness of conglomerate beds between significant sand lenses within the L5a lithofacies, individual flow units vary from 2 to 4 m thick; however, one example contains down-channel accreting bar sets with ~6 m of relief (Figs. 8A and 8B). Full FA3 sections range from 8 to 100 m thick, with an average thickness of 49 m (n = 20).

Interpretation. FA3 generally contains very little architectural organization, with sporadically distributed sand lenses, internal erosive surfaces that are difficult to follow, and only rare appearances of channel forms. Common mud rip-up clasts, lack of mud in the matrix, internal sand lenses with planar beds (Tb), and rare occurrences of down-channel accreting bar sets lead us to interpret that the bulk of FA3 was deposited by multiple, mostly turbiditic events rather than a few en masse laminar flows.

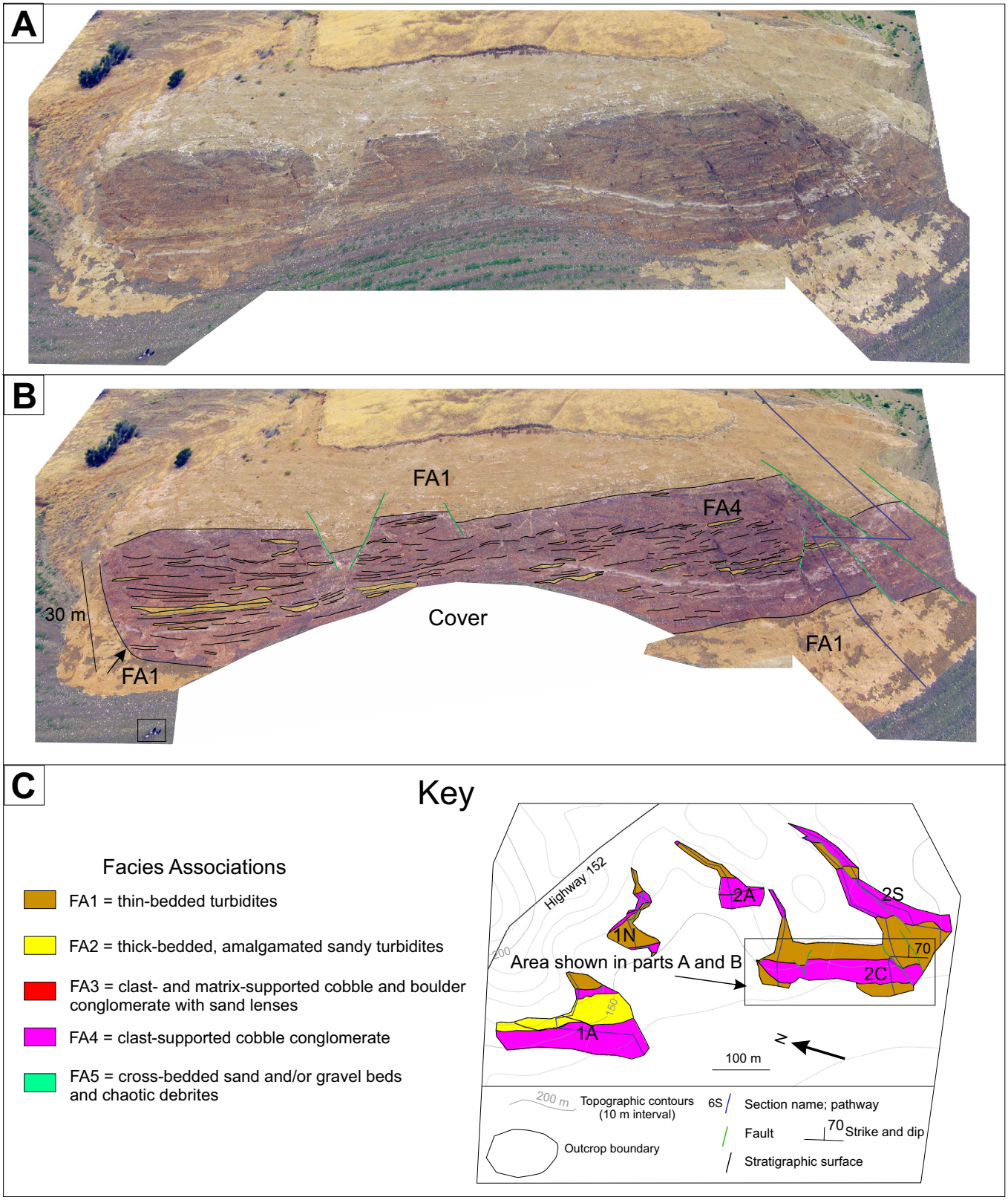

Figure 7. Facies associations for the lowermost channel complex in section 2C (see Plate 1, section 2C for location of photo within CCS-1). (A) Oblique perspective photomosaic from drone photos interpreted in part B. (B) Interpreted photomosaic from part A with facies associations dominated by the clast-supported cobble conglomerate in FA4. FA4 also displays ~1-m-thick sand lenses (colored yellow within FA4). Note the ~30 m erosional surface marked by arrow. This surface was probably reactivated by later faulting. Box in lower left shows three people for scale. (C) Key and map of facies associations showing location of photomosaic and symbol definitions; see Plate 1 location map for reference.

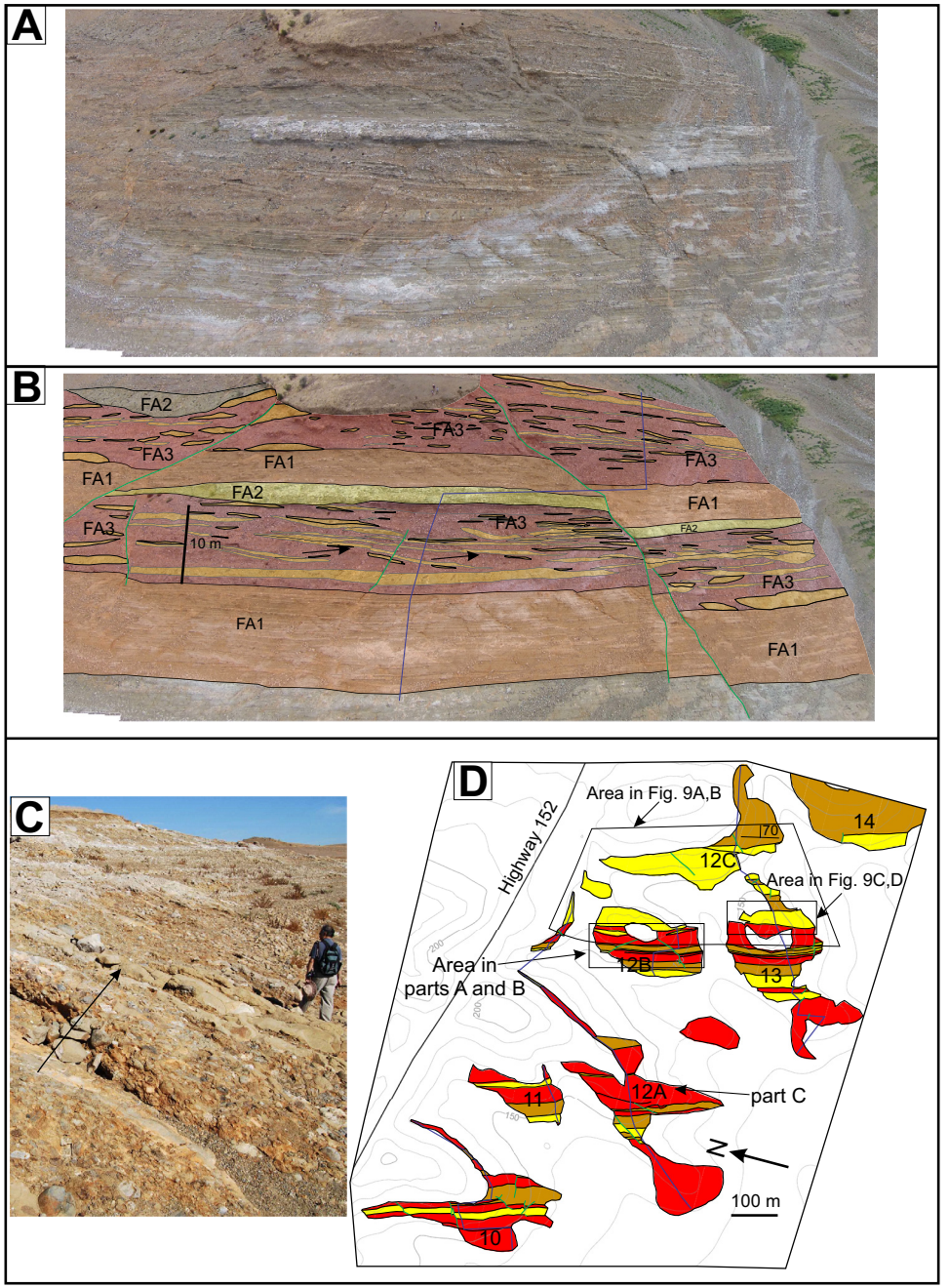

Figure 8. Facies associations of the upper portion at sections 12A and 12B (see Plate 1, sections 12A and 12B for location of photo within CCS-4). (A) Photomosaic interpreted in part B. The perspective is vertical taken from drone photos directly above outcrop. (B) Interpreted photomosaic from part A with facies associations of section 12B. FA3 also shows interbedded sands of L5a. Arrows point to downward accreting bar sets with ~6 m relief. Note the contrasting styles of FA2: lensoidal in the upper left corner and tabular in the center. See Figure 7C for symbol definitions. (C) Photo showing mostly L5a within the thickest FA3 interval of the SLR deposits (section 12A). Arrow points in stratigraphic-up direction (person for scale). (D) Map of facies associations showing locations for parts A, B, C, and Figure 9; see Figure 7C for symbol definitions and Plate 1 location map for reference.

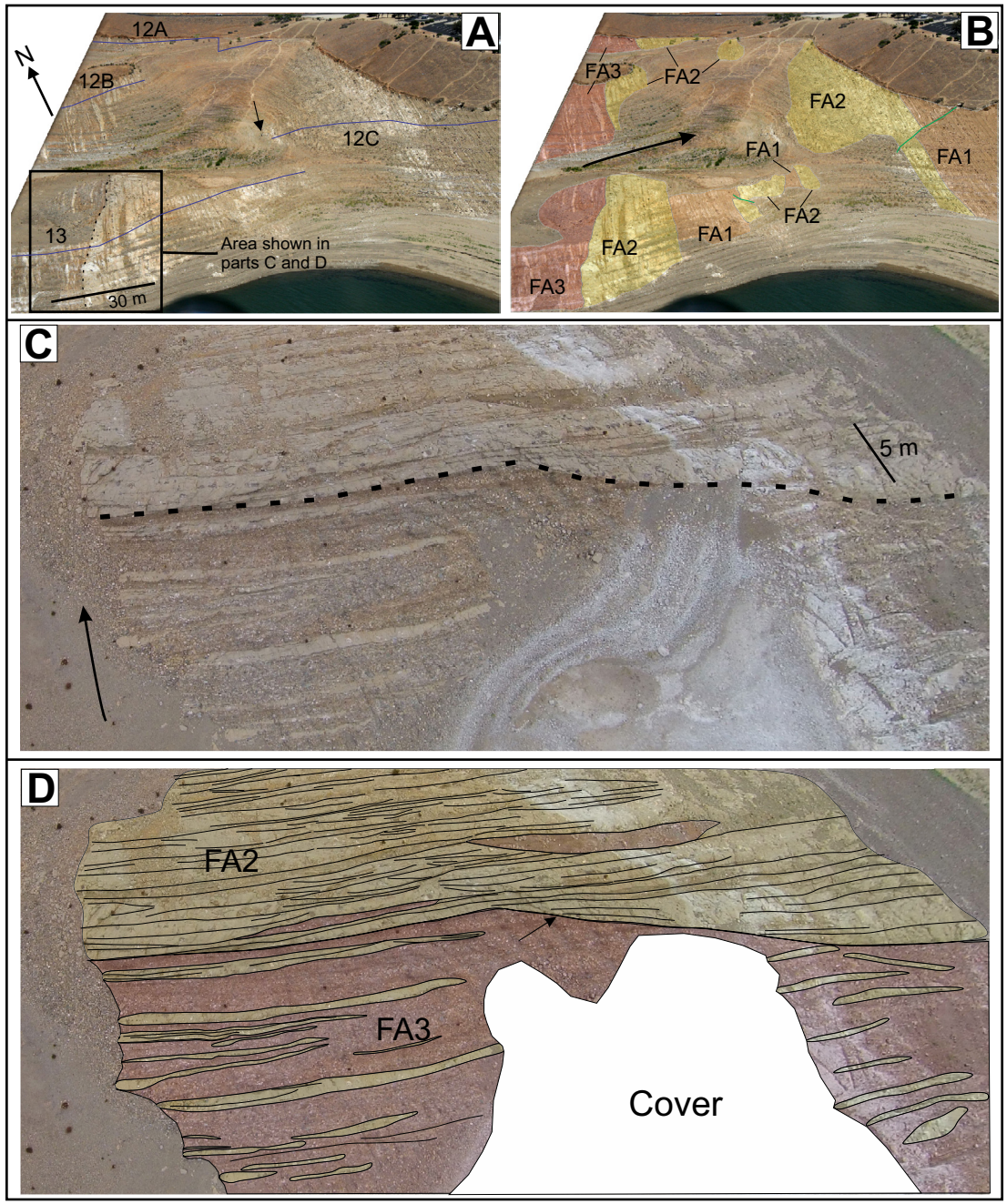

Figure 9. Facies associations of upper portion of the channelized fill from section 13 characteristic of the abandonment phase (see Fig. 8D and Plate 1, section 13 for location of photo within CCS-4). (A) Oblique perspective on-strike aerial view photo taken from a small fixed-wing aircraft showing portions of sections 12A, 12B, 12C, and 13 (pathway of sections shown with purple lines). Arrow within the photo points to person for scale. Box shows area in parts C and D. Dashed stratigraphic surface is included to help link the photo to part C. (B) Interpreted facies associations of photo from part A. Arrow points in the stratigraphic-up direction. Faults are shown in green. (C) Photomosaic interpreted in part D. The perspective is vertical taken from drone photos directly above outcrop. Arrow points in stratigraphic-up direction. (D) Interpreted photomosaic from part C with facies associations. Note the erosional surface with ~5 m of relief cutting into FA3 with overlying, highly amalgamated FA2 deposits. FA2 also shows a small conglomeratic lens representing the stratigraphically highest conglomerate bed of the SLR channelized fill. See Figure 7C for symbol definitions.

The boulder- and/or cobble-rich portions of FA3 were either deposited out of suspension or by traction processes. We interpret the largest of the boulders (e.g., Fig. 6G and 10C) were sourced from bedrock exposures that were weathered, eroded, and eventually incorporated into the deep-water setting by avalanching along steep channel walls. Incoming gravity flows then remobilized the boulders as they rolled along the base of the flow. As these energetic flows deposited the coarsest fraction (FA3), high concentrations of sand and mud continued down channel where they were deposited as FA2 and FA1.

We interpret the bulk of FA3 as on-axis channel deposits based on their greater thickness, degree of amalgamation, blocky vertical grain-size profile, and relative proportions of coarser-grained material (Sullivan et al., 2004; McHargue et al., 2011; Covault et al., 2016). FA1 and FA2 occupy an off-axis and channel margin to overbank position, respectively, relative to the on-axis FA3 flows (cf. McHargue et al., 2011). An example occurs between the lowermost conglomerate in section 12A (on-axis) and the equivalent deposits in section 10 (off-axis; Plate 1). Any interpretation of channel axes is hampered, however, from both the amount of covered section and the depositional dip-parallel orientation of the outcrops.

- ***Facies Association 4 (FA4): Clast-Supported Cobble Conglomerate***

Description. FA4 deposits only appear in the lowermost section of the SLR area (Fig. 7; Plate 1). A majority of the deposits (L6) are clast-supported, well-sorted, cobble conglomerate with common imbrication and internal erosive surfaces (1–3 m relief), gravel lenses, and rare 1–2-m-thick medium-grained sand lenses (Figs. 6H and 7). Unlike FA3, boulder-sized clasts are extremely rare. FA4 has very sharp, planar bases, although one occurrence displays an erosional base with 30 m of relief (Fig. 7). Tops fine upward rapidly and are commonly overlain by fine-grained sediments of FA1. Thickness of FA4 varies from 15 to 76 m (average = 42 m; n = 6).

Interpretation. FA4 is architecturally organized into cobble-filled channels and down-channel accreting bar sets (Fig. 7). The dominant support mechanism was turbulence, as indicated by the well-sorted, clast-supported cobbles, imbrication, and general lack of sand and mud (cf. facies IIIscg of Hubbard et al., 2008; Jobe et al., 2010). With one exception, FA4 is also bounded by the mud-rich FA1 deposits, indicating significant bypass by the sand-rich portion of the flows (Fig. 7C). Only after the thick, amalgamated FA4 deposits formed were the muddy overbank sediments of FA1 deposited, most likely as turbiditic tails adjacent to other FA4 channels (Plate 1).

Similar to FA3 deposits, FA4 represents on-axis channelized deposition. However, fast lateral and vertical facies transitions as well as rapid thickness changes suggest that these channels are more confined. For example, the uppermost conglomerate in section 1A and the lowermost conglomerate in section 2C (Plate 1) show lateral thinning of FA4 deposits (50% thickness reduction across ~500 m). The uppermost conglomerate in section 1N also represents a 50% reduction relative to correlative FA4 deposits to the south.

- ***Facies Association 5 (FA5): Cross-Bedded Sand and/or Gravel Beds and Chaotic Debrites***

Description. FA5 deposits are generally found at the bases of thick conglomeratic FA3 deposits (Fig. 10; Plate 1). They are dominated by crosscutting scour-and-fill structures with well-sorted, very coarse-grained sands and occasional gravels and rare boulders (L4; Fig. 6F). They include common trough cross-bedding, planar beds (L4), and chaotic beds (L3; Fig. 6E). Some bar sets have up to 1.5 m in relief. Thickness ranges from 5 to 36 m (average = 18 m; n = 7). We differentiate FA5 from FA2 sandy deposits by FA5's coarser sand size, better sorting, more traction structures, and less lateral continuity of beds (Fig. 10D).

Interpretation. Turbulence was the dominant support mechanism for the L4 beds; the rare L3 chaotic beds were probably supported by matrix strength. Some FA5 deposits can also be correlated along erosional surfaces at the base of channels (Fig. 10D). Therefore, based on FA5's stratigraphic position, internal structure, texture, and common association with thick FA3 conglomerate, we interpret FA5 as channel-lag deposits recording significant bypass before deposition of the conglomeratic fill of channels (Stevenson et al., 2015).

Paleocurrents

Clast imbrication measurements were taken at two localities within the study area (Fig. 5; Plate 1): (1) lowest channel complex set: CCS-1 (section 2C; n = 100) and (2) highest channel complex set: CCS-4 (section 12B; n = 100). Data from section 2C plotted toward the southeast (mean 140° and 18° circular standard deviation). Similarly, section 12B data also plotted toward the southeast (mean 121°; 15° circular standard deviation). These paleocurrent directions corroborate results of Bennison (1991), Bennison et al. (1991), and V. Cherven (2015, personal commun.).

Stratigraphic Framework

The architectural framework used in this study includes channels, channel complexes, and channel complex sets (cf. Campion et al., 2000; Sprague et al., 2002; Schwarz and Arnott, 2007; McHargue et al., 2011; Macauley and Hubbard, 2013; Bain and Hubbard, 2016). Although individual channel forms rarely manifest, we interpret channels as a heterogeneous mix of lithofacies or facies associations that are dominated by tractional or turbulent structures that may or may not display general fining-upward trends. Channels that appear to be genetically linked form channel complexes; a channel complex may or may not show fining-upward trends but is sometimes marked by an erosive base overlain by bypass deposits (e.g., FA5). Channel complex sets are marked by erosional surfaces at their bases and their tops are generally fine-grained.

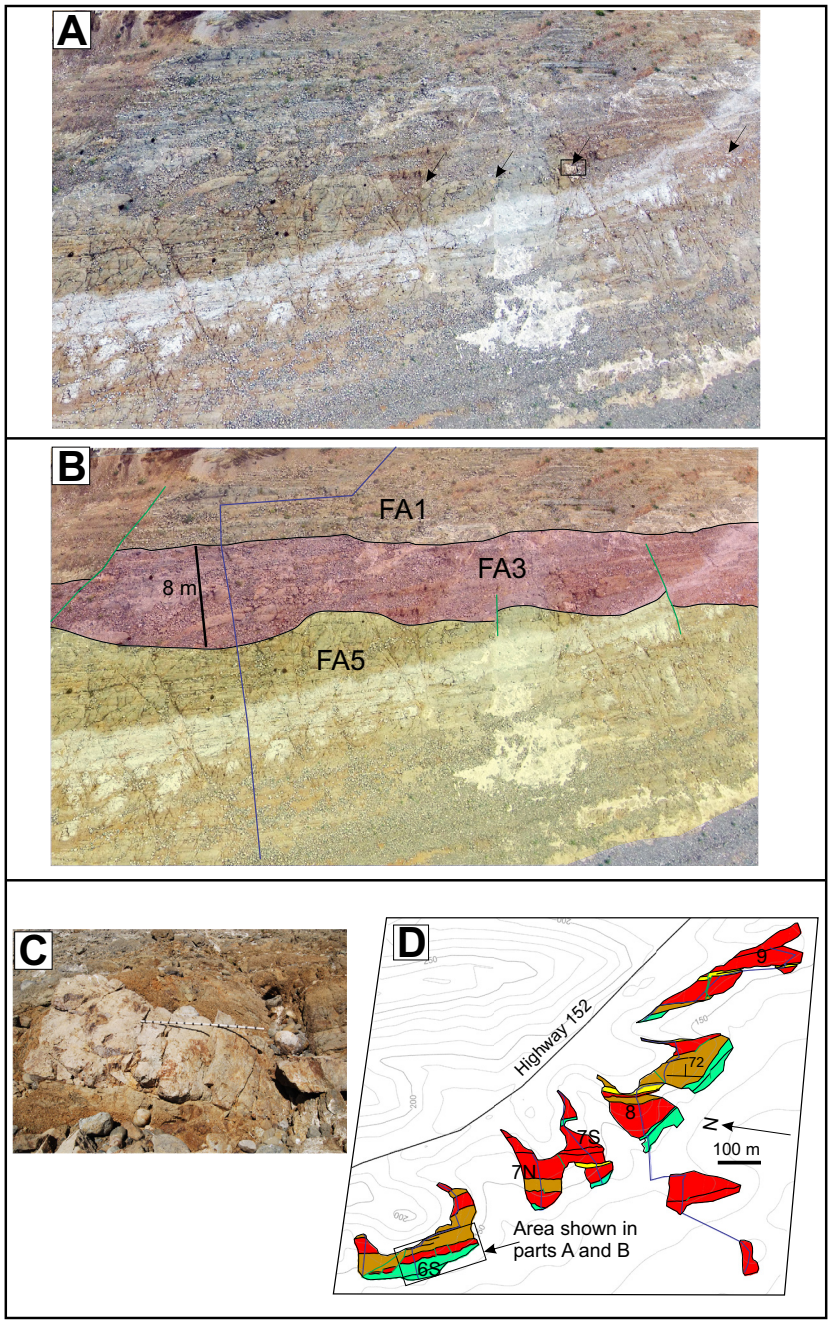

Figure 10. Facies associations for the middle portion of the channelized fill from section 6S (see Plate 1, section 6S for location of photo within CCS-2). (A) Photomosaic interpreted in part B. The perspective is vertical taken from drone photos directly above outcrop. Arrows point to out-sized boulders; boxed area is in part C. (B) Interpreted photomosaic from part A with facies associations showing a major incision surface with overlying boulder conglomerate. The 8-m-thick FA3 layer contains the most abundant out-sized boulder clasts in the study area. (C) Photo of an out-sized boulder clast shown in boxed area of part A. The clast is a 3-m-long, angular, metavolcanic boulder. Staff is 1.5 m long. (D) Map of facies associations showing location of photomosaic; see Figure 7C for symbol definitions and Plate 1 location map for reference.

Vertical changes in facies association stacking patterns and accompanying stratigraphic surfaces were used to package the SLR study area into four channel complex sets that display an upward decrease in depositional energy followed by abandonment. These channel complex sets (CCS) from oldest to youngest are named CCS-1, CCS-2, CCS-3, and CCS-4 (Fig. 5; Plate 1). Each channel complex set contains channel complexes that display varying degrees of lateral continuity. Due to lack of lateral exposure, it is difficult to assess lateral variability, and therefore we do not emphasize the detailed 3-D architectural elements within channel complexes or channel complex sets. In addition, most channel complex and channel complex set widths cannot be determined and are therefore drawn schematically on Plate 1. Nevertheless, channel complex set thickness stratigraphically increases from 390 m (minimum thickness due to lack of a basal exposure) for CCS-1, 410 m for CCS-2, 450 m for CCS-3, and 560 m for CCS-4. The youngest channel complex set (CCS-4) is overlain by 620 m of laterally continuous FA1 deposits that we interpret resulted from regional abandonment.

The lowermost channel complex set (CCS-1) represents the most energetic deposition, which we interpret as having the most confined channel complexes (Fig. 7; Plate 1). The channel complexes are dominated by FA4 deposits (up to 75 m thick) separated by the thin-bedded FA1. CCS-1 also displays the most amalgamated, clast-supported, and well-sorted conglomerate in all of the channel complex sets, indicating the highest degree of consistent turbulent flow.

CCS-2 and CCS-3 represent the main portion of the fill (Fig. 10; Plate 1). They are composed of vertically aggrading channel complexes filled with FA3; the complexes contain some of the largest boulder clasts in the study area (e.g., sections 6S and 10). CCS-2 and CCS-3 both contain bypass facies association (FA5) at their bases (Fig. 10D; Plate 1).

CCS-4 also has abundant channel complexes filled with FA3 deposits; however, CCS-4 contains more amalgamated channel complexes and downward accreting bar sets than CCS-2 or CCS-3 (Figs. 8 and 9; Plate 1). We interpret this to reflect a decrease in accommodation as the entire system aggraded. Other indicators of decreasing depositional energy within CCS-4 include higher proportions of sandy facies associations (e.g., FA2) and a gradual upward decrease in grain size (Fig. 9; Plate 1).

Provenance of Sediments

Conglomerate Clast Counts

Deep-water conglomerates have the potential to capture local sources through large-caliber clasts (e.g., Seiders, 1983; Ingersoll, 1990; Doebbert et al., 2012) and may also include clasts that have traversed confined pathways across exposed shelves and coastal plains during relative sea-level lowstands. We completed five conglomerate clast counts evenly distributed throughout the SLR field area (Figs. 5 and 11; Plate 1). Clast lithology

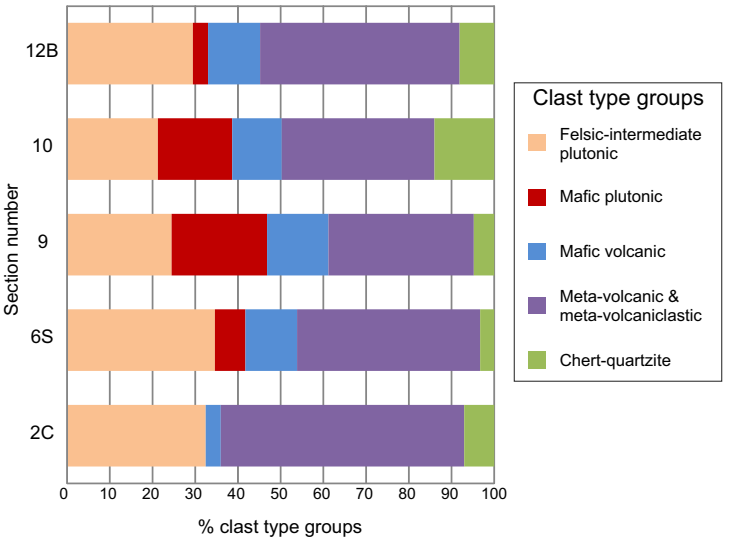

Figure 11. Conglomerate clast count data for five San Luis Reservoir (SLR) localities (n = 200 for each locality). Section localities young from bottom to top. See Figure 5 and Plate 1 for location of counts for each section. See text for discussion of clast type groupings and data.

varied considerably, reflecting the diverse sources contributing to these deposits. To simplify our counts, we created five clast groupings: (1) felsic and/or intermediate plutonic (granitoids and diorite); (2) mafic plutonic (hornblende gabbro and diabase); (3) mafic volcanic (basalt and brecciated basalt); (4) metavolcanic and/or metavolcaniclastic; and (5) chert/quartzite. The metavolcanic and/or metavolcaniclastic and the felsic and/or intermediate plutonic groups make up the majority of the clast types (Fig. 11). The former includes keratophyre (metamorphosed andesite and rhyolite), quartz keratophyre, intermediate-felsic volcanics, silicified metatuffs, metasedimentary, and other lithologies typical of upper portions of arc-related crust (e.g., island arcs and ophiolites). With the exception of the mafic plutonic group in the lowermost locality, all clast groups are present in all localities, indicating similar sources throughout the fill history. Although the mafic plutonic group shows the largest variation in percentage, no obvious vertical trends occur in the data set. In addition, out-sized boulders (greater than 1.5 m in diameter) have a more narrow range of lithologies. The largest clast (3.5 m) is a brecciated basalt boulder with radial pumpellyite (Fig. 6G); most other out-sized clast lithologies include metamorphosed and silicified volcaniclastics and metavolcanics (Fig. 10C). In general, clast counts in SLR conglomerate indicate a mixed source signature: (1) granitoid and other arc rocks likely sourced from the Sierran arc and (2) significant basement clasts derived from the CRO and/or the WSNMB (Fig. 2).

Sandstone Petrography

The seven sandstone samples collected for petrographic analysis contain common diagenetic products, including seritization, alteration of volcanic grains, albitization of plagioclase, minor calcite cement, and crushing of lithic grains. When plotted on tectonic discrimination ternary plots of Dickinson and Suczek (1979) and Dickinson et al. (1983), all seven samples cluster together near the magmatic arc provenance field as well as the San Joaquin subbasin field of Ingersoll (1983; Figs. 5 and 12; Table 1). Based on Ingersoll's (1983) statistically derived petrofacies parameters for GVG sandstone across the entire forearc basin, our samples plot within the range of the Grabast petrofacies (Mansfield, 1979). The parameters, in order of greatest to least importance, are P/F, Lv/L, M, Qp/Q, Q, F, and L (see Table 1 for definitions). Grabast is distinguished by its higher metamorphic signature, as indicated by relatively high P/F and M and low Lv/L values. This was also predicted by petrofacies distribution maps by Ingersoll (1983), wherein the Grabast petrofacies corresponds to Cenomanian through Santonian GVG rocks that only occur in the San Joaquin subbasin. We therefore interpret the SLR sandstone to be derived from the more "continental," dissected southern Sierran arc, similar to other San Joaquin GVG samples.

Major- and Trace-Element Mudrock Geochemistry

Deep-water mudrock geochemistry records a more homogenized provenance signal relative to the coarser sedimentary fractions (e.g., McLennan et al., 1993; Mahoney, 2005) and therefore helps us recognize large-scale provenance shifts rather than more localized variation. Furthermore, mudrocks may

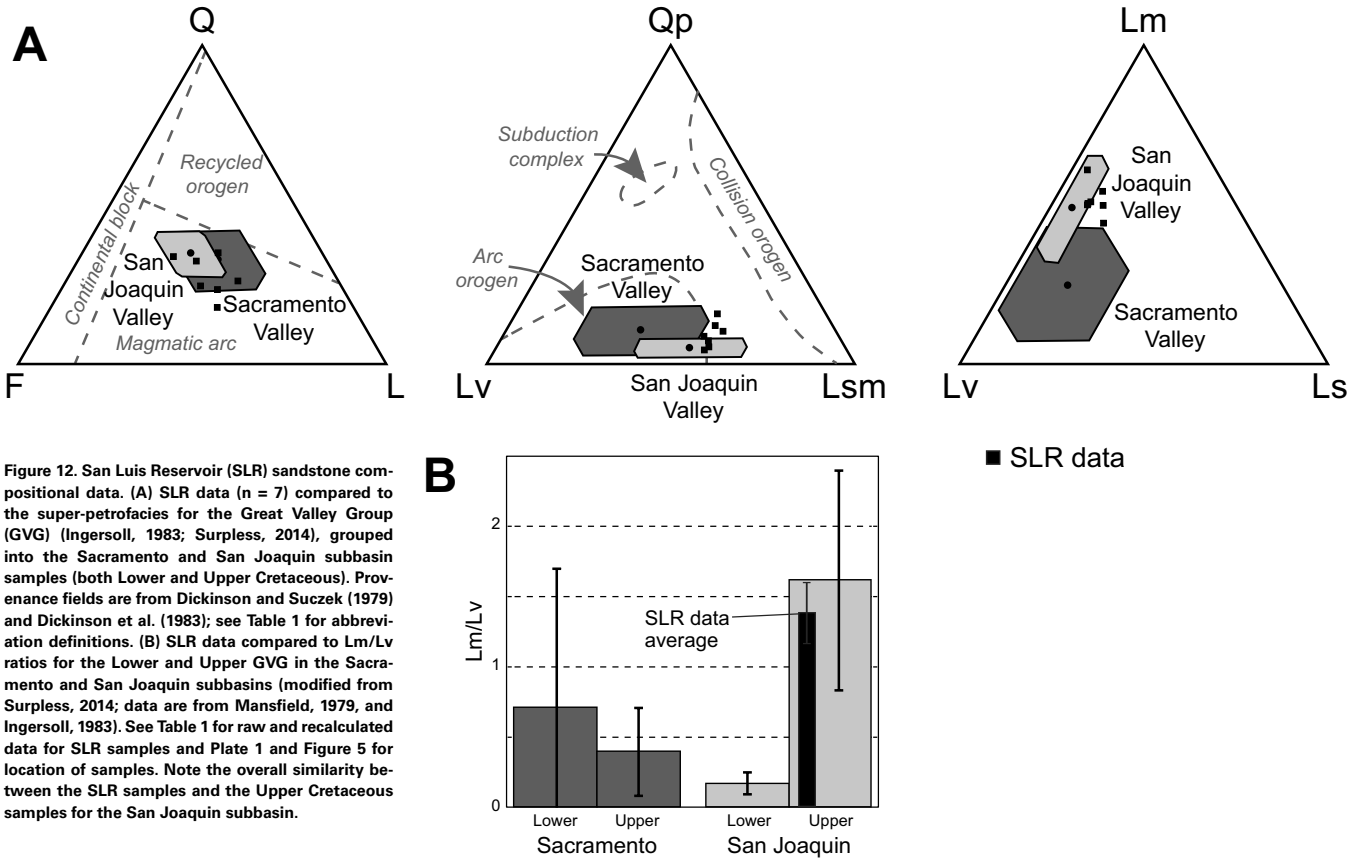

Figure 12. San Luis Reservoir (SLR) sandstone compositional data. (A) SLR data (n = 7) compared to the super-petrofacies for the Great Valley Group (GVG) (Ingersoll, 1983; Surpless, 2014), grouped into the Sacramento and San Joaquin subbasin samples (both Lower and Upper Cretaceous). Provenance fields are from Dickinson and Suczek (1979) and Dickinson et al. (1983); see Table 1 for abbreviation definitions. (B) SLR data compared to Lm/Lv ratios for the Lower and Upper GVG in the Sacramento and San Joaquin subbasins (modified from Surpless, 2014; data are from Mansfield, 1979, and Ingersoll, 1983). See Table 1 for raw and recalculated data for SLR samples and Plate 1 and Figure 5 for location of samples. Note the overall similarity between the SLR samples and the Upper Cretaceous samples for the San Joaquin subbasin.

better represent the more mafic minerals and volcanic clasts of the provenance record than either sandstone or conglomerate (e.g., McLennan et al., 1993). The four SLR samples are compared to Upper Cretaceous mudrock samples from the Sacramento and San Joaquin subbasins (Figs. 5 and 13; Tables 2 and 3; data from Surpless, 2014, and this study). More juvenile or evolved sources may be distinguished on plots of wt% TiO_2 and Al_2O_3/SiO_2 versus Fe_2O_3 + MgO (Bhatia and Crook, 1986; Ryan and Williams, 2007; LaMaskin et al., 2008) because Ti and Al are considered immobile up to greenschist-grade conditions (MacLean, 1990; Jenner, 1996). The four SLR samples cluster together with the more evolved San Joaquin samples (Figs. 13A and 13B).

Comparing incompatible elements Th and La against the compatible element Sc can help distinguish contributions of juvenile and evolved crust (Bhatia and Crook, 1986; McLennan et al., 1990, 1993; Fralick, 2003). San Luis Reservoir samples plot with San Joaquin sample compositions between Continental Arc and North American Shale Composite values on a La-Th-Sc ternary diagram (Fig. 13C). Vanadium, Ni, and Th*10 indicate the relative contributions

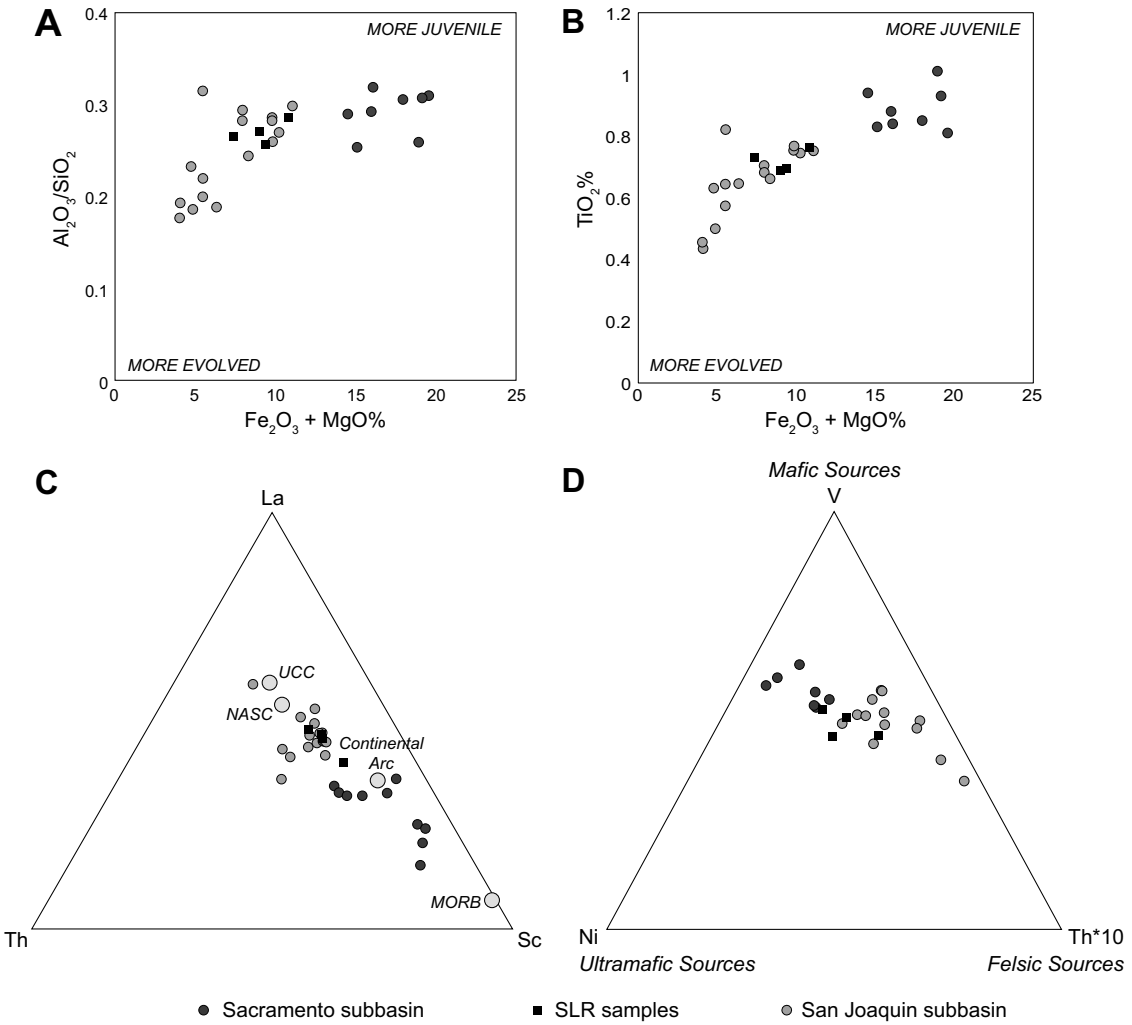

Figure 13. Mudrock geochemical plots displaying San Luis Reservoir (SLR) samples grouping with Upper Cretaceous San Joaquin samples relative to Sacramento subbasin. See Plate 1 and Figure 5 for sample locations and Tables 2 and 3 for data. (A) and (B) Major-element provenance diagrams after Bhatia and Crook (1986). (C) Ternary plot of V-Ni-Th*10 to represent relative contributions of mafic, ultramafic, and felsic sources, respectively (after Bracciali et al., 2007). Values of potential source rocks are from Taylor and McLennan (1985) and McLennan et al. (1993). MORB—mid-oceanic ridge basalt; NASC—North American Shale Composite; UCC—Upper Continental Crust. (D) Ternary plot of La-Th-Sc.

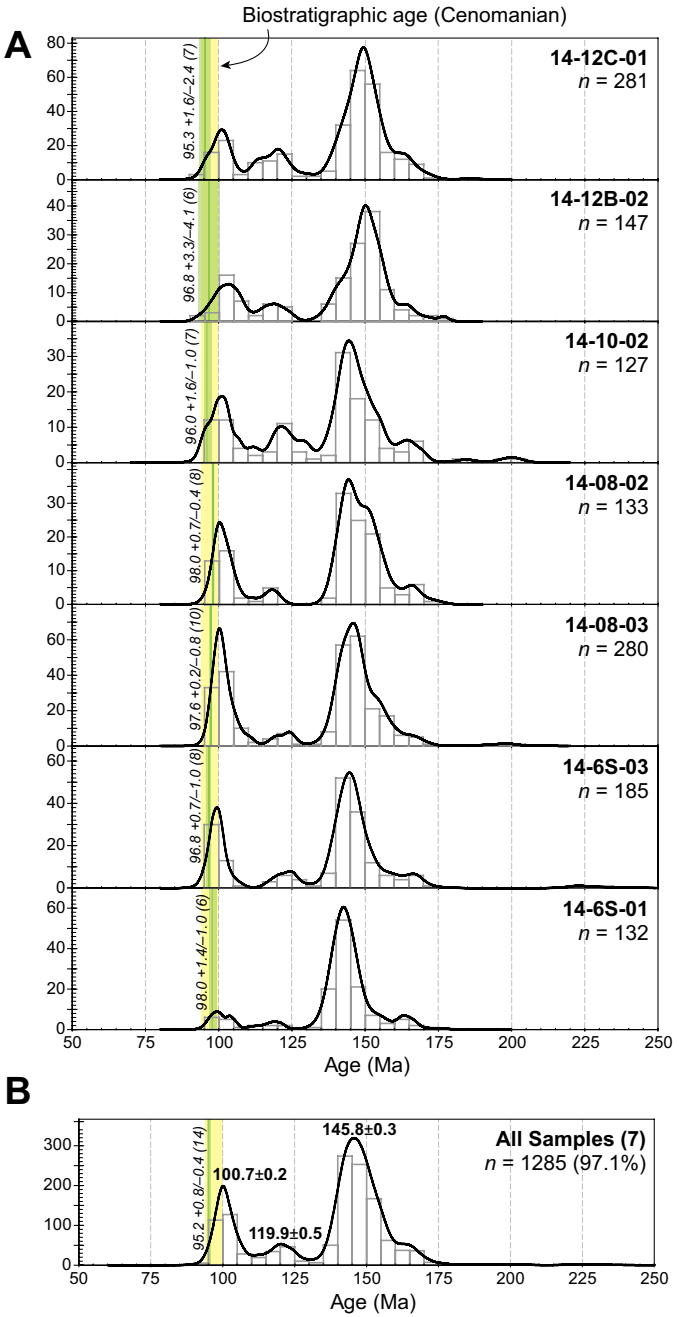

Figure 14. Detrital-zircon age histograms and superimposed probability density curves for the San Luis Reservoir (SLR) deposits (N = 7; see Table DR1 (see footnote 1) for data; see Plate 1 and Figure 5 for sample locations). (A) Mesozoic age distributions (50–250 Ma) with superimposed relative-probability curves. Cenomanian biostratigraphic depositional age is shown as yellow bar (see Fig. 4) and calculated maximum depositional ages are shown as green bars for each sample (see text for discussion); samples are presented in stratigraphic order with the youngest at the top. (B) Compiled Mesozoic data from all samples plotted with the same format as part A. (C) Compiled pre-Mesozoic data from all samples.

of mafic, ultramafic, and felsic sources, respectively (Bracciali et al., 2007). San Luis Reservoir samples plot in the overlap regions between more felsic San Joaquin samples and more mafic Sacramento Valley samples (Fig. 13D).

Overall, our four SLR mudrock samples plot in the overlap region between more mafic Sacramento Valley samples and more felsic San Joaquin samples but tend to show greater affinity with San Joaquin samples. These San Joaquin sample compositions suggest a mixed provenance that includes both juvenile, active continental arc sources, and more evolved, passive-margin type sources.

Detrital-Zircon U-Pb Results

Mesozoic detrital-zircon age distributions are shown in stratigraphic order on Figure 14A as histograms with superimposed relative probability curves generated using routines in Isoplot (Ludwig, 2008). Maximum depositional ages and associated uncertainties are represented on each curve as a green bar and are calculated using the zircon age extractor routine in Isoplot. Youngest maximum depositional ages range from 98 to 95.3 Ma, indicating Cenomanian or younger deposition. Because these maximum depositional ages are consistent with Cenomanian biostratigraphy (yellow vertical bar on Fig. 14; Goudkoff, 1945), we conclude that deposition was Cenomanian.

All samples display remarkably similar age distributions, with prominent Latest Jurassic, Early Cretaceous, and mid-Cretaceous peaks (Figs. 5 and 14). These results suggest that sediment sources did not change significantly during deposition, and thus all strata can be represented with a composite age distribution (Fig. 14B). Maximum depositional age for the compiled strata is 95.2 +0.8/–0.4 Ma, based on the youngest 14 grains. A total of 1285 (97.1%) analyzed grains are Mesozoic age, forming distinct peaks at 145.8 Ma (56% of Mesozoic grains) and 100.7 Ma (21%), with smaller peaks at 160.3 Ma (13%) and 119.9 Ma (9%; peak ages calculated using Unmix routine in Isoplot). Thirty-eight (2.9%) analyzed grains are pre-Mesozoic, ranging in age from 342 to 2733 Ma (Fig. 14C).

DISCUSSION

Aggrading Channelized System versus Submarine Canyon Depositional Model

Differentiating the stratigraphic architecture of an aggrading submarine channel system from a submarine canyon depositional model using outcrops with limited exposure is problematic (Bain and Hubbard, 2016), yet the paleogeographic implications are significantly different. While submarine canyons are often linked to more allocyclic controls (eustasy, denudation, and tectonics), aggrading channelized systems respond more to autocyclic, localized processes (Posamentier et al., 1991; Posamentier and Kolla, 2003; Mountjoy et al., 2009; Sylvester et al., 2011; Di Celma et al., 2014). We define submarine canyons as deeply incised, long-lived sediment conduits with hundreds of

meters to a km of bathymetric relief (Bain and Hubbard, 2016). Alternatively, aggrading submarine channelized systems build as highly amalgamated low-relief channels that are confined by external levees (Sylvester et al., 2011). Due to the lack of lateral exposure in the SLR deposit (Plate 1), a definitive interpretation is not possible because submarine canyon walls or floors as well as any external levee deposits cannot be identified.

However, despite these limitations, we interpret the SLR deposits as an aggrading submarine channel system built along the lower slope. We base this interpretation on: (1) middle-to-lower bathyal paleowater depth determination from benthic foraminifera within the SLR deposits (Fig. 3); (2) numerous examples of erosive surfaces, some with relief up to 30 m (Fig. 7); (3) the highly amalgamated architecture of the channel complexes within all of the channel complex sets (Plate 1); (4) common examples of rafted blocks of thin-bedded turbidites presumably derived from the confining interval levees; and (5) the overall proportion of the coarse-grained facies associations (e.g., FA3 and FA4) being uncharacteristic of other documented GVG submarine canyon fills (cf. Williams et al., 1998; Williams and Graham, 2013).

The forces required to roll, move, and suspend this caliber of sediment most likely involved steep depositional slopes or steep channel walls. As a slightly younger analog, Ingersoll (1979) used well-log data of Coniacian deposits that onlap basement to the east to calculate a steep depositional slope of 8° at the SLR area and determined that the SLR site was less than 30 km away from its time-equivalent shoreline.

The SLR study area records a nearly 1.8-km-thick submarine channelized deposit that extends 4 km along structural strike (Fig. 5; Plate 1). Given the southeastward paleocurrent directions, the SLR outcrops represent a stratigraphic cross section roughly oriented in a depositional-dip direction. Regionally, however, the SLR area is part of a much larger, coeval, deep-water conglomeratic outcrop that extends to the north ~20 km along strike in the depositional up-dip direction (Fig. 3; Schilling, 1962; Bennison et al., 1991; Dibblee, 2007a, 2007b, 2007c). Using Schilling's (1962) stratigraphic chart, the SLR area is in the southernmost (distal) position relative to other time-equivalent outcrops. Coeval conglomeratic units thicken to the north to 3.2 km thick and further thin to 850 m before pinching out into mudstone at the northernmost (proximal) section (Fig. 3). Due to the orientation of the outcrop relative to the paleoflow direction, the steep dip of the beds, and the lack of continuous exposure outside the SLR area, we are unable to estimate overall submarine channel system width. However, we infer the projection of the fill meanders in and out of the outcrop belt and therefore could continue into the subsurface to the north and south. Regardless of dimensions and orientation, we infer the source area had a steep gradient and narrow shelf.

Submarine Channelized System Depositional Analogs

Other well-studied, forearc, deep-water conglomerate in GVG or equivalent outcrops include the Juniper Ridge Conglomerate, near Coalinga (Fig. 2; Hickson and Lowe, 2002), the various conglomerate lenses in the Stony Creek Formation in the Sacramento subbasin (Bertucci, 1983; Campion et al., 2000), and the Nanaimo Group in British Columbia, Canada (Bain and Hubbard, 2016). All of these examples contain similar conglomeratic facies associations and hierarchical elements with the SLR deposits; however, unlike the SLR deposits, they all feature well-exposed, out-of-channel facies, which strengthens the interpretations of submarine channel complex sets or channel-levee complexes.

Although in a foreland basin setting, the Cerro Toro axial channel belt in the Cretaceous Magallanes Basin, Chile, also contains deep-water conglomerate with similar depositional elements to the SLR area (Jobe et al., 2010). Thickness and clast size of coarse-gained strata are comparable, although the Cerro Toro contains evidence for even greater, more powerful turbiditic flows (e.g., canoe-sized flute casts; Jobe et al. [2010]). In addition, the Cerro Toro deposits are well-exposed for longer lateral distances, and they display an overall greater architectural organization than the SLR deposits, with well-defined lateral facies relationships, channel forms, and regional correlation surfaces.

Possible Sources for San Luis Reservoir (SLR) Deposits

Many studies point to the Sierran arc as the dominant source for GVG deposits in the San Joaquin subbasin (Ingersoll, 1983; Linn et al., 1992; DeGraaff-Surpless et al., 2002; Surpless, 2014). However, the changes associated with the ca. 100 Ma time period combined with the coeval deposition of thick deep-water boulder conglomerate at SLR warrant a more detailed investigation into possible sources. These sources include the Sierran arc, WSNMB, CRO, and Franciscan Complex.

Sierran Arc

Relatively continuous subduction-related magmatism associated with the Sierran arc between 248 and 80 Ma (Bateman and Dodge, 1970; Evernden and Kistler, 1970; Stern et al., 1981; Chen and Moore, 1982; Bateman, 1983; Saleeby et al., 1989b; Saleeby, 1990; Coleman et al., 2004; Cecil et al., 2012; Paterson et al., 2014) built a nearly 600-km-long batholith along eastern California with up to at least 35-km-thick intermediate to felsic intrusive rocks and associated metamorphic pendants (Fig. 1; Pickett and Saleeby, 1993; Ducea, 2001). Periods of significant Jurassic and younger plutonism include: (1) Middle Jurassic to Early Cretaceous in the western arc (ca. 194–130 Ma, peaks at ca. 161 ± 14 Ma), which we combine with the WSNMB; and (2) mid-Late Cretaceous in the eastern arc (ca. 124–76 Ma, peak at ca. 98 ± 8.5 Ma; Coleman and Glazner, 1997; Paterson and Ducea, 2015). Scattered borehole penetrations indicate that the western extent of the former phase lies underneath the eastern Great Valley forearc; both phases crosscut portions of the WSNMB (May and Hewitt, 1948; California Division of Oil and Gas, 1964; Bateman, 1983; Harwood and Helley, 1987; Saleeby et al., 1989a; Cecil et al., 2012). Compositional trends across the Sierra indicate more continental signatures to the east and more juvenile signatures in the north (Kistler and Peterman, 1973; DePaolo, 1981; Bateman, 1983).

The mid-Late Cretaceous magmatic flare-up is represented by nearly 50% of exposed Sierran plutons (Chen and Moore, 1982; Irwin and Wooden, 2001). Many of these plutons have been associated with various right-stepping, dextral shear zones within the eastern Sierra that formed concurrently with shallow (8–10 km) pluton emplacement (e.g., Sierran Crest shear zone, proto–Kern Canyon shear zone, and the Mojave–Snow Lake shear zone; Glazner, 1991; McNulty, 1995; Tikoff and Greene, 1997; Tikoff and de Saint Blanquat, 1997; Tobisch et al., 2000; Tikoff et al., 2005; Hirt, 2007). In particular, the northern portion of the Sierran Crest shear zone contains the Gem Lake–Bench Canyon–Quartz Mountain–Cascade Lake shear zone system adjacent to the Tuolumne Igneous Complex (TIC; Fig. 15A; McNulty, 1995; Greene and Schweickert, 1995; Coleman et al., 2004; Tikoff et al., 2005; Memeti et al., 2014). The TIC and surrounding localities host various plutonic and volcanic rocks within the range of the SLR ca. 100 Ma zircon age population (McNulty, 1995; Tobisch et al., 1995; Coleman et al., 2004): Sentinel Granodiorite (95 ± 1 Ma), Red Devil Lake pluton (95 ± 1 Ma), Jackass Lakes pluton (98.5 ± 0.3 Ma), Shellenbarger pluton (99 Ma), Illilouette Creek pluton (99 ± 1 Ma), and the Minarets caldera sequence (98–101 Ma).

Western Sierra Nevada Metamorphic Belt (WSNMB)

The highly complex WSNMB is an amalgamation of oceanic-affinity terranes consisting of Triassic and Jurassic accretionary metasedimentary units, metavolcanic arc rocks, ophiolite, and mélange units (Fig. 2; Saleeby, 1982; Sharp, 1988; Moores et al., 2003; Snow and Scherer, 2006; Ernst et al., 2008; Schweickert, 2015). In general, the WSNMB consists of two island arcs and related ophiolites and accretionary complexes that collided with North America no later than 152 Ma during the Nevadan orogeny (Schweickert and Cowan, 1975; Saleeby et al., 1989a; Schweickert et al., 1999; Schweickert, 2015). No consensus exists on how to divide the WSNMB into various tectonostratigraphic terranes, and it is unclear how far west the belt extends under forearc basin strata (Schweickert et al., 1999; Ernst et al., 2008; Schweickert, 2015). However, the WSNMB probably served as basement to at least the eastern Great Valley forearc (Bailey and Blake, 1969; Harwood and Helley, 1987) and therefore could be a potential source for the SLR deposits.

We also include the Late Jurassic–Early Cretaceous Sierran arc source as part of the WSNMB (Dickinson, 2008). Limited available outcrops, borehole penetrations, and geophysical data suggest the Late Jurassic–Early Cretaceous phase of arc magmatism was prevalent in the western Sierra near the SLR area (Fig. 15A; May and Hewitt, 1948; California Division of Oil and Gas, 1964; Bateman, 1983; Harwood and Helley, 1987; Saleeby et al., 1989a; Ingersoll, 2000; Cecil et al., 2012). According to Cecil et al. (2012), the western boundary of the Late Jurassic–Early Cretaceous arc lies under the San Joaquin subbasin as close as 35 km to the SLR deposits (Figs. 2 and 15A). In particular, the Guadalupe Igneous Complex (GIC), due east of the SLR area (Fig. 2), contains a full suite of intrusive rocks from gabbro through granite emplaced at relatively shallow depths (<15 km) ca. 151 Ma (Putirka et al., 2014). Other small plutons to the northwest have been dated between 150 and 141 Ma (Saleeby et al., 1989a; Schweickert et al., 1999; Dickinson, 2008; Putirka et al., 2014; Schweickert, 2015). In addition, Clemens-Knott and Saleeby (2013) suggest that the GIC was already exposed and supplying sediment to the Early Cretaceous Goldstein Peak basin between 144 and 138 Ma and therefore could also have been emergent during Cenomanian deposition of the SLR deposits.

Coast Range Ophiolite (CRO)

Stretching nearly 700 km in the Coast Ranges, the Middle and Upper Jurassic (168–144 Ma) CRO consists of erratic broken remnants and intact sequences of typical ophiolite assemblages lying structurally above the Franciscan Complex (Fig. 2; Ernst, 1970; Dickinson, 1971; Hopson et al., 1981, 2008; Saleeby et al., 1982; Saleeby, 1983; Ingersoll et al., 1999; Coleman, 2000; Shervais et al., 2004, 2005). CRO has island-arc geochemistry (Shervais and Kimbrough, 1985; Shervais, 1990; Giaramita et al., 1998; Evarts et al., 1999), but tectonic origin interpretations vary (see Dickinson et al. [1996] for a summary) from supra-subduction zone (Shervais and Kimbrough, 1985; Robertson, 1989; Shervais, 1990; Stern and Bloomer, 1992; Shervais et al., 2004, 2005), mid-ocean ridge (Hopson et al., 1996, 2008), and backarc oceanic crust (Schweickert et al., 1984; Schweickert, 1997; Godfrey and Klemperer, 1998; Ingersoll, 2000). The CRO most likely served as basement for the western forearc basin and was periodically affected by accretionary wedge tectonism (Shervais et al., 2004; Mitchell et al., 2010; Wakabayashi, 2015). CRO outcrops that could represent sources for SLR deposits include the Del Puerto (167–143 Ma; Hopson et al., 2008) and the Quinto Creek (Late Jurassic; Hopson et al., 1981; Robertson, 1989) ophiolites, where typical lithologies include hornblende gabbro, diorite, tonalite, peridotite, basalt, keratophyre, plagiogranite, chert, and tuff (Fig. 2; Hopson et al., 1981, 2008; Evarts et al., 1999; Shervais et al., 2004).

Franciscan Complex

The Coast Ranges are dominated by accretionary wedge material of the Franciscan Complex (170–12 Ma), which records nearly 160 m.y. of east-dipping subduction underneath North America (Ernst, 1970; McLaughlin et al., 1982; Wentworth et al., 1984; Dumitru, 1991; Wakabayashi, 1992, 1999, 2015; Unruh et al., 2007; Dumitru et al., 2010). Major divisions (eastern, central, and coastal belts) of the Franciscan typically young from east to west and are composed mainly of serpentinized mélange with semi-coherent blocks of metagraywacke, shale, basalt, greenstone, chert, blueschist, and rare allochthonous upper plate slide blocks (Fig. 2; Irwin, 1960; Bailey et al., 1964, 1970; McLaughlin et al., 1982; Wakabayashi and Rowe, 2015). Most of the mélange is interpreted to be sedimentary in origin with evidence depicting upper-plate–derived (North American) submarine debris depositing into the trench (Jacobson, 1978; Dickinson et al., 1982; MacPherson et al., 1990; Jacobson et al., 2011; Wakabayashi, 2015).

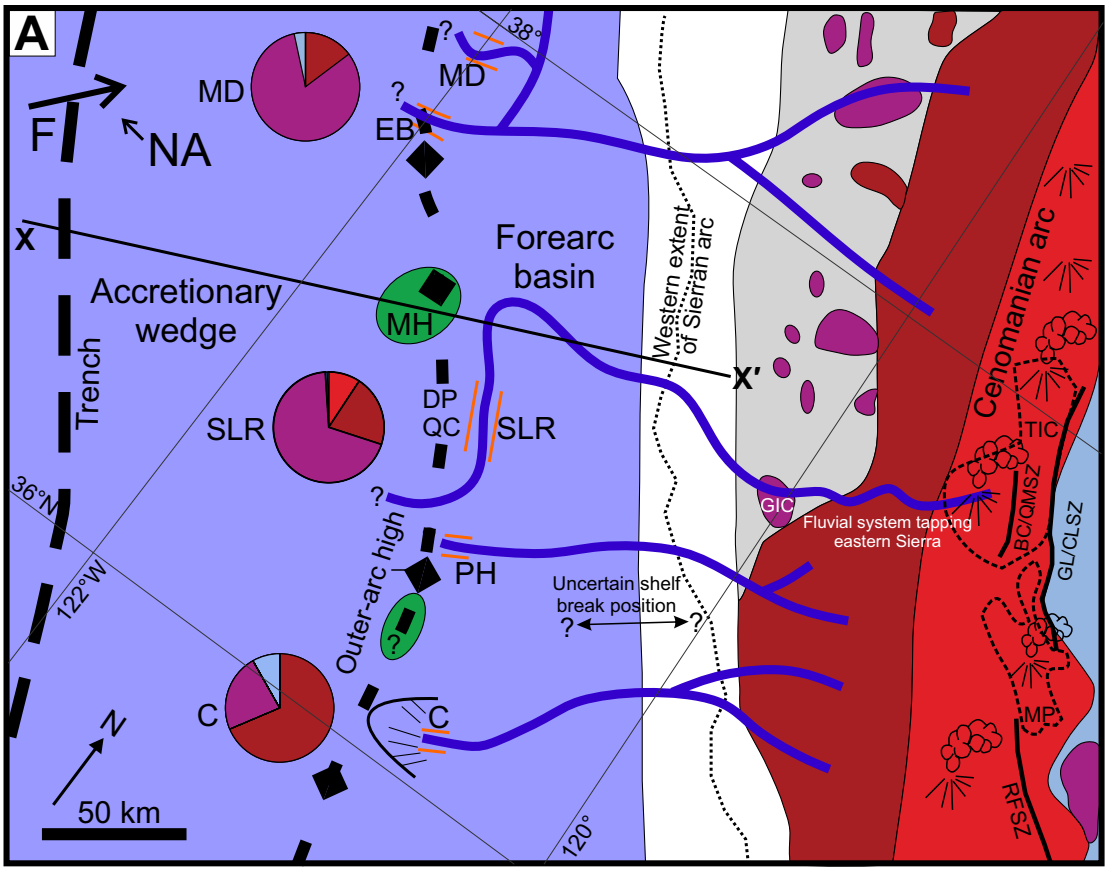

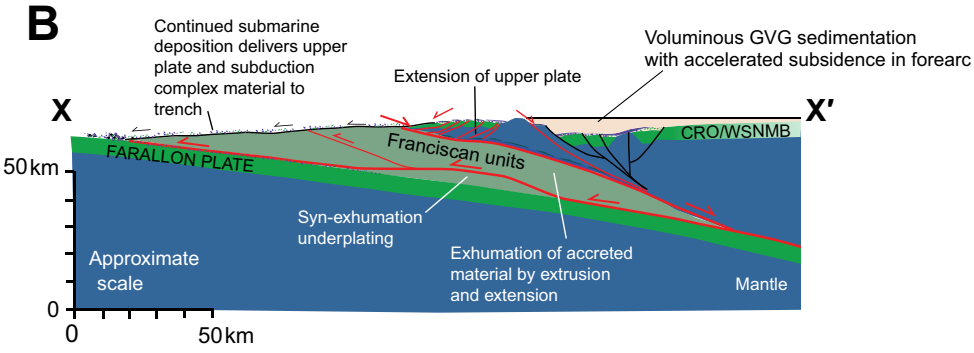

Figure 15. (A) Possible Cenomanian paleogeographic model for a portion of the arc-forearc-prism triad near the San Joaquin subbasin. Both Models #1 and #2 are depicted, although the latter model would not require uplift of the outer-arc high. See text for further explanation. The position of the western extent of the Sierran arc is from Cecil et al. (2012). Abbreviations: TIC—Tuolumne Igneous Complex; GIC—Guadalupe Igneous Complex; MP—Mono Pass igneous complex; GL/CLSZ—Gem Lake and Cascade Lake shear zones; BC/QMSZ—Bench Canyon and Quartz Mountain shear zones; RFSZ—Rosy Finch shear zone; SLR—San Luis Reservoir; MD—Mount Diablo; DP—Del Puerto ophiolite; QC—Quinto Creek ophiolite; MH—Mount Hamilton; C—Coalinga; PH—Panoche Hills; EB—East Bay; F—Farallon plate; NA—North American plate. Pie charts show detrital-zircon age populations for MD and C (Sharman et al., 2015) and SLR (this study); color guide for pie charts is the same as the map key. Arrows for F and NA plates show relative magnitude and direction of plate motions for ca. 90 Ma (Liu et al., 2008). X–X′ schematic cross section is shown in part B. (B) Model #1 only: schematic cross section modified from Wakabayashi (2015) for the 100–70 Ma time frame. Position of X–X′ cross-section line is shown in part A; however, the position is arbitrary and is not meant to exactly match surface features; see text for discussion.

The off-scraped and underplated sedimentary debris commonly formed thrust nappes. These nappes show accretionary (incorporation into subduction complex) ages that young structurally downward (Maxwell, 1974; Blake et al., 1984; Wakabayashi, 1992, 2015; Ernst et al., 2009; Dumitru et al., 2010, 2015; Snow et al., 2010; Wakabayashi and Rowe, 2015). Geochemical and geochronological evidence from coeval GVG and Franciscan strata indicate a similar North American source (Dickinson et al., 1982; DeGraaff-Surpless et al., 2002; Joesten et al., 2004; Tripathy et al., 2005; Ernst et al., 2009; Dumitru et al., 2010, 2015; Snow et al., 2010; Jacobson et al., 2011; Sharman et al., 2015).

Mixed Provenance of San Luis Reservoir (SLR) Sediments

Similar to other Upper Cretaceous GVG samples from the San Joaquin subbasin (Ingersoll, 1983; Linn et al., 1992; DeGraaff-Surpless et al., 2002; Surpless, 2014), SLR sandstone composition and mudrock geochemistry both suggest sources from metamorphic and continental arc signatures of a dissected southern Sierran arc (Figs. 12 and 13). The addition of conglomerate clast data (Fig. 11) and detrital-zircon geochronology (Fig. 14) suggests two main sources contributing sediment to the Cenomanian SLR deposits: (1) mid-Late Cretaceous Sierran arc and (2) Jurassic WSNMB and/or CRO.

Mid-Late Cretaceous Sierran Arc Sources

The small 121 Ma peak in the Cenomanian SLR detrital-zircon signature occurs in coeval samples to the north and south as well as the prominent mid-Cretaceous Sierran arc magmatism (DeGraaff-Surpless et al., 2002; Sharman et al., 2015). However, the ca. 100 Ma age population is unexpected, given the paucity of these ages in Cenomanian–Coniacian strata (<2%; Sharman et al., 2015). Sharman et al. (2015) explain the lack of 100–85 Ma detrital-zircon despite a contemporaneous magmatic flare-up period in the eastern Sierran arc between 125 and 76 Ma (peak 98 ± 8.5 Ma; Paterson and Ducea, 2015) by hypothesizing that a drainage divide blocked detritus from the eastern Sierra from reaching the Cenomanian–Coniacian basin; these Late Cretaceous detrital zircon became increasingly abundant in younger Cretaceous strata due to progressive unroofing (cf. DeGraaff-Surpless et al., 2002).

However, the post–105 Ma population (19% of Mesozoic population; 18.5% of total grains) in the Cenomanian SLR deposits could mean that the submarine channel system was depositionally connected to a source that was not widely available to other Cenomanian–Coniacian deposits (Fig. 15). In addition, the overlap between the maximum depositional age (95.2 Ma) calculated from the youngest detrital zircon (n = 14) and the Cenomanian biostratigraphic age (100–94 Ma) of the SLR deposits indicates that the submarine channel system was linked to a fluvial system that tapped the coeval ca. 100 Ma eastern Sierran volcanic carapace (Fig. 15A; cf. House et al., 1998). Only later did other localities to the north and south of the SLR location receive abundant post–105 Ma zircon.

Western Sierra Nevada Metamorphic Belt (WSNMB) and/or the Coast Range Ophiolite (CRO)

The 145.8 Ma and 160.3 Ma detrital-zircon peaks of the SLR deposits (Fig. 14B) fall within the "Middle Jurassic Sierran flare-up" period (Paterson and Ducea, 2015) of 194–130 Ma (peak at 161 ± 14 Ma) and also overlap with WSNMB and CRO history (Dickinson, 2008; Hopson et al., 2008). In fact, Sharman et al. (2015) suggest that the WSNMB may have provided 200–135 Ma detrital zircon to Cenomanian–Coniacian strata (Fig. 2), and they noted a sharp decrease in this age population to the south between the Mount Diablo and Coalinga localities, mirroring the southern termination of the Jurassic WSNMB (Fig. 2).

The basement terranes of the WSNMB (eastern side of the forearc) and CRO (western side of the forearc) share similar tectonic origins and rock types, and it remains unresolved where and how the two entities became adjacent to one another prior to deposition of the GVG. Although considerable post-Cenomanian deformation occurred regionally, we accept that both entities were in their present position with respect to North America by Cenomanian time (Cady, 1975; Robertson, 1989; Stern and Bloomer, 1992). Therefore, we consider local CRO and WSNMB outcrops as possible analogs for ophiolitic and island-arc sources for the SLR deposits (Fig. 2).

The SLR sandstone composition and mudrock geochemistry data do not show signatures of typical ocean crust or island arcs (Figs. 12 and 13). However, the large conglomerate clasts of the SLR deposits contain a variety of lithologies that also occur in local outcrops of the CRO and WSNMB (Fig. 11; Schweickert et al., 1999; Hopson et al., 2008; Schweickert, 2015). The overlap of rock type, age, and tectonic setting in potential source areas precludes a unique interpretation, and the SLR deposits could have been sourced in part from either the CRO or the WSNMB rocks.

Paleogeographic Models

We suggest that a combination of tectonic events during a time of reorganization (ca. 100 Ma) in the Cretaceous arc-forearc-prism history of California led to the unique Cenomanian SLR deposits. Furthermore, these mid-Cretaceous events most likely resulted from an abrupt increase in plate-motion rates parallel to the arc (obliquity) between the Farallon plate and North American plate (Page and Engebretson, 1984; Engebretson et al., 1985; Liu et al., 2008). Page and Engebretson (1984) report convergence normal to the margin was 5 cm/yr prior to 100 Ma and nearly doubled to 9 cm/yr during 100–85 Ma. In addition, Liu et al. (2008) display plate-motion vectors that shift counterclockwise 38° between 100 Ma and 90 Ma. This change from nearly head-on convergence to oblique transpression likely triggered large-scale effects throughout the arc-forearc-prism system.

In the arc, eastern Sierran shear zones developed contemporaneously with voluminous magmatism associated with the mid-Late Cretaceous magmatic flare-up (peak 98.5 ± 8.5 Ma; Glazner, 1991; Tobisch et al., 1995, 2000; Tikoff and Greene, 1997). The overlap between SLR deposition and the youngest detrital-

zircon ages, as well as the lack of post–100 Ma zircons in other Cenomanian localities (Sharman et al., 2015), suggest that volcanic rocks associated with the flare-up were quickly eroded, transported along confined fluvial drainages, and deposited in the deep-water setting in the SLR area (Fig. 15A).

Other possibly related events in the forearc system include accelerated Late Cretaceous subsidence beginning in the Cenomanian (Moxon and Graham, 1987; Moxon, 1990) and deposition of multiple Cenomanian deep-water conglomerates along strike south of the SLR area, including the Panoche Hills and Coalinga deposits (Figs. 2 and 15A; Moxon, 1990; Hickson and Lowe, 2002) as well as the Rosario Group adjacent to the Peninsular Ranges in southernmost California and northern Baja California (Kimbrough et al., 2001). Similarly, in the Sacramento subbasin to the north, accelerated subsidence began in Cenomanian time (Moxon and Graham, 1987; Moxon, 1990; Williams and Graham, 2013), and deformation of pre–100 Ma strata in the Sites Anticline (Chuber, 1961) was dated to ca. 100 Ma and associated with tectonic wedging of Franciscan material (Wentworth et al., 1984; Williams et al., 1998). Finally, throughout the entire forearc, DeGraaff-Surpless et al. (2002) suggested a range of possible scenarios to explain a fundamental change in detrital-zircon age spectra at the beginning of Cenomanian time: (1) broad shift in the Sierran drainage divide; (2) increased dissection of the magmatic arc with headward erosion of transverse drainage systems; and/or (3) increased sediment mixing on a broadening shelf during eastward shoreline migration.

Here, we present two possible paleogeographic models of the middle Cretaceous San Joaquin subbasin (Fig. 15). Our possible models derive from the interpretation of the SLR as a submarine channelized system with mixed provenance from the Sierran arc and WSNMB with (Model #1) or without (Model #2) the CRO as a source.

Model #1: Coast Range Ophiolite (CRO) as a Potential Contributing Source

We can readily account for Sierran arc and WSNMB sources, but a potential CRO source requires a unique tectonic explanation. Exposure of the CRO adjacent to the SLR submarine channel system would require uplift of basement rocks concurrent with erosion of cover strata. Wakabayashi (2015) reports periods of accelerated accretion in the accretionary prism led to uplift of basement rocks within a forearc deep-water setting (Fig. 15B). Specifically, increased sedimentation to the trench would promote underplating of material, resulting in imbricate thrust stacks separated by paleomegathrust horizons (Wakabayashi, 2015). Because this stacking is commonly accommodated by extension and subsidence in the upper plate, accompanied by exhumation of accreted material (Wakabayashi, 2015), periods of accelerated accretion provide abundant opportunity to uplift, exhume, and erode previously deposited material. These changes would lead to unstable conditions that promote submarine mass wasting and exposure of basement material (Figs. 15A and 15B).

Furthermore, the Diablo Range shows evidence of thrust stacking, coincident with a significant unconformity in the San Joaquin subbasin, followed by SLR deposition. Structurally adjacent to the SLR deposits are blueschist-grade metagraywackes interpreted to be coherent imbricate thrust nappes (Ernst, 1970, 1993; Cloos, 1986; Ernst et al., 2009). Based on detrital- zircon ages and interpreted critical P-T exhumation pathways for these metagraywackes, clastics were deposited in the trench between 102 and 86 Ma (roughly coeval with SLR deposition), buried to 20–30 km depths, and then rapidly exhumed in Late Cretaceous time and again later in Cenozoic time (Dalla Torre et al., 1996; Kimura et al., 1996; Wakabayashi, 2015). In the northern Diablo Range near Mount Hamilton (Fig. 2), Tagami and Dumitru (1996) inferred that ~20 km of exhumation between 100 and 70 Ma led to extensional thinning at shallower levels, triggering massive sediment influx (Fig. 15B).

Within the Diablo Range, there is a significant unconformity between variable thicknesses (20–400 m) of Late Jurassic sediments (e.g., Lotta Creek Tuff) that overlie CRO material and nearly 7.5-km-thick Upper Cretaceous (Cenomanian–Campanian: 100–72 Ma) deep-water deposits. Most of the intervening Lower Cretaceous (Hauterivian–Albian: 132–100 Ma) strata are missing, even though the Sacramento subbasin contains 4.5 km of equivalent material (Fig. 4; Bartow and Nilsen, 1990; Moxon, 1990). Approximately 50 km to the northwest of the SLR area near Mount Hamilton (Fig. 2), a 100–70 Ma uplift event (Tagami and Dumitru, 1996) may have led to erosion of Lower Cretaceous sediment and provided the channel system with newly uplifted CRO sediment sources (Ernst, 1970; Hopson et al., 1981; Moxon, 1990).

The influence of the outer-arc ridge as a paleobathymetric barrier is common in modern examples of "ridged forearcs" (Dickinson and Seely, 1979; Ingersoll, 1979; Moxon, 1990; Williams, 1997). For example, in the Java arc-trench system, a commonly cited analog to the Great Valley forearc (Ingersoll, 1979), the outer-arc ridge, is actually above sea level and strongly influences axial depositional systems in the forearc setting (Beaudry and Moore, 1985). In addition, Williams and Graham's (2013) study of Cenomanian–Campanian strata in the Sacramento subbasin invoked modern examples in the southern Kamchatka Basin and the Unalaska Basin of the Aleutian Terrace where outer-arc ridges create ponded forearc depocenters in some areas, while other areas contain canyons that bypass the ridge and allow sediment deposition in trench-slope basins.

Model #2: Western Sierra Nevada Metamorphic Belt (WSNMB) Source for the Ophiolitic Sediments

Alternatively, if the Western Sierra Nevada Metamorphic Belt (WSNMB) terranes provided the out-sized ophiolitic clasts rather than the CRO, then the WSNMB must have been quite proximal to reconcile the short travel distance indicated by the size of the extrabasinal boulders within the SLR deep-water deposits (Fig. 15A). Ingersoll (1981) hypothesized the time-equivalent shoreline for the slightly younger Coniacian deposits was only 30 km to the east of SLR area. Likewise, Cecil et al. (2012) reported that the western extent of the Sierran arc (which intruded WSNMB rocks) was ~35 km to the east of the SLR area (Fig. 15A). Given steep depositional slopes and potentially proximal WSNMB, the out-sized ophiolitic clasts may have been derived from the WSNMB to the east instead of uplift of an outer-arc ridge.

CONCLUSIONS

We combine facies and comprehensive provenance analyses of the SLR submarine channel system in the San Joaquin subbasin to document a detailed sedimentary record of middle Cretaceous changes in plate motion rates and obliquity ca. 100 Ma along California's convergent margin. The SLR area contains a Cenomanian, 1.8-km-thick, deep-water boulder conglomerate along a 4 km depositional-dip cross section at the SLR, the thickest and coarsest deep-water outcrop ever recorded in the GVG. Furthermore, the SLR outcrop occurs within a 20-km-long outcrop belt previously reported by other workers.

We interpret the SLR as a submarine channel system based on six lithofacies (three lithofacies have two sublithofacies) and five facies associations. The two coarsest facies associations contain abundant clast-supported conglomerate with cobbles and boulders up to 3.5 m in axial length and significant evidence of turbulent flow. The overall architectural framework includes four channel complex sets, with southeast-directed paleoflow indicating an axially-oriented submarine channel system.

Within the context of other basin-wide data sets, our combined provenance approach of mudrock geochemistry, sandstone composition, detrital-zircon geochronology, and conglomerate clast counts suggests a mixed source provided sediment to the SLR deposits. Sediment sources likely included the Sierran arc, WSNMB, and/or CRO. We interpret the change in plate-motion rate and obliquity ca. 100 Ma caused deformation along the eastern Sierra shear zones; this deformation induced large-scale plutonism during the mid-Late Cretaceous magmatic flare-up. We also suggest that the anomalous ca. 100 Ma detrital-zircon age population in SLR strata was derived from the eastern Sierran arc, reflecting erosion of the nearly contemporaneous volcanic carapace.

We offer two possible paleogeographic models for the northern San Joaquin subbasin dependent on the potential contribution of the CRO to SLR deposits. If the CRO provided detritus to the basin, we invoke uplift of an outer-arc ridge to provide ophiolitic out-sized boulders in SLR strata. If the WSNMB provided the ophiolitic detritus, this would require a nearby WSNMB source to reconcile the short travel distance indicated by the size of the extrabasinal boulders.

Our study emphasizes the importance of integrating multiple provenance indicators with detailed sedimentologic analysis within forearc basins to document greater complexity and construct plausible paleogeographic models.

ACKNOWLEDGMENTS

We wish to acknowledge the very thorough review efforts of G. Sharman, who greatly improved an earlier version of this manuscript. We also wish to thank California State University, Chico's Research Foundation and the Department of Geological and Environmental Sciences for partially funding this project. Detrital-zircon geochronology sample preparation and analyses were funded by National Science Foundation (NSF) grant EAR ICER 846695 (KDS) and subsidized by University of Arizona LaserChron Center NSF grant EAR 1032156. Nora Nieminski and Jared Gooley (Stanford University) provided drone and piloting expertise. Bruce Cruikshank piloted small fixed-wing aircraft to assist in aerial photography. Invaluable field and laboratory assistance was provided by Michelle Melosh and Russell Shapiro. The ideas presented in this study greatly benefitted from discussions with Terry Kato, Steve Graham, Don Lowe, Tim McHargue, Vic Cherven, Ray Ingersoll, Cal Stevens, Steven Hubbard, William Hirt, and John Wakabayashi.

REFERENCES CITED

Almgren, A.A., 1986, Benthic foraminiferal zonation and correlations of Upper Cretaceous strata of the Great Valley of California—A modification, *in* Abbott, P.L., ed., Cretaceous Stratigraphy, Western North America: Society of Economic Paleontologists and Mineralogists, Pacific section, v. 46, p. 37–152.

Anderson, R., and Pack, R.W., 1915, Geology and oil resources of the west border of the San Joaquin Valley north of Coalinga, California: U.S. Geological Survey Bulletin 603, 220 p.

Atwater, T., 1970, Implications of plate tectonics for the Cenozoic tectonic evolution of western North America: Geological Society of America Bulletin, v. 81, p. 3513–3536, doi:10.1130/0016-7606(1970)81[3513:IOPTFT]2.0.CO;2.

Bailey, E.H., and Blake, M.C.J., 1969, Tectonic development of western California during the late Mesozoic: Geotectonics, v. 3, p. 148–154.

Bailey, E.H., Irwin, W.P., and Jones, D.L., 1964, Franciscan and related rocks, and their significance in the geology of western California: California Division of Mines and Geology Bulletin 183, 177 p.

Bailey, E.H., Blake, M.C.J., and Jones, D.L., 1970, On-land Mesozoic oceanic crust in California Coast Ranges: U.S. Geological Survey Professional Paper 700-C, p. 70–80.

Bain, H.A., and Hubbard, S.M., 2016, Stratigraphic evolution of a long-lived submarine channel system in the Late Cretaceous Nanaimo Group, British Columbia, Canada: Sedimentary Geology, v. 337, p. 113–132, doi:10.1016/j.sedgeo.2016.03.010.

Bartow, J.A., and Nilsen, T.H., 1990, Review of the Great Valley sequence, eastern Diablo Range and northern San Joaquin Valley, central California: U.S. Geological Survey Open-File Report 90-226, 25 p.

Bateman, P.C., 1983, A summary of critical relations in the central part of the Sierra Nevada batholith, California, U.S.A., *in* Roddick, J.A., ed., Circum-Pacific Plutonic Terranes: Geological Society of America Memoir 159, p. 241–254, doi:10.1130/MEM159-p241.

Bateman, P.C., and Dodge, F.C.W., 1970, Variations of major chemical constituents across the central Sierra Nevada batholith: Geological Society of America Bulletin, v. 81, p. 409–420, doi:10.1130/0016-7606(1970)81[409:VOMCCA]2.0.CO;2.

Beaudry, D., and Moore, G.F., 1985, Seismic stratigraphy and Cenozoic evolution of West Sumatra forearc basin: American Association of Petroleum Geologists Bulletin, v. 69, p. 742–759.

Bennison, A.P., 1991, Great Valley Sequence east of Pacheco Pass in central California: Geological Society of America Abstracts with Programs, v. 23, no. 2, p. 6.

Bennison, A.P., Blake, M.C., Jr., Cox, B.F., Elder, W.P., Ernst, W.G., Harms, T., and Nilsen, T.H., 1991, Franciscan Complex, Coast Range Ophiolite and Great Valley Sequence: Pacheco Pass to Del Puerto Canyon, California, *in* Sloan, D., and Wagner, D.L., eds., Geologic Excursions in Northern California: San Francisco to Sierra Nevada: California Division of Mines and Geology Special Publication 109, p. 85–100.

Berry, K.D., 1974, Mesozoic foraminiferal zonation, Turonian to Tithonian stages, Pacific Coast province: Society of Economic Paleontologists and Mineralogists, Pacific Section, Annual Meeting Preprints, p. 1–29.

Bertucci, P.F., 1983, Petrology and provenance of the Stony Creek Formation, northwestern Sacramento Valley, California, *in* Bertucci, P.F., and Ingersoll, R.V., eds., Guidebook to the Stony Creek Formation, Great Valley Group, Sacramento Valley, California: Annual Meeting Pacific Section Society of Economic Paleontologists and Mineralogists Field Trips, p. 1–16.

Bhatia, M.R., and Crook, K.A.W., 1986, Trace element characteristics of graywackes and tectonic setting discrimination of sedimentary basins: Contributions to Mineralogy and Petrology, v. 92, p. 181–193, doi:10.1007/BF00375292.

Blake, M.C., Jr., Howell, D.G., and Jayko, A.S., 1984, Tectonostratigraphic terranes of the San Francisco Bay Region, *in* Blake, M.C., Jr., ed., Franciscan Geology of Northern California: Los Angeles, California, Pacific Section, Society of Economic Paleontologists and Mineralogists, v. 43, p. 5–22.

Bouma, A.H., 1962, Sedimentology of Some Flysch Deposits: A Graphic Approach to Facies Interpretation: Amsterdam, Elsevier, 168 p.

Bracciali, L., Marroni, M., Pandolfi, L., and Rocchi, S., 2007, Geochemistry and petrography of Western Tethys Cretaceous sedimentary covers (Corsica and Northern Apennines): From source areas to configuration of margins, *in* Arribas, J., Critelli, S., and Johnsson, M.J., eds., Sedimentary Provenance and Petrogenesis: Perspectives from Petrography and Geochemistry: Geological Society of America Special Paper 420, p. 73–93, doi:10.1130/2006.2420(06).

Cady, J.W., 1975, Magnetic and Gravity Anomalies in the Great Valley and Western Sierra Nevada Metamorphic Belt, California: Geological Society America Special Paper 168, 56 p., doi:10.1130/SPE168-p1.

California Division of Oil and Gas, 1964, Exploratory wells drilled outside of oil and gas fields in California: San Francisco, California Division of Oil and Gas, 320 p.
Campion, K.M., Sprague, A.R., Mohrig, D., Lovell, R.W., Drzewiecki, P.A., Sullivan, M.D., Ardill, J.A., Jensen, G.N., and Sickafoose, D.K., 2000, Outcrop expression of confined channel complexes, *in* Weimer, P., Slatt, R., Coleman, J., Rosen, N.C., Nelson, H., Bouma, A.H., Styzen, M.J., and Lawrence, D.T., eds., Deep-water Reservoirs of the World: Dallas, Texas, Gulf Coast Section Society of Economic Paleontologists and Mineralogists Foundation, 20th Annual Bob F. Perkins Research Conference, Society for Sedimentary Geology, Gulf Coast Section, v. 20, p. 127–151.
Cecil, M.R., Rotberg, G.L., Ducea, M.N., Saleeby, J.B., and Gehrels, G.E., 2012, Magmatic growth and batholithic root development in the northern Sierra Nevada, California: Geosphere, v. 8, p. 592–606, doi:10.1130/GES00729.1.
Chen, J.H., and Moore, J.G., 1982, Uranium-lead isotopic ages from the Sierra Nevada batholith, California: Journal of Geophysical Research, v. 87, p. 4761–4784, doi:10.1029/JB087iB06p04761.
Cherven, V.B., 1983, A delta-slope-submarine fan model for Maestrichtian part of Great Valley sequence, Sacramento and San Joaquin basins, California: American Association of Petroleum Geologists Bulletin, v. 67, p. 772–816.
Chuber, S., 1961, Late Mesozoic stratigraphy of the Elk Creek–Fruto area, Glenn County, California [Ph.D. thesis]: Stanford, California, Stanford University, 115 p.
Chuber, S., 1962, Late Mesozoic stratigraphy of the Sacramento Valley: San Joaquin Geological Society Selected Papers, v. 1, p. 3–16.
Clemens-Knott, D., and Saleeby, J.B., 2013, Mesozoic metasedimentary framework and gabbroids of the Early Cretaceous Sierra Nevada batholith, California, *in* Putirka, K., ed., Geologic Excursions from Fresno, California, and the Central Valley: A Tour of California's Iconic Geology: Geological Society of America Field Guide 32, p. 79–98, doi:10.1130/2013.0032(05).
Cloos, M., 1986, Blueschists in the Franciscan Complex of California: Petrotectonic constraints on uplift mechanisms, *in* Evans, B.W., and Brown, E.H., eds., Blueschists and Eclogites: Geological Society of America Memoir 164, p. 77–94, doi:10.1130/MEM164-p77.
Coleman, D.S., and Glazner, A.F., 1997, The Sierra Crest magmatic event: Rapid formation of juvenile crust during the Late Cretaceous in California: International Geology Review, v. 39, p. 768–787, doi:10.1080/00206819709465302.
Coleman, D.S., Gray, W., and Glazner, A.F., 2004, Rethinking the emplacement and evolution of zoned plutons: Geochronologic evidence for incremental assembly of the Tuolumne Intrusive Suite, California: Geology, v. 32, p. 433–436, doi:10.1130/G20220.1.
Coleman, R.G., 2000, Prospecting for ophiolites along the California continental margin, *in* Dilek, Y., Moores, E.M., Elthon, D., and Nicolas, A., eds., Ophiolites and Oceanic Crust: New Insights from Field Studies and the Ocean Drilling Program: Geological Society of America Special Paper 349, p. 351–364, doi:10.1130/0-8137-2349-3.351.
Covault, J.A., Sylvester, Z., Hubbard, S.M., Jobe, Z.R., and Sech, R.P., 2016, The stratigraphic record of submarine-channel evolution: The Sedimentary Record, v. 14, p. 4–11.
Dalla Torre, M., De Capitani, C., Frey, M., Underwood, M.B., Mullis, J., and Cox, R., 1996, Very low temperature metamorphism of shales from the Diablo Range, Franciscan Complex, California: New constraints on the exhumation path: Geological Society of America Bulletin, v. 108, p. 578–601, doi:10.1130/0016-7606(1996)108<0578:VLTMOS>2.3.CO;2.
DeGraaff-Surpless, K., Graham, S.A., Wooden, J.L., and McWilliams, M.O., 2002, Detrital-zircon provenance analysis of the Great Valley Group, California: Evolution of an arc-forearc system: Geological Society of America Bulletin, v. 114, p. 1564–1580, doi:10.1130/0016-7606(2002)114<1564:DZPAOT>2.0.CO;2.
DePaolo, D.J., 1981, A neodymium and strontium isotopic study of the Mesozoic calc-alkaline granitic batholiths of the Sierra Nevada and Peninsular ranges, California: Journal of Geophysical Research, v. 86, p. 10,470–10,488, doi:10.1029/JB086iB11p10470.
Dibblee, T., Jr., 2007a, Geologic map of the Crevison Peak and Howard Ranch Quadrangles, Merced, Santa Clara, and Stanislaus Counties, California, Minch, J.A., ed.: Dibblee Geology Center Map #DF-345, 1:24,000.
Dibblee, T., Jr., 2007b, Geologic map of the Pacheco Pass Quadrangles, Merced and Santa Clara Counties, California, Minch, J.A., ed.: Dibblee Geology Center Map #DF-336, 1:24,000.
Dibblee, T., Jr., 2007c, Geologic map of the San Luis Dam and Volta Quadrangles, Merced County, California, Minch, J.A., ed.: Dibblee Geology Center Map #DF-335, 1:24,000.
Di Celma, C., Teloni, R., and Rustichelli, A., 2014, Large-scale stratigraphic architecture and sequence analysis of an early Pleistocene submarine canyon fill, Monte Ascensione succession (Peri-Adriatic Basin, eastern central Italy): International Journal of Earth Sciences, v. 103, p. 843–875, doi:10.1007/s00531-013-0984-3.
Dickinson, W.R., 1970, Relations of andesites, granites and derivative sandstones to arc-trench tectonics: Reviews of Geophysics and Space Physics, v. 8, p. 813–860, doi:10.1029/RG008i004p00813.
Dickinson, W.R., 1971, Plate tectonic models for orogeny at continental margins: Nature, v. 232, p. 41–42, doi:10.1038/232041a0.
Dickinson, W.R., 1976, Sedimentary basins developed during evolution of Mesozoic–Cenozoic arc trench system in western North America: Canadian Journal of Earth Sciences, v. 13, p. 1268–1287, doi:10.1139/e76-129.
Dickinson, W.R., 1995, Forearc basins, *in* Busby, C.J., and Ingersoll, R.V., eds., Tectonics of Sedimentary Basins: Cambridge, Massachusetts, Blackwell Science, p. 221–261.
Dickinson, W.R., 2008, Accretionary Mesozoic–Cenozoic expansion of the Cordilleran continental margin in California and adjacent Oregon: Geosphere, v. 4, p. 329–353, doi:10.1130/GES00105.1.
Dickinson, W.R., and Rich, E.I., 1972, Petrologic intervals and petrofacies in the Great Valley Sequence, Sacramento Valley, California: Geological Society of America Bulletin, v. 83, p. 3007–3024, doi:10.1130/0016-7606(1972)83[3007:PIAPIT]2.0.CO;2.
Dickinson, W.R., and Seely, D.R., 1979, Structure and stratigraphy of forearc regions: The American Association of Petroleum Geologists Bulletin, v. 63, p. 2–31.
Dickinson, W.R., and Suczek, C.A., 1979, Plate tectonics and sandstone compositions: American Association of Petroleum Geologists Bulletin, v. 63, p. 2164–2182.
Dickinson, W.R., Ingersoll, R.V., and Graham, S.A., 1979, Paleogene sediment dispersal and paleotectonics in northern California: Geological Society of America Bulletin, v. 90, pt. I, p. 897–898, doi:10.1130/0016-7606(1979)90<897:PSDAPI>2.0.CO;2; pt. II, p. 1458–1528, doi:10.1130/GSAB-P2-90-1458.
Dickinson, W.R., Ingersoll, R.V., Cowan, D.S., Helmold, K.P., and Suczek, C.A., 1982, Provenance of Franciscan graywackes in coastal California: Geological Society of America Bulletin, v. 93, p. 95–107, doi:10.1130/0016-7606(1982)93<95:POFGIC>2.0.CO;2.
Dickinson, W.R., Beard, L.S., Brakenridge, G.R., Erjavec, J.L., Ferguson, R.C., Inman, K.F., Knepp, R.A., Lindberg, F.A., and Ryberg, P.T., 1983, Provenance of North American Phanerozoic sandstones in relation to tectonic setting: Geological Society of America Bulletin, v. 94, p. 222–235, doi:10.1130/0016-7606(1983)94<222:PONAPS>2.0.CO;2.
Dickinson, W.R., Hopson, C.A., and Saleeby, J.B., 1996, Alternate origins of the Coast Range ophiolite (California): Introduction and implications: GSA Today, v. 6, no. 2, p. 1–10.
Doebbert, A.C., Carroll, A.R., and Johnson, C., 2012, The sandstone-derived provenance record of the Gualala Basin, Northern California, USA: Journal of Sedimentary Research, v. 82, p. 841–858, doi:10.2110/jsr.2012.72.
Douglas, R.G., 1966, Upper Cretaceous planktonic foraminiferal biostratigraphy of the western Sacramento Valley, California [Ph.D. thesis]: Los Angeles, California, University of California, 508 p.
Ducea, M., 2001, The California arc: Thick granitic batholiths, eclogitic residues, lithospheric-scale thrusting and magmatic flare-ups: GSA Today, v. 11, no. 11, p. 4–10, doi:10.1130/1052 5173(2001)011<0004:TCATGB>2.0.CO;2.
Dumitru, T.A., 1991, Effects of subduction parameters on geothermal gradients in forearcs, with an application to Franciscan subduction in California: Journal of Geophysical Research, v. 96, p. 621–641, doi:10.1029/90JB01913.
Dumitru, T.A., Wakabayashi, J., Wright, J.E., and Wooden, J.L., 2010, Early Cretaceous transition from nonaccretionary behavior to strongly accretionary behavior within the Franciscan subduction complex: Tectonics, v. 29, TC5001, doi:10.1029/2009TC002542.
Dumitru, T.A., Ernst, W.G., Hourigan, J.K., and McLaughlin, R.J., 2015, Detrital zircon U-Pb reconnaissance of the Franciscan subduction complex in northwestern California: International Geology Review, v. 57, p. 767–800, doi:10.1080/00206814.2015.1008060.
Dykstra, M., and Kneller, B., 2009, Lateral accretion in a deep marine channel complex: Implications for channelized flow processes in turbidity currents: Sedimentology, v. 56, p. 1411–1432, doi:10.1111/j.1365-3091.2008.01040.x.
Elder, W.P., and Miller, J.W., 1993, Map and checklist of Jurassic and Cretaceous macrofossil localities within the San Jose 1:100,000 quadrangle, California, and discussion of paleontological results: U.S. Geological Survey Open-File Report 93-503, 49 p.
Engebretson, D.C., Cox, A., and Gordon, R.G., 1985, Relative Motions between Oceanic and Continental Plates in the Pacific Basin: Geological Society of America Special Paper 206, 59 p, doi:10.1130/SPE206-p1, doi:10.1130/SPE206-p1.
Ernst, W.G., 1970, Tectonic contact between the Franciscan mélange and the Great Valley Sequence, crustal expression of a Late Mesozoic Benioff Zone: Journal of Geophysical Research, v. 75, p. 886–901, doi:10.1029/JB075i005p00886.

Ernst, W.G., 1993, Metamorphism of Franciscan tectonostratigraphic assemblage, Pacheco Pass area, east-central Diablo Range, California Coast Ranges: Geological Society of America Bulletin, v. 105, p. 618–636, doi:10.1130/0016-7606(1993)105<0618:MOFTAP>2.3.CO;2.

Ernst, W.G., Snow, C.A., and Scherer, H.H., 2008, Contrasting early and late Mesozoic petrotectonic evolution of northern California: Geological Society of America Bulletin, v. 120, p. 179–194, doi: 10.1130/B26173.1.

Ernst, W.G., Martens, U., and Valencia, V., 2009, U-Pb ages of detrital zircons in Pacheco Pass metagraywackes: Sierran-Klamath source of Mid-Cretaceous and Late Cretaceous Franciscan deposition and underplating: Tectonics, v. 28, TC6011, doi:10.1029/2008TC002352.

Evarts, R.C., Coleman, R.G., and Schiffman, P., 1999, The Del Puerto ophiolite: Petrology and tectonic setting, *in* Wagner, D.L., and Graham, S.A., eds., Geologic Field Trips in Northern California; Centennial Meeting of the Cordilleran Section of the Geological Society of America, Special Publication 119: Sacramento, California, Department of Conservation, Division of Mines and Geology, p. 136–149.

Evernden, J.F., and Kistler, R.W., 1970, Chronology of emplacement of Mesozoic batholithic complexes in California and western Nevada: U.S. Geological Survey Professional Paper 623, 42 p.

Fralick, P.W., 2003, Geochemistry of clastic sedimentary rocks: ratio techniques, *in* Lentz, D.R., ed., Geochemistry of Sediments and Sedimentary Rocks: Evolutionary Considerations to Mineral Deposit-Forming Environments: Geological Association of Canada, GeoText 4, p. 85–103.

Gehrels, G., and Pecha, M., 2014, Detrital zircon U-Pb geochronology and Hf isotope geochemistry of Paleozoic and Triassic passive margin strata of western North America: Geosphere, v. 10, p. 49–65, doi:10.1130/GES00889.1.

Gehrels, G.E., Valencia, V., and Ruiz, J., 2008, Enhanced precision, accuracy, efficiency, and spatial resolution of U-Pb ages by laser ablation–multicollector–inductively coupled plasma mass spectrometry: Geochemistry Geophysics Geosystems, v. 9, Q03017, doi:10.1029 /2007GC001805.

Giaramita, M., MacPherson, G.J., and Phipps, S.P., 1998, Petrologically diverse basalts from a fossil oceanic forearc in California: The Llanada and Black Mountain remnants of the Coast Range ophiolite: Geological Society of America Bulletin, v. 110, p. 553–571, doi:10.1130/0016-7606 (1998)110<0553:PDBFAF>2.3.CO;2.

Glazner, A.F., 1991, Plutonism, oblique subduction, and continental growth: An example from the Mesozoic of California: Geology, v. 19, p. 784–786, doi:10.1130/0091-7613(1991)019<0784: POSACG>2.3.CO;2.

Godfrey, N.J., and Klemperer, S.L., 1998, Ophiolitic basement to a forearc basin and implications for continental growth: The Coast Range/Great Valley Ophiolite, California: Tectonics, v. 17, p. 558–570, doi:10.1029/98TC01536.

Godfrey, N.J., Beaudoin, B.C., Klemperer, S.L., Levander, A.R., Luetgert, J.H., Meltzer, A.S., Mooney, W.D., and Trehu, A.M., 1997, Ophiolitic basement to the Great Valley forearc basin, northern California, from seismic and gravity data: Implications for crustal growth at the North American continental margin: Geological Society of America Bulletin, v. 109, p. 1536–1562, doi:10.1130/0016-7606(1997)109<1536:OBTTGV>2.3.CO;2.

Goudkoff, P.P., 1945, Stratigraphic relations of Upper Cretaceous in Great Valley, California: American Association of Petroleum Geologists Bulletin, v. 29, p. 956–1007.

Gradstein, F.M., Ogg, J.G., Hardenbol, J., Schmitz, M., and Ogg, G., 2012, The Geologic Time Scale 2012: Amsterdam, Elsevier, 1176 p.

Graham, S.A., and Ingersoll, R.V., 1981, Field trip road log; Great Valley Group submarine fan facies and Sacramento Valley forearc gas province (Part I), Sacramento to Cache Creek and return, *in* Graham, S.A., ed., Field Guide to the Mesozoic–Cenozoic Convergent Margin of Northern California: Santa Fe Springs, Pacific Section, American Association of Petroleum Geologists, p. 71–78.

Greene, D.C., and Schweickert, R.A., 1995, The Gem Lake shear zone: Cretaceous dextral transpression in the Northern Ritter Range pendant, eastern Sierra Nevada, California: Tectonics, v. 14, p. 945–961, doi:10.1029/95TC01509.

Haig, D.W., 1979, Global distribution patterns for mid-Cretaceous foraminiferids: Journal of Foraminiferal Research, v. 9, p. 29–40, doi:10.2113/gsjfr.9.1.29.

Hamilton, W.B., 1969, Mesozoic California and the underflow of Pacific mantle: Geological Society of America Bulletin, v. 80, p. 2409–2430, doi:10.1130/0016-7606(1969)80[2409:MCATUO]2.0.CO;2.

Harwood, D.S., and Helley, E.J., 1987, Late Cenozoic tectonism of the Sacramento Valley, California: U.S. Geological Survey Professional Paper 1359, 46 p.

Hickson, T.A., and Lowe, D.R., 2002, Facies architecture of a submarine fan channel-levee complex: The Juniper Ridge Conglomerate, Coalinga, California: Sedimentology, v. 49, p. 335–362, doi: 10.1046/j.1365-3091.2002.00447.x.

Hirt, W., 2007, Petrology of the Mount Whitney Intrusive Suite, eastern Sierra Nevada, California: Implications for the emplacement and differentiation of composite felsic intrusions: Geological Society of America Bulletin, v. 119, p. 1185–1200, doi:10.1130/B26054.1.

Hopson, C.A., Mattinson, J.M., and Pessagno, E.A., Jr., 1981, Coast Range Ophiolite, western California, *in* Ernst, W.G., ed., Geotectonic Development of California, Rubey Volume I: Englewood Cliffs, New Jersey, Prentice-Hall, p. 418–510.

Hopson, C., Pessagno, E.A.P., Jr., Mattinson, J., Luyendyk, B., Beebe, W., Hull, D., Munoz, E., and Blome, C., 1996, Coast Range ophiolite as paleoequatorial mid-ocean lithosphere, *in* Dickinson, W.R., Hopson, C.A., and Saleeby, J.B., eds., Alternate Origins of the Coast Range Ophiolite (California): Introduction and Implications: GSA Today, v. 6, no. 2, p. 4–6.

Hopson, C.A., Mattinson, J.M., Pessagno, E.A., Jr., and Luyendyk, B.P., 2008, California Coast Range ophiolite: Composite Middle and Late Jurassic oceanic lithosphere, *in* Wright, J.E., and Shervais, J.W., eds., Ophiolites, Arcs, and Batholiths: A Tribute to Cliff Hopson: Geological Society of America Special Paper 483, p. 1–101, doi:10.1130/2008.2438(01).

Hosford Scheirer, A.H., and Magoon, L.B., 2007, Age, distribution, and stratigraphic relationship of rock units in the San Joaquin Basin Province, California, *in* Hosford Scheirer, A.H., ed., Petroleum Systems and Geologic Assessment of Oil and Gas in the San Joaquin Basin Province, California: U.S. Geological Survey Professional Paper 1713, p. 2–107, doi:10.3133/pp1713.ch05.

House, M.A., Wernicke, B.P., and Farley, K.A., 1998, Dating topography of the Sierra Nevada, California, using apatite (U-Th)/He ages: Nature, v. 396, p. 66–69, doi:10.1038/23926.

Hsü, K.J., 1971, Franciscan mélanges as a model for eugeosynclinal sedimentation and underthrusting tectonics: Journal of Geophysical Research, v. 76, p. 1162–1170, doi:10.1029 /JB076i005p01162.

Hubbard, S.M., Romans, B.W., and Graham, S.A., 2008, Deep-water foreland basin deposits of the Cerro Toro Formation, Magallanes basin, Chile: Architectural elements of a sinuous basin axial channel belt: Sedimentology, v. 55, p. 1333–1359.

Hubbard, S.M., de Ruig, M.J., and Graham, S.A., 2009, Confined channel levee complex development in an elongate depo-center: Deep-water Tertiary strata of the Austrian Molasse basin: Marine and Petroleum Geology, v. 26, p. 85–112, doi:10.1016/j.marpetgeo.2007.11.006.

Ingersoll, R.V., 1976, Evolution of the Late Cretaceous forearc basin of northern and central California [Ph.D. thesis]: Stanford, California, Stanford University, 200 p.

Ingersoll, R.V., 1978, Paleogeography and paleotectonics of the late Mesozoic forearc basin for northern and central California, *in* Howell, D.G., and McDougall, K., eds., Mesozoic Paleogeography of the Western United States: Society of Economic Paleontologists and Mineralogists, Pacific Section, Paleogeography Symposium 2, p. 471–482.

Ingersoll, R.V., 1979, Evolution of the Late Cretaceous forearc basin, northern and central California: Geological Society of America Bulletin, v. 90, p. 813–826, doi:10.1130 /0016–7606 (1979)90 <813:EOTLCF>2.0.CO;2.

Ingersoll, R.V., 1981, Petrofacies, lithofacies, submarine-fan facies of the Great Valley Group (Sequence), *in* Graham, S.A., ed., Field Guide to the Mesozoic–Cenozoic Convergent Margin of Northern California: Santa Fe Springs, Pacific Section, American Association of Petroleum Geologists, p. 59–69.

Ingersoll, R.V., 1982, Initiation and evolution of the Great Valley forearc basin of northern and central California, USA, *in* Leggett, J.K., ed., Trench-Forearc Geology: Sedimentation and Tectonics on Modern and Ancient Active Plate Margins: Geological Society of London Special Publication 10, p. 459–467, doi:10.1144/GSL.SP.1982.010.01.31.

Ingersoll, R.V., 1983, Petrofacies and provenance of late Mesozoic forearc basin, northern and central California: American Association of Petroleum Geologists Bulletin, v. 67, p. 1125–1142.

Ingersoll, R.V., 1988, Development of the Cretaceous forearc basin of central California, *in* Graham, S.A., and Olson, H.C., eds., Studies of the Geology of the San Joaquin Basin: Los Angeles, Society of Economic Paleontologists and Mineralogists, Pacific Section, v. 60, p. 141–155.

Ingersoll, R.V., 1990, Nomenclature of Upper Mesozoic strata of the Sacramento Valley of California: Review and recommendations, *in* Ingersoll, R.V., and Nilsen, T.H., eds., Sacramento Valley Symposium and Guidebook: Society of Economic Paleontologists and Mineralogists, Pacific Section, v. 65, p. 1–3.

Ingersoll, R.V., 2000, Models for origin and emplacement of Jurassic ophiolites of northern California, *in* Dilek, Y., Moores, E., Elthon, D., and Nicolas, A., eds., Ophiolites and Oceanic Crust: New Insights from Field Studies and the Ocean Drilling Program: Geological Society of America Special Paper 349, p. 395–402, doi:10.1130/0-8137-2349-3.395.

Ingersoll, R.V., and Dickinson, W.R., 1981, Great Valley Group (sequence), Sacramento Valley, California, *in* Frizzell, V., ed., Upper Mesozoic Franciscan rocks and Great Valley Sequence, Central

Coast Ranges, California: Society of Economic Paleontologists and Mineralogists, Pacific Section, Annual Meeting 1981, Field trips 1 and 4, Guidebook, p. 1–33.
Ingersoll, R.V., and Schweickert, R.A., 1986, A plate tectonic model for late Jurassic ophiolite genesis, Nevadan orogeny and forearc initiation, northern California: Tectonics, v. 5, p. 901–912, doi:10.1029/TC005i006p00901.
Ingersoll, R.V., Ratajeski, K., Glazner, A.F., and Cloos, M., 1999, Mesozoic convergent margin of Central California, *in* Wagner, D.L., and Graham, S., eds., Geologic Field Trips in Northern California; Centennial Meeting of the Cordilleran Section of the Geological Society of America, Special Publication 119: Sacramento, California, Department of Conservation, Division of Mines and Geology, p. 101–135.
Irwin, W.P., 1960, Geologic reconnaissance of the northern Coast Ranges and the southern Klamath Mountains, California, with a summary of the mineral resources: California Division of Mines and Geology Bulletin, v. 179, 80 p.
Irwin, W.P., and Wooden, J.L., 2001, Maps showing plutons and accreted terranes of the Sierra Nevada, California, with a tabulation of U/Pb isotopic ages: U.S. Geological Survey Open-File Report OF-01-229, scale 1:100,000.
Jachens, R.C., Griscom, A., and Roberts, C.W., 1995, Regional extent of Great Valley basement west of the Great Valley, California: Implications for extensive tectonic wedging in the California Coast Ranges: Journal of Geophysical Research, v. 100, p. 12769–12790, doi:10.1029/95JB00718.
Jacobson, C.E., Grove, M., Pedrick, J.N., Barth, A.P., Marsaglia, K.M., Gehrels, G.E., and Nourse, J.A., 2011, Late Cretaceous–early Cenozoic tectonic evolution of the southern California margin inferred from provenance of trench and forearc sediments: Geological Society of America Bulletin, v. 123, p. 485–506, doi:10.1130/B30238.1.
Jacobson, M.I., 1978, Petrologic variations in Franciscan sandstone from the Diablo Range, California, *in* Howell, D.G., and McDougall, K.A., eds., Mesozoic Paleogeography of the Western United States: Los Angeles, California, Pacific Section Society of Economic Paleontologists and Mineralogists, Pacific Coast Paleogeography Symposium 2, p. 401–417.
Jenner, G.A., 1996, Trace element geochemistry of igneous rocks: Geochemical nomenclature and analytical geochemistry, *in* Wyman, D.A., ed., Trace Element Geochemistry of Volcanic Rocks: Applications for Massive Sulfide Exploration: Geological Association of Canada, Short Course Notes, v. 12, p. 55–71.
Jobe, Z.R., Bernhardt, A., and Lowe, D.R., 2010, Facies and architectural asymmetry in a conglomerate-rich submarine channel fill, Cerro Toro Formation, Sierra Del Toro, Magallanes Basin, Chile: Journal of Sedimentary Research, v. 80, p. 1085–1108, doi:10.2110/jsr.2010.092.
Joesten, R., Wooden, J.L., Silver, L.T., Ernst, W.G., and McWilliams, M.O., 2004, Depositional age and provenance of jadeite-grade metagraywacke from the Franciscan accretionary prism, Diablo Range, central California—SHRIMP Pb-isotope dating of detrital zircon: Geological Society of America Abstracts with Programs, v. 36, no. 5, p. 120.
Johnson, D.M., Hooper, P.R., and Conrey, R.M., 1999, XRF analysis of rocks and minerals for major and trace elements on a single low dilution Li-tetraborate fused bead: Advances in X-Ray Analysis, v. 41, p. 843–867.
Kane, I.A., and Hodgson, D.M., 2011, Sedimentological criteria to differentiate submarine channel levee subenvironments: Exhumed examples from the Rosario Fm. (Upper Cretaceous) of Baja California, Mexico, and the Fort Brown Fm. (Permian), Karoo Basin, S. Africa: Marine and Petroleum Geology, v. 28, p. 807–823, doi:10.1016/j.marpetgeo.2010.05.009.
Kimbrough, D.L., Smith, D.P., Mahoney, J.B., Moore, T.E., Grove, M., Gastil, R.G., Ortega-Rivera, A., and Fanning, C.M., 2001, Forearc-basin sedimentary response to rapid Late Cretaceous batholith emplacement in the Peninsular Ranges of southern and Baja California: Geology, v. 29, p. 491–494, doi:10.1130/0091-7613(2001)029<0491:FBSRTR>2.0.CO;2.
Kimura, G., Maruyama, S., Isozaki, Y., and Terabayashi, M., 1996, Well-preserved underplating structure of the jadeitized Franciscan complex, Pacheco Pass, California: Geology, v. 24, p. 75–78, doi:10.1130/0091-7613(1996)024<0075:WPUSOT>2.3.CO;2.
Kistler, R.W., and Peterman, Z.E., 1973, Variations in Sr, Rb, K, Na, and initial $^{87}Sr/^{86}Sr$ in Mesozoic granitic rocks and intruded wall rocks in central California: Geological Society of America Bulletin, v. 84, p. 3489–3512, doi:10.1130/0016-7606(1973)84<3489:VISRKN>2.0.CO;2.
Knaack, C., Cornelius, S.B., and Hooper, P.R., 1994, Trace element analyses of rocks and minerals by ICP-MS: http://cahnrs.wsu.edu/soe/facilities/geolab/technotes/icp-ms_method/ (Accessed 2016).
LaMaskin, T.A., Dorsey, R.J., and Vervoort, J.D., 2008, Tectonic controls on mudrock geochemistry, Mesozoic rocks of eastern Oregon and western Idaho, U.S.A.: Implications for Cordilleran tectonics: Journal of Sedimentary Research, v. 78, p. 765–783, doi:10.2110/jsr.2008.087.
Linn, A.M., DePaolo, D.J., and Ingersoll, R.V., 1992, Nd-Sr isotopic, geochemical, and petrographic stratigraphy and paleotectonic analysis: Mesozoic Great Valley forearc sedimentary rocks of California: Geological Society of America Bulletin, v. 104, p. 1264–1279, doi:10.1130/0016-7606(1992)104<1264:NSIGAP>2.3.CO;2.
Liu, L., Spasojević, S., and Gurnis, M., 2008, Reconstructing Farallon plate subduction beneath North America back to the Late Cretaceous: Science, v. 322, p. 934–938, doi:10.1126/science.1162921.
Lowe, D.R., 1982, Sediment gravity flows II. Depositional models with special reference to the deposits of high density turbidity currents: Journal of Sedimentary Petrology, v. 52, p. 279–297.
Lowe, D.R., 2004, Deep-water sandstones: Submarine canyon to basin plain, western California: Pacific Section, American Association of Petroleum Geologists, Publication Guidebook GB 79, 79 p.
Ludwig, K.R., 2008, Isoplot 3.60: Berkeley Geochronology Center, Special Publication No. 4, 77 p.
Macauley, R.V., and Hubbard, S.M., 2013, Slope channel sedimentary processes and stratigraphic stacking, Cretaceous Tres Pasos Formation slope system, Chilean Patagonia: Marine and Petroleum Geology, v. 41, p. 146–162, doi:10.1016/j.marpetgeo.2012.02.004.
MacLean, W.H., 1990, Mass change calculations in altered rock series: Mineralium Deposita, v. 25, p. 44–49, doi:10.1007/BF03326382.
MacPherson, G.J., Phipps, S.P., and Grossman, J.N., 1990, Diverse sources for igneous blocks in Franciscan mélanges, California Coast Ranges: The Journal of Geology, v. 98, p. 845–862, doi:10.1086/629457.
Mahoney, J.B., 2005, Nd and Sr isotopic signatures of fine-grained clastic sediments: A case study of western Pacific marginal basins: Sedimentary Geology, v. 182, p. 183–199, doi:10.1016/j.sedgeo.2005.07.009.
Mansfield, C.F., 1979, Upper Mesozoic subsea fan deposits in the southern Diablo Range, California: Record of the Sierra Nevada magmatic arc: Geological Society of America Bulletin, v. 90, p. 1025–1046, doi:10.1130/0016-7606(1979)90<1025:UMSFDI>2.0.CO;2.
Maxwell, J.C., 1974, Anatomy of an orogen: Geological Society of America Bulletin, v. 85, p. 1195–1204, doi:10.1130/0016-7606(1974)85<1195:AOAO>2.0.CO;2.
May, J.C., and Hewitt, R.L., 1948, The basement complex in well samples from the Sacramento and San Joaquin Valleys, California: California Journal of Mines and Geology, v. 44, p. 129–158.
McHargue, T., Pyrcz, M.J., Sullivan, M.D., Clark, J.D., Fildani, A., Romans, B.W., Covault, J.A., Levy, M., Posamentier, H.W., and Drinkwater, N.J., 2011, Architecture of turbidite channel systems on the continental slope: Patterns and predictions: Marine and Petroleum Geology, v. 28, p. 728–743, doi:10.1016/j.marpetgeo.2010.07.008.
McLaughlin, R.J., Kling, S.A., Poore, R.Z., McDougall, K.A., and Buetner, E.C., 1982, Post–Middle Miocene accretion of Franciscan rocks, northwestern California: Geological Society of America Bulletin, v. 93, p. 595–605, doi:10.1130/0016-7606(1982)93<595:PMAOFR>2.0.CO;2.
McLennan, S.M., Taylor, S.R., McCulloch, M.T., and Maynard, J.B., 1990, Geochemical and Nd-Sr isotopic composition of deep-sea turbidites: Crustal evolution and plate tectonic associations: Geochimica et Cosmochimica Acta, v. 54, p. 2015–2050, doi:10.1016/0016-7037(90)90269-Q.
McLennan, S.M., Hemming, S., McDaniel, D.K., and Hanson, G.N., 1993, Geochemical approaches to sedimentation, provenance, and tectonics, *in* Johnson, M.J., and Basu, A., eds., Processes Controlling the Composition of Clastic Sediments: Geological Society of America Special Paper 284, p. 21–40, doi:10.1130/SPE284-p21, doi:10.1130/SPE284-p21.
McNulty, B.A., 1995, Shear zone development during magmatic arc construction: the Bench Canyon shear zone, central Sierra Nevada, California: Geological Society of America Bulletin, v. 107, p. 1094–1107, doi:10.1130/0016-7606(1995)107<1094:SZDDMA>2.3.CO;2.
Memeti, V., Patterson, S.R., and Mudil, R., 2014, Day 4: Magmatic evolution of the Tuolumne Intrusive Complex, *in* Memeti, V., Paterson, S.R., and Putirka, K.D., eds., Formation of the Sierra Nevada Batholith: Magmatic and Tectonic Processes and Their Tempos: Geological Society of America Field Guide 34, p. 43–74, doi:10.1130/2014.0034(04).
Mitchell, C., Graham, S.A., and Suek, D.H., 2010, Subduction complex uplift and exhumation and its influence on Maastrichtian forearc stratigraphy in the Great Valley Basin, northern San Joaquin Valley, California: Geological Society of America Bulletin, v. 122, p. 2063–2078, doi:10.1130/B30180.1.
Moores, E.M., Wakabayashi, J., and Unruh, J.R., 2003, Crustal-scale cross-section of the U.S. Cordillera, California and beyond, its tectonic significance, and speculations on the Andean Orogeny, *in* Klemperer, S., and Ernst, W.G., eds., The George A. Thompson Volume: The Lithosphere of Western North America and Its Geophysical Characterization: Geological Society of America International Book Series, v. 7, p. 191–212.

Mountjoy, J.J., Barnes, P.M., and Pettinga, J.R., 2009, Morphostructure and evolution of submarine canyons across an active margin: Cook Strait sector of the Hikurangi Margin, New Zealand: Marine Geology, v. 260, p. 45–68, doi:10.1016/j.margeo.2009.01.006.

Moxon, I.W., 1990, Stratigraphic and structural architecture of the San Joaquin–Sacramento Basin [Ph.D. thesis]: Stanford, California, Stanford University, 371 p.

Moxon, I.W., and Graham, S.A., 1987, History and controls of subsidence in the Late Cretaceous–Tertiary Great Valley forearc basin, California: Geology, v. 15, p. 626–629, doi:10.1130/0091-7613(1987)15<626:HACOSI>2.0.CO;2.

Nilsen, T.H., and Clarke, S.H., 1975, Sedimentation and tectonics in the Early Tertiary continental borderland of central California: U.S. Geological Survey Professional Paper 925, 64 p.

Ojakangas, R.W., 1964, Petrology and sedimentation of the Cretaceous Sacramento Valley sequence, Cache Creek, California [Ph.D. thesis]: Stanford, California, Stanford University, 190 p.

Ojakangas, R.W., 1968, Cretaceous sedimentation, Sacramento Valley, California: Geological Society of America Bulletin, v. 79, p. 973–1008, doi:10.1130/0016-7606(1968)79[973:CSSVC]2.0.CO;2.

Page, B.M., 1981, The southern Coast Ranges, *in* Ernst, W.G., ed., The Geotectonic Development of California: Englewood Cliffs, Prentice-Hall, Rubey Volume I, p. 329–417.

Page, B.M., and Engebretson, D.C., 1984, Correlation between the geologic record and computed plate motions for central California: Tectonics, v. 3, p. 133–155, doi:10.1029/TC003i002p00133.

Paterson, S.R., and Ducea, M.N., 2015, Arc magmatic tempos: Gathering the evidence: Elements, v. 11, p. 91–98, doi:10.2113/gselements.11.2.91.

Paterson, S.R., Memeti, V., Anderson, L., Cao, W., Lackey, J.S., Putirka, K.D., Miller, R.B., Miller, J.S., and Mundil, R., 2014, Day 6: Overview of arc processes and tempos, *in* Memeti, V., Paterson, S.R., and Putirka, K.D., eds., Formation of the Sierra Nevada Batholith: Magmatic and Tectonic Processes and their Tempos: Geological Society of America Field Guide 34, p. 87–116, doi:10.1130/2014.0034(06).

Payne, M.B., 1962, Type Panoche Group (Upper Cretaceous) and overlying Moreno and Tertiary strata on the west side of the San Joaquin Valley, *in* Bowen, O.E., ed., Geologic Guide to the Gas and Oil Fields of Northern California: California Division of Mines and Geology Bulletin 181, p. 165–175.

Pickett, D.A., and Saleeby, J.B., 1993, Thermobarometric constraints on the depth of exposure and conditions of plutonism and metamorphism at deep levels of the Sierra Nevada batholith, Tehachapi Mountains, California: Journal of Geophysical Research. Solid Earth, v. 98, p. 609–629, doi:10.1029/92JB01889.

Posamentier, H.W., and Kolla, V., 2003, Seismic geomorphology and stratigraphy of depositional elements in deep-water settings: Journal of Sedimentary Research, v. 73, p. 367–388, doi:10.1306/111302730367.

Posamentier, H.W., and Walker, R.G., 2006, Deep-water turbidites and submarine fans, *in* Posamentier, H.W., and Walker, R.G., eds., Facies Models Revisited: Society for Sedimentary Geology Special Publication 84, p. 399–520, doi:10.2110/pec.06.84.0399.

Posamentier, H.W., Erskine, R.D., and Mitchum, R.M., Jr., 1991, Submarine fan deposition in a sequence stratigraphic framework, *in* Weimer, P., and Link, M.H., eds., Seismic Facies and Sedimentary Processes of Submarine Fans and Turbidite Systems: New York, Springer-Verlag, p. 127–136, doi:10.1007/978-1-4684-8276-8_6.

Putirka, K.D., Canchola, J., McNaughton, M., Smith, O., Torrez, G., Paterson, S.R., and Ducea, M., 2014, Day 1: Guadalupe Igneous Complex, *in* Memeti, V., Paterson, S.R., and Putirka, K.D., eds., Formation of the Sierra Nevada Batholith: Magmatic and Tectonic Processes and Their Tempos: Geological Society of America Field Guide 34, p. 1–15, doi:10.1130/2014.0034(01).

Robertson, A.H.F., 1989, Paleoceanography and tectonic setting of the Jurassic Coast Range ophiolite, central California: Evidence from the extrusive rocks and the volcaniclastic sediment cover: Marine and Petroleum Geology, v. 6, p. 194–220, doi:10.1016/0264-8172(89)90001-9.

Ryan, K.M., and Williams, D.M., 2007, Testing the reliability of discrimination diagrams for determining the tectonic depositional environment of ancient sedimentary basins: Chemical Geology, v. 242, p. 103–125, doi:10.1016/j.chemgeo.2007.03.013.

Saleeby, J., 1981, Ocean floor accretion and volcanoplutonic arc evolution of the Mesozoic Sierra Nevada, *in* Ernst, W.G., ed., The Geotectonic Development of California: Englewood Cliffs, New Jersey, Prentice-Hall, Inc., Rubey Volume 1, p. 132–181.

Saleeby, J.B., 1982, Polygenetic ophiolite belt of the California Sierra Nevada: Geochronological and tectonostratigraphic development: Journal of Geophysical Research, v. 87, p. 1803–1824, doi:10.1029/JB087iB03p01803.

Saleeby, J.B., 1983, Accretionary tectonics of the North American Cordillera: Annual Reviews in Earth Science, v. 15, p. 45–73, doi:10.1146/annurev.ea.11.050183.000401.

Saleeby, J.B., 1990, Progress in tectonic and petrogenetic studies in an exposed cross section of young (~100 Ma) continental crust, southern Sierra Nevada, California, *in* Salisbury, M.H., and Fountain, D.M., eds., Exposed Crustal Sections of the Continental Crust: Norwell, Massachusetts, Kluwer Academic, p. 137–158, doi:10.1007/978-94-009-0675-4_6.

Saleeby, J.B., Harper, G.D., Snoke, A.W., and Sharp, W.D., 1982, Time relations and structural stratigraphic patterns in ophiolite accretion, west-central Klamath Mountains, California: Journal of Geophysical Research, v. 87, p. 3831–3848, doi:10.1029/JB087iB05p03831.

Saleeby, J.B., Geary, E.E., Paterson, S.R., and Tobisch, O.T., 1989a, Isotopic systematics of Pb/U (zircon) and $^{40}Ar/^{39}Ar$ (biotite-hornblende) from rocks of the central Foothills Terrane, Sierra Nevada, California: Geological Society of America Bulletin, v. 101, p. 1481–1492, doi:10.1130/0016-7606(1989)101<1481:ISOPUZ>2.3.CO;2.

Saleeby, J.B., Shaw, H.F., Niemeyer, S., Moores, E.M., and Edelman, S.H., 1989b, U/Pb, Sm/Nd and Rb/Sr geochronological and isotopic study of northern Sierra Nevada ophiolitic assemblages, California: Contributions to Mineralogy and Petrology, v. 102, p. 205–220, doi:10.1007/BF00375341.

Sams, D.B., and Saleeby, J.B., 1988, Geology and petrotectonic significance of crystalline rocks of the southernmost Sierra Nevada, California, *in* Ernst, ed., Metamorphism and Crustal Evolution of the Western United States (Rubey Volume VII): Englewood Cliffs, New Jersey, Prentice-Hall, p. 865–893.

Schilling, F.A., Jr., 1962, The Upper Cretaceous stratigraphy of the Pacheco Pass quadrangle, California [Ph.D. thesis]: Stanford, California, Stanford University, 153 p.

Schwarz, E., and Arnott, R.W.C., 2007, Anatomy and evolution of a slope channel-complex set (Neoproterozoic Isaac Formation, Windermere Supergroup, Southern Canadian Cordillera): Implications for reservoir characterization: Journal of Sedimentary Research, v. 77, p. 89–109, doi:10.2110/jsr.2007.015.

Schweickert, R.A., 1997, Critical stratigraphic, structural, and timing relations within the western Sierra Nevada, California, and their bearing on models for origin of the Foothills Terrane and the Great Valley Basin: American Association of Petroleum Geologists Bulletin, v. 81, p. 692.

Schweickert, R.A., 2015, Jurassic evolution of the Western Sierra Nevada metamorphic province, *in* Anderson, T.H., Didenko, A.N., Johnson, C.L., Khanchuk, A.I., and MacDonald, J.H., eds., Late Jurassic Margin of Laurasia—A Record of Faulting Accommodating Plate Rotation: Geological Society of America Special Paper 513, p. 299–358, doi:10.1130/2015.2513(08).

Schweickert, R.A., and Cowan, D.S., 1975, Early Mesozoic tectonic evolution of the western Sierra Nevada, California: Geological Society of America Bulletin, v. 86, p. 1329–1336, doi:10.1130/0016-7606(1975)86<1329:EMTEOT>2.0.CO;2.

Schweickert, R.A., Bogen, N.L., Girty, G.H., Hanson, R.E., and Merguerian, C., 1984, Timing and structural expression of the Nevadan orogeny, Sierra Nevada, California: Geological Society of America Bulletin, v. 95, p. 967–979, doi:10.1130/0016-7606(1984)95<967:TASEOT>2.0.CO;2.

Schweickert, R.A., Hanson, R.E., and Girty, G.H., 1999, Accretionary tectonics of the western Sierra Nevada metamorphic belt, *in* Wagner, D.L., and Graham, S.A., eds., Geologic Field Trips in Northern California: Centennial Meeting of the Cordilleran Section of the Geological Society of America, Special Publication 119; Sacramento, California, Department of Conservation, Division of Mines and Geology, p. 33–79.

Seiders, V.M., 1983, Correlation and provenance of upper Mesozoic chert-rich conglomerate of California: Geological Society of America Bulletin, v. 94, p. 875–888, doi:10.1130/0016-7606(1983)94<875:CAPOUM>2.0.CO;2.

Sharman, G.R., Graham, S.A., Grove, M., Kimbrough, D.L., and Wright, J.E., 2015, Detrital zircon provenance of the Late Cretaceous–Eocene California forearc: Influence of Laramide low-angle subduction on sediment dispersal and paleogeography: Geological Society of America Bulletin, v. 127, p. 38–60, doi:10.1130/B31065.1.

Sharp, W.D., 1988, Pre-Cretaceous crustal evolution of the Sierra Nevada region, *in* Ernst, W.G., ed., Metamorphism and Crustal Evolution of the Western United States: Englewood Cliffs, New Jersey, Prentice-Hall, p. 824–864.

Shervais, J.W., 1990, Island arc and ocean crust ophiolites: Contrasts in the petrology, geochemistry, and tectonic style of ophiolite assemblages in the California Coast Ranges, *in* Malpas, J., Moores, E., Panayiotou, A., and Xenophontos, C., eds., Ophiolites: Oceanic Crust Analogs: Nicosia, Cyprus Geological Survey Department, p. 507–520.

Shervais, J.W., and Kimbrough, D.L., 1985, Geochemical evidence for the tectonic setting of the Coast Range ophiolite: A composite island arc–oceanic crust terrane in western California: Geology, v. 13, p. 35–38, doi:10.1130/0091-7613(1985)13<35:GEFTTS>2.0.CO;2.

Shervais, J.W., Kimbrough, D.L., Renne, P., Hanan, B.B., Murchey, B., Snow, C.A., Zoglman-Schuman, M.M., and Beaman, J., 2004, Multi-stage origin of the Coast Range ophiolite, California: Implications for the life cycle of supra-subduction zone ophiolites: International Geology Review, v. 46, p. 289–315, doi:10.2747/0020-6814.46.4.289.

Shervais, J.W., Murchey, B.L., Kimbrough, D.L., Renne, P.R., and Hanan, B.B., 2005, Radioisotopic and biostratigraphic age relations in the Coast Range ophiolite, northern California: Implications for the tectonic evolution of the western Cordillera: Geological Society of America Bulletin, v. 117, p. 633–653, doi:10.1130/B25443.1.

Short, P.F., and Ingersoll, R.V., 1990, Petrofacies and provenance of the Great Valley Group, southern Klamath Mountains and northern Sacramento Valley, *in* Ingersoll, R.V., and Nilsen, T.H., eds., Sacramento Valley Symposium and Guidebook: Society of Economic Paleontologists and Mineralogists, Pacific Section, v. 65, p. 39–52.

Sliter, W.V., 1975, Foraminiferal life and residue assemblages from Cretaceous slope deposits: Geological Society of America Bulletin, v. 86, p. 897–906, doi:10.1130/0016-7606(1975)86<897:FLARAF>2.0.CO;2.

Sliter, W.V., and Baker, R.A., 1972, Cretaceous bathymetric distribution of benthic foraminifers: Journal of Foraminiferal Research, v. 2, p. 167–183, doi:10.2113/gsjfr.2.4.167.

Snow, C.A., and Scherer, H.H., 2006, Terranes of the western Sierra Nevada Foothills metamorphic belt, California: A critical review: International Geology Review, v. 48, p. 46–62, doi:10.2747/0020-6814.48.1.46.

Snow, C.A., Wakabayashi, J., Ernst, W.G., and Wooden, J.L., 2010, Detrital zircon evidence for progressive underthrusting in Franciscan metagraywackes, west-central California: Geological Society of America Bulletin, v. 122, p. 282–291, doi:10.1130/B26399.1.

Sprague, A.R., Sullivan, M.D., Campion, K.M., Jensen, G.N., Goulding, D.K., Sickafoose, D.K., and Jennette, D.C., 2002, The physical stratigraphy of deep-water strata: A hierarchical approach to the analysis of genetically related elements for improved reservoir prediction: Houston, Texas, American Association of Petroleum Geologists Annual Meeting Abstracts, p. 10–13.

Stacey, J.S., and Kramers, J.D., 1975, Approximation of terrestrial lead isotope evolution by a two stage model: Earth and Planetary Science Letters, v. 26, p. 207–221, doi:10.1016/0012-821X(75)90088-6.

Stern, R.J., and Bloomer, S.H., 1992, Subduction zone-infancy: Examples from the Eocene Izu-Bonin-Mariana and Jurassic California arcs: Geological Society of America Bulletin, v. 104, p. 1621–1636, doi:10.1130/0016-7606(1992)104<1621:SZIEFT>2.3.CO;2.

Stern, T.W., Bateman, P.C., Morgan, B.A., Newell, M.F., and Peck, D.L., 1981, Isotopic U-Pb ages of zircon from the granitoids of the central Sierra Nevada, California: U.S. Geological Survey Professional Paper 1185, 19 p.

Stevenson, C.J., Jackson, C.A.-L., Hodgson, D.M., Hubbard, S.M., and Eggenhuisen, J.T., 2015, Deep-water sediment bypass: Journal of Sedimentary Research, v. 85, p. 1058–1081, doi:10.2110/jsr.2015.63.

Sullivan, M.D., Foreman, J.L., Jennette, D.C., Stern, D., Jensen, G.N., and Goulding, F.J., 2004, An integrated approach to characterization and modeling of deep-water reservoirs, Diana field, western Gulf of Mexico, *in* Grammer, G.M., Harris, P.M., and Eberli, G.P., eds., Integration of Outcrop and Modern Analogs in Reservoir Modeling: American Association of Petroleum Geologists Memoir 80, p. 215–234.

Surpless, K.D., 2014, Geochemistry of the Great Valley Group: An integrated provenance record: International Geology Review, v. 57, p. 747–766, doi:10.1080/00206814.2014.923347.

Sylvester, Z., Pirmez, C., and Cantelli, A., 2011, A model of submarine channel-levee evolution based on channel trajectories: Implications for stratigraphic architecture: Marine and Petroleum Geology, v. 28, p. 716–727, doi:10.1016/j.marpetgeo.2010.05.012.

Tagami, T., and Dumitru, T.A., 1996, Provenance and thermal history of the Franciscan accretionary complex: Constraints from zircon fission track thermochronology: Journal of Geophysical Research, v. 101, p. 11,353–11,364, doi:10.1029/96JB00407.

Taylor, S.R., and McLennan, S.M., 1985, The Continental Crust: Its Composition and Evolution: Oxford, UK, Blackwell, 312 p.

Tikoff, B., and de Saint Blanquat, M., 1997, Transpressional shearing and strike-slip partitioning in the Late Cretaceous Sierra Nevada magmatic arc, California: Tectonics, v. 16, p. 442–459, doi:10.1029/97TC00720.

Tikoff, B., and Greene, D., 1997, Stretching lineations in transpressional shear zones: An example from the Sierra Nevada Batholith, California: Journal of Structural Geology, v. 19, p. 29–39, doi:10.1016/S0191-8141(96)00056-9.

Tikoff, B., and Teyssier, C., 1992, Crustal-scale, en echelon "P-shear" tensional bridges: A possible solution to the batholithic room problem: Geology, v. 20, p. 927–930, doi:10.1130/0091-7613(1992)020<0927:CSEEPS>2.3.CO;2.

Tikoff, B., Davis, M.R., Teyssier, C., and de St. Blanquat, M., Habert, G., and Morgan, S., 2005, Fabric studies within the Cascade Lake shear zone, Sierra Nevada, California: Tectonophysics, v. 400, v. 209–226, doi:10.1016/j.tecto.2005.03.003.

Tobisch, O.T., Saleeby, J.B., Renne, P.R., McNulty, B., and Tong, W., 1995, Variations in deformation fields during development of a large volume magmatic arc, central Sierra Nevada, California: Geological Society of America Bulletin, v. 107, p. 148–166, doi:10.1130/0016-7606(1995)107<0148:VIDFDD>2.3.CO;2.

Tobisch, O.T., Fiske, R.S., Saleeby, J.B., Holt, E., and Sorensen, S.S., 2000, Steep tilting of metavolcanic rocks by multiple mechanisms, central Sierra Nevada, California: Geological Society of America Bulletin, v. 112, p. 1043–1058, doi:10.1130/0016-7606(2000)112<1043:STOMRB>2.0.CO;2.

Tripathy, A., Housh, T.B., Morisani, A.M., and Cloos, M., 2005, Detrital zircon geochronology of coherent jadeitic pyroxene-bearing rocks of the Franciscan Complex, Pacheco Pass, California: Implications for unroofing: Geological Society of America Abstracts with Programs, v. 37, no. 7, p. 18.

Unruh, J.R., Dumitru, T.A., and Sawyer, T.L., 2007, Coupling of Early Tertiary extension in the Great Valley forearc basin with blueschist exhumation in the underlying Franciscan accretionary wedge at Mount Diablo, California: Geological Society of America Bulletin, v. 119, p. 1347–1367, doi:10.1130/B26057.1.

Wakabayashi, J., 1992, Nappes, tectonics of oblique plate convergence, and metamorphic evolution related to 140 million years of continuous subduction, Franciscan Complex, California: The Journal of Geology, v. 100, p. 19–40, doi:10.1086/629569.

Wakabayashi, J., 1999, Subduction and the rock record: Concepts developed in the Franciscan Complex, California, *in* Sloan, D., Moores, E.M., and Stout, D., eds., Classic Cordilleran Concepts: A View from California: Geological Society of America Special Paper 338, p. 123–133, doi:10.1130/0-8137-2338-8.123, doi:10.1130/0-8137-2338-8.123.

Wakabayashi, J., 2015, Anatomy of a subduction complex: Architecture of the Franciscan Complex, California, at multiple length and time scales: International Geology Review, v. 57, p. 669–746, doi:10.1080/00206814.2014.998728.

Wakabayashi, J., and Rowe, C.D., 2015, Whither the Megathrust?: Localization of large-scale subduction slip along the upper contact of a mélange: International Geology Review, v. 57, p. 854–870, doi:10.1080/00206814.2015.1020453.

Wentworth, C.M., Blake, M.C., Jr., Jones, D.L., Walter, A.W., and Zoback, M.D., 1984, Tectonic wedging associated with emplacement of the Franciscan assemblage, California Coast Ranges, *in* Blake, M.C., Jr., ed., Franciscan Geology of Northern California: Los Angeles, California, Society of Economic Paleontologists and Mineralogists, v. 43, p. 163–173.

Williams, T.A., 1997, Basin-fill architecture and forearc tectonics, Cretaceous Great Valley Group, Sacramento Basin, northern California [Ph.D. thesis]: Stanford, California, Stanford University, 412 p.

Williams, T.A., and Graham, S.A., 2013, Controls on forearc basin architecture from seismic and sequence stratigraphy of the Upper Cretaceous Great Valley Group, central Sacramento basin, California: International Geology Review, v. 55, p. 2030–2059, doi:10.1080/00206814.2013.817520.

Williams, T.A., Graham, S.A., and Constenius, K.N., 1998, Recognition of a Santonian submarine canyon, Great Valley Group, Sacramento Basin, California: Implications for petroleum exploration and sequence stratigraphy of deep marine strata: American Association of Petroleum Geologists Bulletin, v. 82, p. 1575–1595.

Wyld, S.J., Umhoefer, P.J., and Wright, J.E., 2006, Reconstructing northern Cordilleran terranes along known Cretaceous and Cenozoic strike-slip faults: Implications for the Baja British Columbia hypothesis and other models, *in* Haggart, J.W., Enkin, R.J., and Monger, J.W.H., eds., Paleogeography of the North American Cordillera: Evidence For and Against Large-Scale Displacements: Geological Association of Canada Special Paper 46, p. 277–298.

Plate 1: Stratigraphic panel, measured sections, and location map of Panoche Fm. deposits surrounding the San Luis Reservoir

KEY

Sedimentology Key

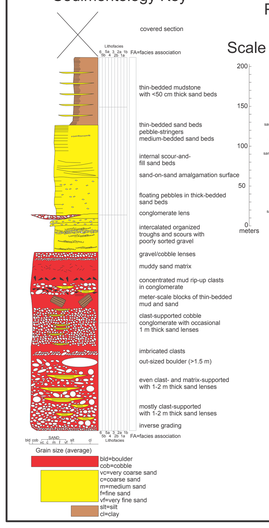

Paleocurrent rose diagram on imbricated clasts

Scale

Detrital zircon and sandstone petrography sample (name)

Sandstone petrography sample only (name)

Conglomerate clast count

Mudrock geochemistry sample (name)

Facies Associations

- FA1 = thin-bedded turbidites
- FA2 = thick-bedded, amalgamated sandy turbidites
- FA3 = clast- and matrix-supported cobble and boulder conglomerate with sand lenses
- FA4 = clast-supported cobble conglomerate
- FA5 = cross-bedded sand and/or gravel beds and chaotic debrites

Channel Complex Sets

(blank areas represent cover)

? = unknown lateral continuity

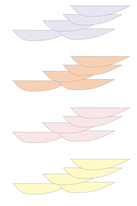

Lithofacies Descriptions

Lithofacies name	Defining features	Grain size R= range, A=average, M=matrix	Support	Grading	Bedding thickness range (m): style	Turbidite divisions (Lowe, 1982; Bouma, 1962)	Sedimentary structures	Other features
L1a	muddy low-density turbidites, bioturbated	R: mud-fine sand A: mud	clast	normal	0.02-0.5: thin	S3/Ta, Tabc, Tab, Tcd, Tde	common planar beds, rare ripples	horizontal trace fossils common
L1b	muddy low-density turbidites, non-bioturbated	R: mud-fine sand A: mud	clast	normal	0.02-0.5: thin	S3/Ta, Tabcd, Tab, Tcd	common planar beds, rare ripples	laterally continuous
L2a	sandy, mostly low-density turbidites	R: fine-medium sand A: medium sand	clast	normal	0.1-0.5: thin	Ta, Tab, Tabcd	common planar beds, rare ripples	laterally grades into L2b
L2b	sandy, mostly high-density turbidites	R: fine sand-cobble A: medium sand	clast	normal	0.5-3.0: medium-thick	S3, Tab, Tb	common planar beds	moderately sorted, amalgamated sand beds, rare cobble lenses, interbedded within L5a and L5b, laterally continuous bed can grade into L2a
L3	debrites	R: mud-cobble A: mud M: mud-sand	matrix	chaotic	1.0-3.0: medium-thick	chaotic	concentrated mud rip-ups	chaotic beds of poorly-sorted mud, sand, gravel, rare cobbles; mud rip-ups are angular blocks of thin-beds
L4	sandy/gravel high-density turbidites	R: medium sand-cobble A: very coarse sand	clast	normal	1.0-3.0: thick	R3, S1, S3/Ta, Tab,Tb	trough cross-bedding with aligned gravel, common internal scour surfaces with on-lapping gravel (channels), common planar beds and mud rip-ups	well-organized, well-sorted, commonly found at bases of thick conglomerate, rare outsized cobbles and boulders, common inclined bar surfaces
L5a	conglomeratic high-density turbidites, mixed support	R: medium sand-boulder A: cobble/boulder M: medium sand	clast and matrix	mostly absent, rare inverse	1.0-10: thick	R3, S3/Ta, Tab,Tb	common planar beds in sand lenses, occasional mud rip-ups	laterally and vertically grades to L5b, moderate to poor sorting, contains largest boulders (up to 3.5 m), most clasts are well-rounded to sub-rounded, common 0.5-2.0 m thick lenses of medium sand with occasional boulders, cobbles, and gravel
L5b	conglomeratic high-density turbidites, mostly clast-supported	R: medium sand-boulder A: cobble/boulder M: medium sand	mostly clast	mostly absent, normal at top	0.5-5.0: thick	R1, R3, S3/Ta, Tab,Tb	aligned gravel and cobbles, common planar beds in sand lenses, mud rip-ups	laterally and vertically grades to L5a, amalgamated cobble/boulder lenses, common imbrication, moderate sorting, common 0.5-2.0 m thick lenses of medium sand with occasional cobbles and gravel
L6	conglomeratic high-density turbidites, clast-supported	R: medium sand-cobble A: cobble M: medium sand	clast	mostly absent, occasional normal	1.0-5.0: thick	R1, R3, S3/Ta, Tab,Tb	aligned gravel and cobbles, rare planar beds in sand lenses	common imbrication, amalgamated cobble lenses, moderate sorting, rare 0.5-1.0 m thick lenses of medium sand with occasional gravel, inclined internal erosive surfaces

Facies association panel with channel complex sets at approximately 1:1 scale

(blank areas represent cover)

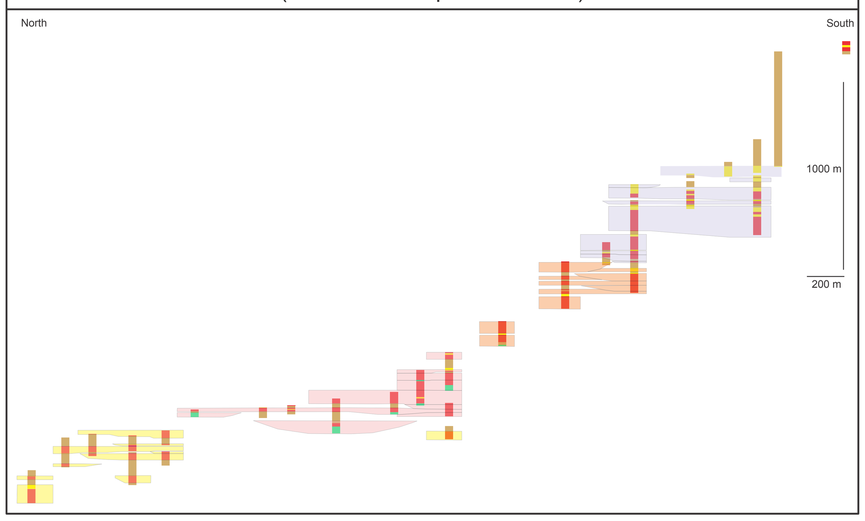

Location map and facies associations for San Luis Reservoir area